

MASTER THESIS

GENERALIZED WANNIER STATES IN INHOMOGENEOUS LATTICES

JONATHAN ENDERS

INSTITUT FÜR THEORETISCHE PHYSIK
GOETHE-UNIVERSITÄT

First examiner and supervisor: Prof. Dr. Hofstetter
Second examiner: Prof. Dr. Valenti
Advisor: Dr. Bissbort

April 3, 2014

Contents

1	Introduction	4
1.1	Generalized Wannier States	5
1.2	References and History	5
2	The Mathematical Procedure to obtain Generalized Wannier States	7
2.1	Wannier States Definitions	7
2.1.1	Common Definition for Wannier States	7
2.1.2	Generalized Wannier States	9
2.2	Overview	10
2.2.1	Basic Operations	10
2.3	Real Space Propagation	12
2.3.1	Lattice in a Well	13
2.3.2	Infinite Lattice	14
2.4	Inhomogeneous Lattice	18
2.4.1	Homogeneous Lattice Wannier States	19
2.4.2	Inhomogeneous Lattice Eigenstates	19
2.4.3	Inhomogeneous Lattice Wannier States	20
2.5	Hubbard Model	21
2.5.1	Hubbard-like Model for Inhomogeneous Lattices	24
2.6	Different Inhomogeneity Strengths	25
2.6.1	Tracking the Energy Eigenvalues	25
2.6.2	Band Assigning	26
2.6.3	Avoided Crossings	27
2.6.4	Measures	27
2.6.5	Tracing the Bands	28
2.7	Boundary Conditions	31
2.7.1	Periodic versus Non-Periodic Localized Basis	32
3	Numerical Implementation	34
3.1	Propagation	35
3.1.1	Extraction of Energy Eigenstates from Bulirsch Stoer Solver	35
3.1.2	Spline Interpolation	35
3.2	Multiple Root Finding	36
3.2.1	Fast Homogeneous System Eigenvalues	36
3.3	Wannier Functions	38
3.3.1	Different System Size for the Homogeneous and the Inhomogeneous System	38

3.3.2	Spread of the Homogeneous Wannier Functions	39
3.4	Homogeneous System Results	39
3.5	Diagonalization of Complete System Hamiltonian	43
3.5.1	Basis for Diagonalizing the complete Hamiltonian	43
3.5.2	Cut-off for Off-site Elements	43
3.5.3	Restricting Integration Length	43
3.6	Verification	44
3.6.1	Comparison with Foreign Implementation	44
3.6.2	Determining Calculation Inaccuracies	45
3.6.3	Limits	49
3.6.4	Validity Checks	51
3.7	Performance	52
3.7.1	Complexity of Operations	52
3.7.2	Execution Speed and Program Output	53
3.7.3	Own Implementations of Numerical Routines	53
3.8	Units	54
4	Results for a Lattice in a Well	56
4.1	Additional Linear Potential	58
4.2	Conclusion	60
5	Results for a Lattice in a Harmonic Trap	61
5.1	Qualitative Behaviour Portrayed in a Small System	62
5.1.1	Eigenstates and Wannier States for Shallow Trap	62
5.1.2	Hubbard Parameters for a Shallow Trap	64
5.1.3	Avoided Crossing	65
5.1.4	Hubbard Parameters at Avoided Crossing	68
5.1.5	Strong Trap	68
5.2	Realistic Systems	71
5.2.1	Shallow Trap	71
5.2.2	Strong Trap	72
5.2.3	Large System	74
5.3	Conclusion	76
6	Results for a Lattice with Quasi-Disorder	77
6.1	General Analysis for Incommensurate Lattices	78
6.1.1	Energy Eigenvalues	78
6.1.2	Energy and Wannier States	79
6.1.3	On-site Energy, Hopping and On-site Interaction	81
6.1.4	Statistics for Hubbard Model Parameters	82
6.2	Localization in Incommensurate Lattices	87
6.2.1	Extended Aubry-André Model	87
6.2.2	Discretized Real Space Schrödinger Equation	89
6.3	Conclusion	97
7	Outlook	98

A Derivations and non-implemented material	100
A.1 Conversion of Effective Schrödinger Equation to Real-Valued First Order DGL	100
A.2 Infinite System Band Projection Operator	102
A.2.1 Accelerated Calculation	103
A.3 Calculation of State Position	104
A.3.1 Expectation Value of \hat{x}	104
A.3.2 Expectation Value of $\sum_{\alpha} \hat{x}_{\alpha}$	104
A.3.3 Relation between the Expectation Values of \hat{x} and $\sum_{\alpha} \hat{x}_{\alpha}$	104
A.4 Fast Calculation of the Localization	105
A.5 Exact Diagonalization	106
A.5.1 Localized States at Avoided Crossing	109

Chapter 1

Introduction

Throughout history, humans have benefited from an understanding of how the materials that fill the world around them behave. A simple qualitative understanding enabled cavemen to store fire, blacksmiths to forge harder steel and telegraph operators to transport information much faster than thought possible before. **Solid state physics** brought the art of understanding materials' behaviours to a new level. Rooted on an extremely accurate microscopic description, it is today possible to predict phenomena through mere calculation.

While the fundamental laws that govern the behaviour of materials have been deciphered and are astonishingly simple¹, applying them to real life situations proves incredibly demanding in terms of calculatory effort. Fortunately more complex relations can be derived from the fundamentals, oftentimes using approximations that lower the calculatory demands to regions accessible by today's **computers**. The existence of the latter can be almost exclusively accredited to solid state physics. The last point illustrates the self-supporting and self-accelerating properties of this field of science, which, on its way to perfection, nurtures almost every other field of science and throughout everyday life along the way.

A more recent advancement in the field is the synthesis of systems which obey the laws of a solid, but are in fact much larger with respect to particle distances (lattice constant) and particle masses ($\approx 10,000\times$). Such a system can be used as a **quantum simulator** because dynamics are much slower and therefore easier to follow. Additionally, probing is easier. Finally and most importantly the way these systems are implemented offers new means of control unimaginable for actual solids, see [ASSK⁺06]. An example of such a quantum simulator is given by [SBM⁺11].

A normal solid state system can be described by a periodic potential, i.e. the periodically aligned almost motionless nuclei and the electrons around them. With this potential, the dynamics of a single electron in the crystal can be described. In the novel approach mentioned earlier, so-called **optical lattices**[Blo05] are used to create a periodic potential in which atoms behave like the electrons in a actual solid state system. In contrast to an actual solid, the potential strength and its periodicity can be changed easily by changing the wavelength or intensity of a laser. In addition, even the interaction strength

¹regarding only electromagnetic interactions and disregarding relativistic effects

between the mobile particles can be tuned. These interactions can be controlled by *Feshbach Resonances* which can be adjusted all the way from repulsive to attractive via an external magnetic field. Many of the formerly mentioned systems' properties can, just like the properties for most solids, be described using Hubbard models.

The **Hubbard model** is the simplest model to describe solid state systems. Despite this, it can describe a remarkable range of phenomena, especially when its many variations are taken into account. Formulated in the framework of second quantization, it relies on a localized basis that takes advantage of the periodicity of the potential. The states that make up this localized basis are the Wannier states, named after the person who first introduced them in [Wan37]. The goal in this thesis is to investigate a generalized but broadly unknown procedure to calculate this basis.

1.1 Generalized Wannier States

In the **commonly** used procedure, **Wannier states** are obtained through a Fourier series over the Bloch states. While the states obtained in this way obey the properties demanded by the definition for Wannier states (orthogonality, translationally symmetry, inversion symmetry), the resulting states are not unique. This is due to the phases of the Bloch states which can be chosen arbitrarily thus leading to different Wannier states. Demanding further properties, the choice can be made unique. A minimal spatial variance is the additional property requested in the common procedure. While it is easy to fulfill this requirement for some lattice geometries (cubic lattices), others require a very computation demanding minimum search.

Using another procedure can help. In a procedure published by S. Kivelson in [KS82] in 1982, the Wannier states are shown to be the eigenstates of the band projected position operator. Given a band projector, Wannier states can **systematically** and **uniquely** be calculated in this way without a complex minimization procedure. The resulting states don't just fulfill the properties demanded by the Wannier state definition in a homogeneous lattice, but are also maximally localized, i.e. they have minimal spatial variance with respect to the Bloch phases. This method was first applied in [BDH12].

Relying only on a defined band projector, Kivelson's procedure also has the benefit of being more general than the common procedure. In an **inhomogeneous lattice**, i.e. a lattice potential which has some foreign contribution that interrupts the strict periodicity, bands are expected to prevail to some degree. This offers the possibility to evoke Wannier states for inhomogeneous lattices. This procedure, being more general than the commonly used procedure, the states are also referred to as **generalized Wannier states**.

1.2 References and History

The research field of optical lattices developed continuously from the field of laser cooling. One of the first experimental realizations using a standing wave to cool atoms is explained in [PC89]. *Optical molasses* are one of the precursors to optical lattices [LCV⁺92]. One of the first experimental realizations using

standing wave laser beams to trap atoms is explained in [HH93]. The term *optical lattice* in this context was introduced in [HZH94]. A much more detailed description for optical lattice systems is given in [Blo05].

Chapter 2

The Mathematical Procedure to obtain Generalized Wannier States

In this chapter the paths that lead to generalized Wannier functions will be explained from a theoretical, mathematical point of view. The definitions for Wannier functions will be discussed first so that the goal is known. Then a multitude of different paths will be presented and some of the steps involved will be discussed in greater detail. Also, the follow-up quantities that result from the generalized Wannier functions and their use in Hubbard-like models will be explained.

2.1 Wannier States Definitions

Having a localized basis in which to perform calculations, brings remarkable benefits. Aside from the advantage mentioned in section 2.4, one of the strongest arguments for this statement is the success of the Hubbard model, see section 2.5. It relies on a localized basis and can thus take advantage of the benefits of the tight binding approximation.

Wannier states constitute such a localized basis.¹

2.1.1 Common Definition for Wannier States

Wannier functions are the real-space representation of the Wannier states

$$w_{l,\alpha}(x) = \langle x | l, \alpha \rangle$$

In the commonly established definition, Wannier states are defined through a **Fourier series** over the Bloch states (see section 2.3.2) in a band

¹A proof that Wannier functions are exponentially localized in insulators can be found in [BPC⁺07].

$$|l, \alpha\rangle = \frac{1}{\sqrt{N}} \sum_k e^{-ikla} |k, \alpha\rangle$$

This definition causes all the resulting states in one band to be **connected through translation** in real space

$$w_{l,\alpha}(x) = w_{l+\Delta l,\alpha}(x + \Delta l a)$$

with a being the lattice constant
which can be proven easily through the use of the Bloch theorem

$$\begin{aligned} w_{l+\Delta l,\alpha}(x + \Delta l a) &= \frac{1}{\sqrt{N}} \sum_k e^{-ik(l+\Delta l)a} \varphi_{k,\alpha}(x + \Delta l a) \\ &= \frac{1}{\sqrt{N}} \sum_k e^{-ik(l+\Delta l)a} e^{ik(x+\Delta l a)} u_{k,\alpha}(x + \Delta l a) \\ &= \frac{1}{\sqrt{N}} \sum_k e^{-ikla} e^{ikx} u_{k,\alpha}(x) \\ &= \frac{1}{\sqrt{N}} \sum_k e^{-ikla} \varphi_{k,\alpha}(x) \\ &= w_{l,\alpha}(x) \end{aligned}$$

Also, all the Wannier states are mutually **orthogonal**

$$\begin{aligned} \langle l, \alpha | l', \alpha' \rangle &= \frac{1}{N} \sum_{k,k'} e^{ikla} e^{-ik'l'a} \langle k, \alpha | k', \alpha' \rangle \\ &= \frac{1}{N} \sum_{k,k'} e^{i(kl - k'l')a} \delta_{k,k'} \delta_{\alpha,\alpha'} \\ &= \frac{1}{N} \sum_k e^{ik(l-l')a} \delta_{\alpha,\alpha'} \\ &= \delta_{l,l'} \delta_{\alpha,\alpha'} \end{aligned}$$

All the Wannier states in a band span the same space as all the energy eigenstates in a band. Thus all the Wannier states form a **complete basis**.

But the Wannier states which are defined in the upper way are **not unique** because the phases of the Bloch states can be chosen arbitrarily. The choice can be made unique by demanding that the spatial variance of the Wannier states is minimal. This constraint together with the requirement of the Wannier functions being real allows for only one specific choice of all of the Bloch phases.

In simple cubic lattice geometries, Wannier states can be localized easily. This is accomplished with a simple **recipe** that advises to choose the phases of all the Bloch functions such that they are all solely real (phase=0) in a certain lattice site for odd bands. For Wannier states in even bands, the phase of the derivative of the Bloch functions has to be chosen 0. Obviously the amplitude

of the resulting Wannier states will be high at this lattice site and experience yields that it is also maximally localized there with respect to the available energy eigenstate phases. The remaining Wannier states can then be obtained by translation of the first state obtained for each band in this way.

When the lattice geometry is more complex and particularly when treating multiple dimensions, obtaining the Wannier states is not that simple. In such a case the phases of the Bloch functions have to be chosen through a minimization condition on the localization of the Wannier functions. Given n states in a band the minimization is a minimum search in the space spanned by the n phases of the Bloch functions. This is **computationally demanding** especially because there is the possibility to find only a local minimum instead of the desired global minimum. This problem arises for example in [JInA13].

An in-depth description of methods to obtain maximally-localized Wannier functions can be found in [MSV03] and [MMY⁺12]. A software that performs this task is presented in [MYL⁺08].

2.1.2 Generalized Wannier States

In the paper [KS82], S. Kivelson looks at the **band projected position operator** $\hat{x}_\alpha = \hat{P}_\alpha \hat{x} \hat{P}_\alpha$ (with \hat{P}_α being the projection operator onto band α). He finds that the eigenstates $|l, \alpha\rangle$ of this operator have the **same properties** as the Wannier states that were discussed in section 2.1.1, i.e. for homogeneous lattices they are translationally invariant and orthogonal. In addition, they are by construction already **maximally localized** in homogeneous lattices.

As already discussed in section 1.1 this definition is the core idea for this thesis because it is more general and thus more versatile than the common definition. That is to say, localized states can be calculated whenever a band projection operator can be reasonably defined. To do this, merely the states that belong to a certain band α need to be chosen $|n\rangle \rightarrow |n, \alpha\rangle$. A band projection operator can then be defined in terms of a sum over the energy eigenstates:

$$P_\alpha = \sum_n |n, \alpha\rangle \langle n, \alpha|$$

Here the versatility of this definition can be seen. Whenever there is a band gap or whenever a set of states are used to **define** a **band projector** in the upper way, the eigenstates of the band projected position operator can be calculated. As a result, to some extent, inhomogeneous lattice systems can be treated with this definition.

While for homogeneous lattices assigning a band index to every state is not an issue thanks to the Bloch theorem, for **inhomogeneous lattices** this causes a bigger challenge as discussed in section 2.6.2.

After the band projector is defined, the matrix elements of the band projected position operator can be calculated

$$\begin{aligned} X_{n,n'} &= \langle n, \alpha | \hat{x}_{\bar{\alpha}} | n', \alpha' \rangle = \langle n, \alpha | \left(\sum_{\bar{n}} |\bar{n}, \bar{\alpha}\rangle \langle \bar{n}, \bar{\alpha}| \right) \hat{x} \left(\sum_{\bar{n}'} |\bar{n}', \bar{\alpha}\rangle \langle \bar{n}', \bar{\alpha}| \right) | n', \alpha' \rangle \\ &= \delta_{\alpha, \bar{\alpha}} \delta_{\alpha', \bar{\alpha}} \langle n, \alpha | \hat{x} | n', \alpha' \rangle \end{aligned}$$

Then $X_{n,n'}$ can be diagonalized as explained in section 2.2.1. This will yield the overlap matrix between the energy eigenstates and the Wannier states $\langle n, \alpha | l, \alpha' \rangle = \delta_{\alpha, \alpha'} \langle n, \alpha | l, \alpha' \rangle$. These are simply the common Wannier states in the specific Bloch representation.

The Wannier functions can then be calculated from the overlap and the energy eigenfunctions:

$$w_{l,\alpha}(x) = \sum_n \langle n, \alpha | l, \alpha \rangle \varphi_{n,\alpha}(x)$$

Another peculiarity should be noted. While this definition, applied to inhomogeneous lattice systems, causes the resulting Wannier states to still be orthogonal, they are generally **no longer translationally symmetric**. This is not a problem however, as all the Wannier states are obtained through the diagonalization.

The states calculated using S. Kivelson's definition are referred to as the *generalized Wannier states* throughout this thesis.

2.2 Overview

There are different paths that can be used to acquire generalized Wannier functions. In this chapter the properties of these **different paths (simplicity, numerical effort and accuracy)** and the detailed steps that are involved with each path are discussed.

Figure 2.1 visualizes the complexity that is involved with choosing a path. The starting point is at the top with a given inhomogeneous lattice potential. To proceed with this potential, at least the three listed actions right below can be taken. Note that even though using the left path using a real space propagation of the stationary Schrödinger equation seems to be the most direct path to the inhomogeneous eigenstates, this path has major drawbacks in terms of numerical efficiency. Thus, even though the right paths may seem more complex, they are really more practical.

2.2.1 Basic Operations

Diagonalization of an Observable

Every useful observable (e.g. Hamiltonian) needs to be defined in some basis (other than its eigenbasis in which every observable is by definition diagonal). The eigenvalues and -states for the observable can then be obtained in that basis by diagonalizing the observable. Consider an observable \hat{O} with its eigenstates $|O\rangle$ and eigenvalues O . Let the states $|b\rangle$ be the basis that \hat{O} is defined in.

$$\begin{aligned} \hat{O} &|O\rangle = O |O\rangle \\ \sum_b \langle b' | \hat{O} | b \rangle \langle b | O \rangle &= O \langle b' | O \rangle \end{aligned}$$

$O_{b',b} = \langle b' | \hat{O} | b \rangle$ is given by the definition of the observable. The second equation can be read as an **eigenvalue equation**. Solving the corresponding

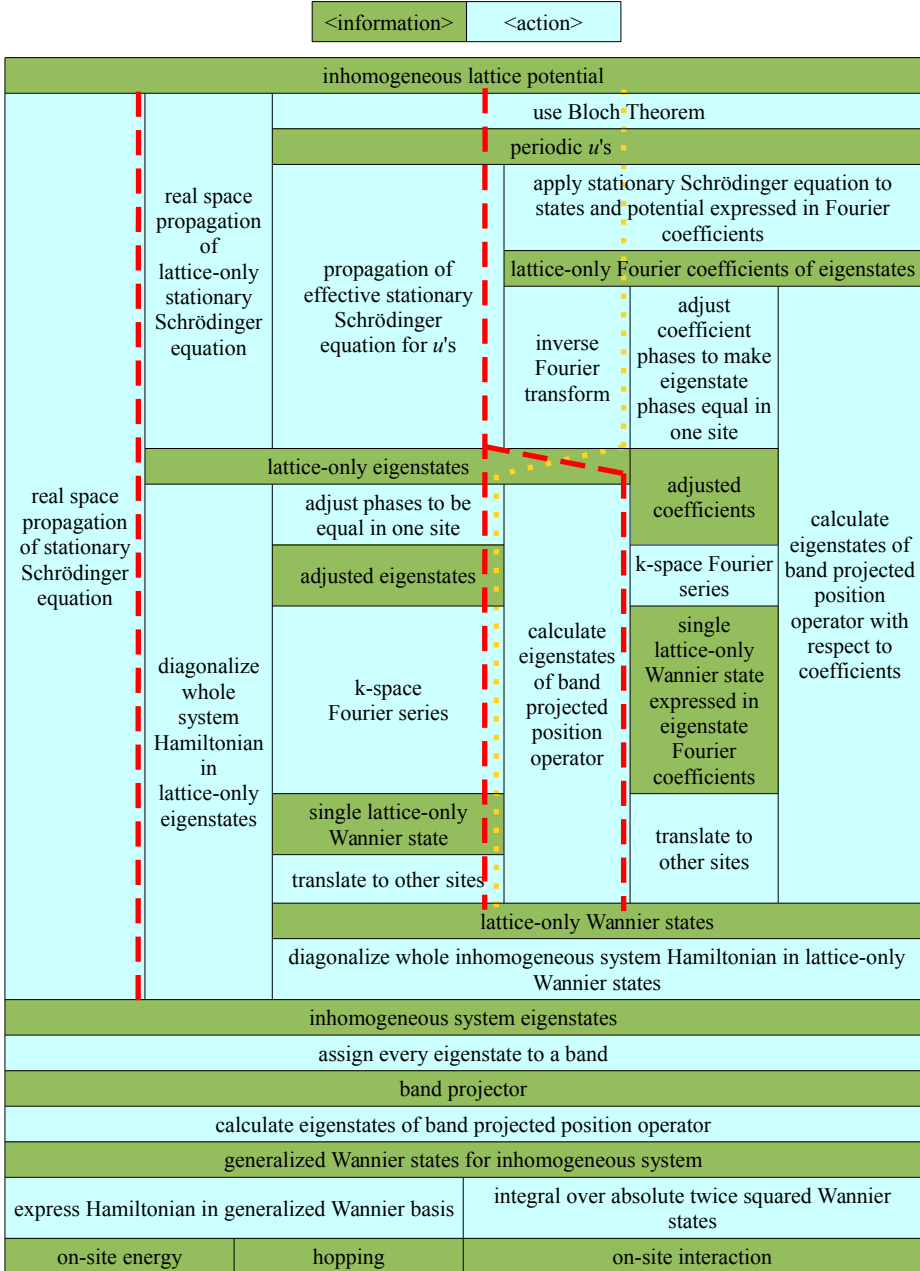


Figure 2.1: The many possible paths to obtain generalized Wannier functions. The starting point is at the top with an expression for the potential assumed as given. At the bottom are the final results, i.e. hopping, on-site energy and -interaction obtained through the generalized Wannier functions. Four path are marked, three with a dashed red and one with a dotted yellow line. The red lines correspond to the paths that have been implemented in the course of this thesis. The yellow line corresponds to an alternative implementation by Ulf Bissbort which was used to compare results. All implementations continue beyond the shown paths to arrive at the generalized Wannier states (not shown so as to improve readability).

eigenvalue problem gives the overlap $\langle b|O \rangle$ between the observable's eigenstates and the basis states.

Basis Transformation for an Observable

A state $|O\rangle$ can be expressed in another basis $|b\rangle$ using

$$|O\rangle = \sum_b c_{b,O} |b\rangle$$

with $c_{b,O} = \langle b|O \rangle$.

To represent an observable (e.g. Hamiltonian) in another basis, the above basis transformation can be applied twice

$$\begin{aligned} O_{b,b'} &= \langle b|\hat{O}|b'\rangle = \sum_O \langle b|O\rangle O \langle O|b'\rangle \\ &= \sum_O c_{b,O} O c_{b',O}^* \end{aligned}$$

It should be noted that this requires the knowledge about the elements $c_{b,O}$ of the basis in the observable's eigenstates. This transformation will be useful in calculating the **Hubbard parameters** in section 2.5.1.

2.3 Real Space Propagation

As mentioned before, in order to get the eigenstates of some Hamiltonian \hat{H} in some basis it has to be diagonalized in that basis. Most Hamiltonians can be expressed in real space easily, because in many problems the potential terms are initially given in real space. Despite this, they are usually not diagonal in real space because the kinetic term has to be expressed in terms of spatial derivatives (e.g. $\frac{d^2}{dx^2}$).

In order to diagonalize the Hamilton operator in real space, a **discretization** of the real space has to be applied first. With this discretization the differential operator in the Hamiltonian could be written in terms of neighboring space points yielding a matrix whose eigenstates could be found as described in section 2.2.1. A numerically advantageous equivalent is the propagation of the differential equation that results from the Hamiltonian eigenvalue equation (stationary Schrödinger equation) in real space. This also yields the desired elements $\langle x|n\rangle$ with $\hat{H}|n\rangle = E_n|n\rangle$.

Propagating an equation is particularly easy when the **boundary conditions** in one point x_0 are given.

$$\begin{aligned}
\hat{H}|\varphi\rangle &= E|\varphi\rangle \\
(T(\hat{x}) + V(x))|\varphi\rangle &= E|\varphi\rangle \\
\left(\frac{-\hbar^2}{2m} \frac{\partial^2}{\partial x^2} + V(x) \right) \varphi(x) &= E\varphi(x) \\
\frac{\partial^2}{\partial x^2} \varphi(x) &= \frac{2m}{\hbar^2} (V(x) - E) \varphi(x) \\
\rightarrow \varphi'(x) &= \frac{\partial}{\partial x} \varphi(x) \\
\rightarrow \frac{\partial}{\partial x} \varphi'(x) &= \frac{2m}{\hbar^2} (V(x) - E) \varphi(x)
\end{aligned}$$

Using the discretization in real space, an approximate solution in the form of the Euler method can be written as

$$\begin{aligned}
\rightarrow \varphi'(x_0 + \Delta x) &\approx \varphi'(x_0) + \frac{2m}{\hbar^2} (V(x_0) - E) \varphi(x_0) \Delta x \\
\rightarrow \varphi(x_0 + \Delta x) &\approx \varphi(x_0) + \varphi'(x_0) \Delta x
\end{aligned}$$

This relation provides the means to obtain the value for φ at some arbitrary point x_1 by repetitively iterating forward (or backward) from x_0 . The accuracy of this iteration is greater the smaller Δx .

This procedure is very simple and also very general as it can be applied to arbitrary potentials in real space.

If applied to the inhomogeneous potential directly this corresponds to the most leftward path in Figure 2.1. This is done for the lattice in a well system where boundary conditions are obvious, see section 2.3.1. But in general this method is computationally too demanding.

Further problems arise when a system is infinitely large. In such cases looking at a finite subsystem might help.

Another option in an inhomogeneous lattice is to **solve the homogeneous lattice system**, i.e. an infinite system with periodicity, **first**. This can be done by either propagating the Schrödinger equation for the homogeneous system directly, corresponding to the second most leftward column in Figure 2.1. Alternatively and much more practically is the use of the Bloch theorem. Its application yields an effective Schrödinger equation acting on functions with small periodicity (u -functions) which are easily converted into the homogeneous lattice eigenfunctions. This corresponds to the third column in Figure 2.1. After the solution for the homogeneous system is known, the methods explained in section 2.4 can be used to obtain the inhomogeneous system solutions.

In the following, the paths taken in the implementation will be discussed more thoroughly.

2.3.1 Lattice in a Well

For every potential whose value jumps to ∞ instantly on the boundaries (Figure 2.2), the stationary Schrödinger equation can be propagated easily.

The value of the eigenfunction $\varphi(x)$ at either boundary needs to vanish $\varphi(x_{1,\text{boundary}}) = \varphi(x_{2,\text{boundary}}) = 0$. So either of the boundaries promises to be a good point to start the propagation.

As the stationary Schrödinger equation is a second order differential equation in space, the first derivative of the solution $\frac{\partial}{\partial x}\varphi(x)$ also needs to be set in the point where the propagation is to be started. The derivative can be chosen arbitrarily non-zero as it only affects a prefactor of the eigenfunction $\varphi(x)$. The normalization that takes place once the propagation is completed eliminates this prefactor.

With an arbitrary energy E the propagated function $\varphi_E(x)$ will in general not fulfill the boundary condition on the other edge of the potential $x_{2,\text{boundary}}$. In order to find a proper eigenstate of the problem the second boundary condition needs to be fulfilled. This can be achieved by propagating the differential equation with different values for the energy and trying to find the right energy E_{state} at which the value of the propagated function fulfills the second boundary condition. This is analogous to the problem of **finding the roots** of the function $f(E) := \varphi_E(x_{2,\text{boundary}})$.

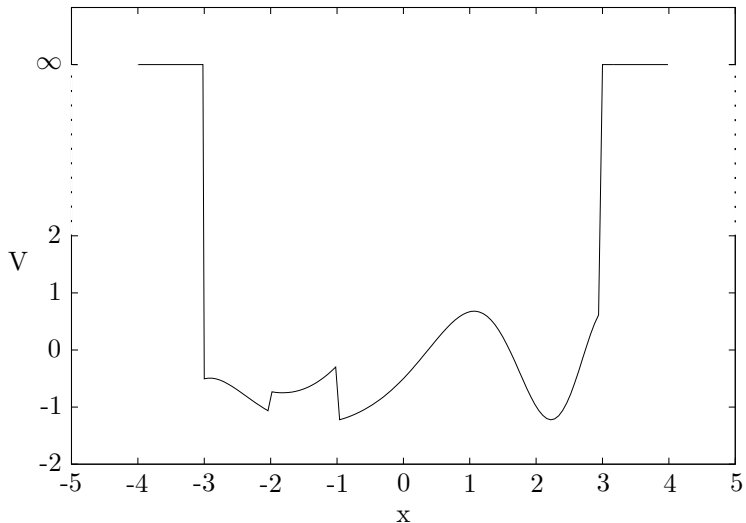


Figure 2.2: A potential with hard boundaries schematically. Eigenfunctions for such potentials can be found by propagating the stationary Schrödinger equation, starting on one of the infinite boundaries. This has to be done multiple times by a root finding procedure until the boundary condition on the other system boundary is fulfilled.

2.3.2 Infinite Lattice

All the energy eigenvalues of a particle in an infinite lattice potential taken together form intervals (bands) which are separated by intervals without eigenvalues (band gaps). Each eigenstate can also be assigned a quasi momentum k . k is determined by the **Bloch theorem** which states that every eigenfunction $\varphi_{k,\alpha}$ on the lattice can be written in terms of a periodic function $u_k(x)$ such that

$$\varphi_{k,\alpha}(x) = e^{ikx} u_{k,\alpha}(x)$$

while $u_{k,\alpha}(x)$ has the same periodicity as the lattice potential.

Plugging this expression into the stationary Schrödinger equation yields another k -dependent differential equation which can be used to determine $u_k(x)$.

$$\begin{aligned} \left(V(x) - \frac{\hbar^2}{2m} \frac{\partial^2}{\partial x^2} \right) \varphi_k(x) &= E \varphi_k(x) \\ \left(V(x) - E - \frac{\hbar^2}{2m} \frac{\partial^2}{\partial x^2} \right) e^{ikx} u_k(x) &= 0 \\ e^{ikx} \left(V(x) - E - \frac{\hbar^2}{2m} \left(ik + \frac{\partial}{\partial x} \right)^2 \right) u_k(x) &= 0 \end{aligned} \quad (2.1)$$

Given the equation above, $u_k(x)$ is periodic iff

$$u(-s) = u(s) \quad (2.2)$$

and

$$\left. \frac{\partial}{\partial x} u(x) \right|_{x=-s} = \left. \frac{\partial}{\partial x} u(x) \right|_{x=s} \quad (2.3)$$

with s being the length of half the periodicity.

With (2.1) further properties of $u(x)$ can also be derived that prove helpful. Reversing the coordinate system yields

$$\left(V(-x) - E - \frac{\hbar^2}{2m} \left(ik + \frac{\partial}{\partial(-x)} \right)^2 \right) u_k(-x) = 0$$

Assuming a symmetric potential $V(x) = V(-x)$ yields

$$\left(V(x) - E - \frac{\hbar^2}{2m} \left(-(-ik + \frac{\partial}{\partial x}) \right)^2 \right) u_k(-x) = 0$$

Complex conjugation yields

$$\left(V(x) - E - \frac{\hbar^2}{2m} \left(ik + \frac{\partial}{\partial x} \right)^2 \right) u_k^*(-x) = 0$$

So $u_k(x)$ complex conjugated and vertically flipped fulfills the same differential equation as $u_k(x)$ itself. Together with the common point at $x = s$ where the conditions (2.2) and (2.3) hold this ensures that

$$u_k(x) = u_k^*(-x)$$

for all x . Rephrased: The real part of $u_k(x)$ is symmetric and the imaginary part is antisymmetric.

It follows for the derivative:

$$\frac{\partial}{\partial x} u_k(x) = -\frac{\partial}{\partial(-x)} u_k^*(-x) \quad (2.7)$$

or rephrased:

$$\left. \frac{\partial}{\partial y} u_k(y) \right|_{y=x} = - \left. \frac{\partial}{\partial y} u_k^*(y) \right|_{y=-x} \quad (2.8)$$

Being a second order differential equation the general solution of $u(x)$ can be constructed using two linearly independent special solutions of the propagated equation.

$$u(x) = c_1 f_1(x) + c_2 f_2(x)$$

A special solution $f_1(x)$ of the differential equation can be found using arbitrary initial conditions. To be able to obey Bloch's theorem also the conditions (2.7) and (2.8) need to be fulfilled (for a symmetric potential). Here this restriction is exploited to simplify the work: The initial conditions chosen in the implementation are:

$$\begin{aligned} f_1(0) &= 1 & f_2(0) &= 0 \\ \left. \frac{\partial}{\partial x} f_1(x) \right|_{x=0} &= 0 & \left. \frac{\partial}{\partial x} f_2(x) \right|_{x=0} &= i \end{aligned}$$

Thus because the restriction requires the real part to be symmetric and the imaginary part to be antisymmetric the coefficients c_1 and c_2 are guaranteed to be real otherwise the restrictions would be violated.

Plugging the general solution into the upper conditions results in

$$\begin{aligned} c_1 f_1(s) + c_2 f_2(s) &= c_1 f_1(-s) + c_2 f_2(-s) && \text{using(2.2)} \\ &= c_1 f_1^*(s) + c_2 f_2^*(s) && \text{using(2.7)} \end{aligned}$$

and

$$\begin{aligned} c_1 \left. \frac{\partial}{\partial x} f_1(x) \right|_{x=s} + c_2 \left. \frac{\partial}{\partial x} f_2(x) \right|_{x=s} &= c_1 \left. \frac{\partial}{\partial x} f_1(x) \right|_{x=-s} + c_2 \left. \frac{\partial}{\partial x} f_2(x) \right|_{x=-s} && \text{using(2.3)} \\ &= -c_1 \left. \frac{\partial}{\partial x} f_1^*(x) \right|_{x=s} - c_2 \left. \frac{\partial}{\partial x} f_2^*(x) \right|_{x=s} && \text{using(2.8)} \end{aligned}$$

which can be rewritten

$$c_1 \Im(f_1(s)) + c_2 \Im(f_2(s)) = 0$$

and

$$c_1 \left. \frac{\partial}{\partial x} \Re(f_1(x)) \right|_{x=s} + c_2 \left. \frac{\partial}{\partial x} \Re(f_2(x)) \right|_{x=s} = 0$$

eliminating c_1 and c_2 the condition becomes

$$\frac{\partial}{\partial x} \Re(f_2(x)) \Big|_{x=s} \Im(f_1(s)) - \frac{\partial}{\partial x} \Re(f_1(x)) \Big|_{x=s} \Im(f_2(s)) = 0$$

or re-expressed in matrix form

$$\begin{vmatrix} \Im(f_1(s)) & \Im(f_2(s)) \\ \frac{\partial}{\partial x} \Re(f_1(x)) \Big|_{x=s} & \frac{\partial}{\partial x} \Re(f_2(x)) \Big|_{x=s} \end{vmatrix} = 0 \quad (2.9)$$

To find the actual eigenvalues an arbitrary k can be chosen then E has to be varied until condition (2.9) is fulfilled. This is again a **root finding problem**. Multiple energy values can be found for every k which belong to different bands. To get the dispersion relation the energy values for multiple k in an interval of 2π have to be found. Then the energy eigenvalues are plotted as a function of k , see Figure 3.5.

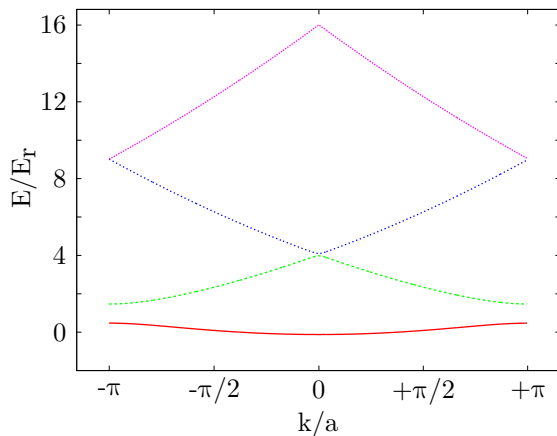


Figure 2.3: A dispersion relation for an infinite optical lattice potential (sine function) showing the first four bands each in a different color. An energy is assigned to every quasi momentum k . All energy eigenstates except those with $k = n\pi$ ($n \in \mathbb{Z}$) are twice-degenerate.

An infinite lattice system without inhomogeneity is also referred to as a homogeneous system throughout this thesis.

Exact Diagonalization

Another method to obtain system eigenstates should be mentioned. Especially for potentials that have a periodic structure this method is beneficial in that it allows further analytical treatment and thus also faster numerics.

A periodic function can usually be represented well by a Fourier series. This can be applied to a lattice potential and the associated periodic u -functions from the Bloch theorem. Plugging these series expressions into the effective stationary Schrödinger equation for the u -functions, a **discretized** version of

the **stationary Schrödinger equation** in terms of the **Fourier coefficients** for the u -functions is obtained. After a cut-off for high frequency components has been applied, the diagonalization of a relatively sparse matrix (very sparse for a sine-like potential) is all that is needed to get the energy eigenfunctions. Furthermore, the matrix elements of the band projected position operator can be calculated more efficiently with the u -functions decomposed into their Fourier coefficients.

This procedure corresponds to the yellow dotted path shown in Figure 2.1, except that there the common definition for the Wannier states was used. The method was implemented by U. Bissbort who also supervised this thesis. Some of the results gained in the local implementation have been reproduced with the implementation by U. Bissbort to ensure their correctness.

In section A.5 some of the steps required for this method are explained in greater detail. The method is also explained in [Bis12].

2.4 Inhomogeneous Lattice

Now that the homogeneous lattice eigenstates are known, the solution for the inhomogeneous lattice is the next step.

An inhomogeneous lattice is a system in which a lattice potential has some foreign potential contribution that has no or different periodicity than the lattice potential. This foreign potential is referred to as the inhomogeneity.

$$\hat{H} = \hat{T} + \hat{V}_{lat} + \hat{V}_{inh} = \hat{H}_{lat} + \hat{V}_{inh}$$

For such a Hamiltonian it is often more convenient to calculate the eigenstates $|n_{lat}\rangle$ of the homogeneous lattice \hat{H}_{lat} first. This can be accomplished using the methods explained in section 2.3. The eigenstates for the lattice constitute a complete basis which could be used to diagonalize the complete Hamiltonian \hat{H} in ².

$$\langle n_{lat} | \hat{H} | n'_{lat} \rangle = \langle n_{lat} | \hat{H}_{lat} | n'_{lat} \rangle + \langle n_{lat} | \hat{V}_{inh} | n'_{lat} \rangle$$

The first term is trivially diagonal. The second term which is the non-lattice potential is most likely given in real space. So an integral has to be evaluated.

$$\langle n_{lat} | \hat{H} | n'_{lat} \rangle = \delta_{n_{lat}, n'_{lat}} E_{n_{lat}} + \int \langle n_{lat} | x \rangle V_{inh}(x) \langle x | n'_{lat} \rangle dx$$

Evaluating such an integral is computationally demanding. This wouldn't be the case if the functions that the integral runs over were spatially localized. Luckily such a basis can be obtained through one of the methods explained in section 2.1 which can be used to calculate the **Wannier basis** of the homogeneous lattice with elements $|l_0, \alpha\rangle$. If this basis is used to diagonalize \hat{H} the following terms have to be evaluated³

²this procedure corresponds to the second column in Figure 2.1

³this procedure corresponds to the two red dashed lines to the right in Figure 2.1

$$\langle l_0, \alpha | \hat{H} | l'_0, \alpha' \rangle = \langle l_0, \alpha | \hat{H}_{lat} | l'_0, \alpha' \rangle + \langle l_0, \alpha | \hat{V}_{inh} | l'_0, \alpha' \rangle$$

Here the first term is the on-site energy and hopping for the homogeneous lattice. The second term is the potential in the homogeneous Wannier basis which can be evaluated because both are available in real space. So in order to proceed the homogeneous lattice Wannier states and the Hubbard parameters for the homogeneous lattice are needed.

2.4.1 Homogeneous Lattice Wannier States

When the energy eigenstates for the homogeneous system have been obtained, the Wannier states for the homogeneous system can be calculated using either of the two definitions presented in section 2.1. Thanks to the Bloch theorem every state **can be assigned to a band clearly**, because there is just one energy value per band for every quasi momentum k . So in short either the Fourier transformation over the phase adjusted energy eigenstates per band is performed or the band projected position operator \hat{x}_α is diagonalized.

With the overlap matrix between the energy and Wannier states the homogeneous system Hamiltonian can be calculated in the homogeneous system Wannier basis

$$\begin{aligned} \langle l_0, \alpha | \hat{H}_{lat} | l'_0, \alpha' \rangle &= \sum_{k, \bar{\alpha}} \langle l_0, \alpha | k, \bar{\alpha} \rangle E_{lat}^{k, \bar{\alpha}} \langle k, \bar{\alpha} | l'_0, \alpha' \rangle \\ &= \frac{\delta_{\alpha, \alpha'}}{N} \sum_k e^{ik(l-l')} E_{lat}^{k, \alpha} \end{aligned}$$

This quantity corresponds to the **homogeneous system Hubbard parameters** on-site energy and hopping, see section 2.5. It is also useful when the inhomogeneous lattice Hamiltonian matrix elements are calculated as was seen in the last section.

To describe the homogeneous system via a Hubbard model only the **on-site interaction** would be left to be calculated. But for the description of the inhomogeneous system the homogeneous system on-site interaction is of no use.

2.4.2 Inhomogeneous Lattice Eigenstates

To get the complete system Hamiltonian in the homogeneous system Wannier basis the term

$$\langle l_0, \alpha | \hat{V}_{inh} | l'_0, \alpha' \rangle = \int \langle l_0, \alpha | x \rangle V_{inh}(x) \langle x | l'_0, \alpha' \rangle dx$$

has to be evaluated. With the inhomogeneous potential given in real space, it can be evaluated using an integration over the Wannier functions and the potential, as shown above.

This integral is similar to the one encountered in section 2.4 where the inhomogeneous Hamiltonian is written in the homogeneous system energy basis

but different in that it integrates over localized functions. This means that the integration can be restricted to just the interval where there is a notable overlap of the integrand functions, i.e. the two localized Wannier functions and the potential. This **reduces computation effort** immensely especially for big lattice systems and a low band description.

Now the complete Hamiltonian $\langle l_0, \alpha | \hat{H} | l'_0, \alpha' \rangle$ can be calculated. Diagonalizing it then yields the energy eigenvalues and the energy eigenstates, i.e. the overlap elements between the complete system energy eigenstates and the homogeneous system Wannier states $\langle E | l_0, \alpha \rangle$.

From the diagonalization routine **no information** which of the eigenstates belongs to what **band** is obtained. There is no strict way to assign the states to bands as in the homogeneous case where the Bloch theorem yielded this information. Instead, the distribution of energy eigenvalues or various other observables for the energy eigenstates can be regarded to motivate a certain assignment. For now, it will be assumed that the band gap is still present in the inhomogeneous system and thus the order of the energy eigenvalues can be used to assign states to bands $|E\rangle \rightarrow |E, \alpha\rangle$. But in general, the band gap will become smaller with the inhomogeneity strength as shown in Figure 2.4 and will eventually be gone. Then the methods explained in section 2.6.2 may become necessary.

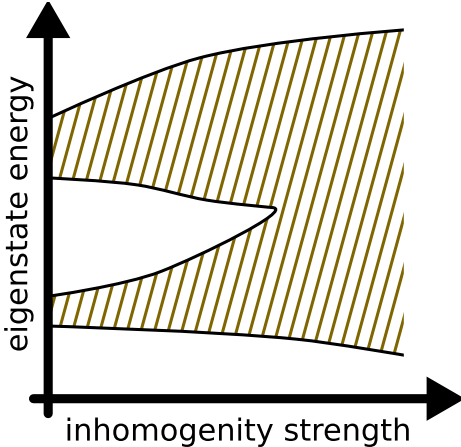


Figure 2.4: Schematic view of energy spectrum as function of the inhomogeneity strength. The homogeneous system bands start to broaden once the inhomogeneity strength is increased. Eventually the band gaps disappear.

A second look at the complete Hamiltonian shown above is worthwhile. The $|l_0, \alpha\rangle$ constitute a localized basis in which the Hamiltonian is expanded. That is just what is needed to formulate a **Hubbard model**. But this is not the desired Hubbard model yet, which ought to use the generalized Wannier functions. More information about this can be found under section 2.5.1.

2.4.3 Inhomogeneous Lattice Wannier States

Once the eigenstates are assigned to bands, applying the generalized definition for Wannier states is easy. The band projection operator is defined in terms

of the assigned eigenstates. Then the elements of the band projected position operator can be calculated in the energy eigenbasis.

$$\begin{aligned}\langle E, \alpha | x_{\bar{\alpha}} | E', \alpha' \rangle &= \langle E, \alpha | \left(\sum_{\bar{E}} |\bar{E}, \bar{\alpha} \rangle \langle \bar{E}, \bar{\alpha}| \right) \hat{x} \left(\sum_{\bar{E}'} |\bar{E}', \bar{\alpha} \rangle \langle \bar{E}', \bar{\alpha}| \right) |E', \alpha' \rangle \\ &= \delta_{\alpha, \bar{\alpha}} \delta_{\alpha', \bar{\alpha}} \langle E, \alpha | \hat{x} | E', \alpha' \rangle \\ &= \delta_{\alpha, \bar{\alpha}} \delta_{\alpha', \bar{\alpha}} \int_x x \varphi'_{E, \alpha}(x) \varphi_{E', \alpha'}(x) dx\end{aligned}$$

This matrix is **block diagonal**, i.e. bands are not mixed. If lots of bands are used, this reduces computation effort because less matrix elements have to be computed.

Diagonalization then gives the generalized Wannier states $|l, \alpha\rangle$ as overlaps with the energy eigenstates. The generalized Wannier eigenfunctions can be obtained via the energy eigenfunctions and the overlap elements.

As shown in Figure 2.1, further quantities can be derived. Specifically to construct an optimal single-band Hubbard-type model, Hubbard parameters should be obtained from the generalized Wannier states, so that the inhomogeneous lattice system can be described using a Hubbard-like model formulated in the generalized Wannier basis.

2.5 Hubbard Model

Throughout solid state physics, the Hubbard model is the simplest model to describe strongly correlated lattice systems. The single particle lattice Hamiltonian is expanded in the basis of its Wannier states.

$$\begin{aligned}\hat{H} &= \sum_{l, \alpha} \sum_{l', \alpha'} |l, \alpha\rangle \langle l, \alpha| \hat{H} |l', \alpha'\rangle \langle l', \alpha'| \\ &= \sum_{k, \bar{\alpha}} \sum_{l, \alpha} \sum_{l', \alpha'} |l, \alpha\rangle \langle l, \alpha| k, \bar{\alpha} \rangle E_{k, \bar{\alpha}} \langle k, \bar{\alpha}| l', \alpha'\rangle \langle l', \alpha'| \\ &= \sum_{l, l', \alpha} |l, \alpha\rangle \underbrace{\frac{1}{N} \sum_k E_{k, \alpha} e^{ika(l-l')}}_{H_{l, l'}^{(\alpha)}} \langle l', \alpha|\end{aligned}$$

As shown, every band can be treated separately because off-block-diagonal elements $\langle l, \alpha | \hat{H} | l', \alpha' \rangle$ which obey $\alpha \neq \alpha'$ vanish. For every band there is one matrix $H_{l, l'}^{(\alpha)}$ whose elements are gained, as shown, through a Fourier transformation over the dispersion relation with the band's eigenvalues. For $\Delta l = l - l' = 0$, the matrix elements which correspond to the expectation value of the Hamiltonian in a Wannier state, are called the on-site energies (commonly referred to as $U_l^{(\alpha)}$). For $\Delta l \neq 0$ the elements are called hopping elements (commonly referred to as $J_{l, l'}^{(\alpha)}$). The $\Delta l = 1$ matrix elements are called nearest neighbor hopping, for $\Delta l = 2$ next-nearest neighbor hopping and so on.

If the lattice potential is sufficiently deep, the hopping terms become exponentially small, see Figure 2.5. With increasing Δl the exponential coefficient

grows, such that for moderately deep lattices the trapping elements beyond nearest neighbor are commonly neglected (\rightarrow tridiagonal Hamiltonian). This approximation is referred to as the **tight binding** approximation. In many systems, second band excitations are also neglected in the so-called **lowest band approximation**. The Hamiltonian can then be written

$$\hat{H} \approx \sum_l |l\rangle \frac{1}{N} \sum_k E_k \langle l| + \sum_l |l\rangle \sum_k E_k e^{-ika} \langle l+1| + \text{h.c.}$$

with $|l\rangle$ and E_k being the corresponding first band quantities.

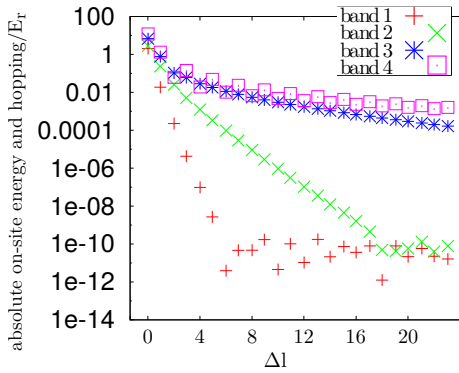


Figure 2.5: Exponential decrease of hopping with Δl for 4 bands. The tight binding approximation is motivated by the fact that the elements with $\Delta l > 1$ are very small. This calculation was performed with a lattice depth of $10 E_r$. The limited numerical accuracy interrupts the exponential decay for values in the order of $10^{-10} E_r$. In the fourth band there is an alternating behaviour with Δl . This is an artifact caused by the discretization of the quasi momenta k .

Neglecting interactions initially, this can be extended to a multi-particle description easily. Furthermore, a distinction between bosons and fermions has to be made. Here only **bosons** are regarded in detail. Let

$$b_l = \sum_{n_1, \dots, n_L=0}^{\infty} \sqrt{n_l} |n_1 \dots n_l - 1 \dots n_L\rangle \langle n_1 \dots n_l \dots n_L|$$

be the particle annihilation operator operating on the l -th site in Fock space⁴ and let b_l^\dagger be the corresponding creation operator. Promoting this single-particle operator to the **many-particle** Fock space, the corresponding Hamiltonian expressed within the framework of second quantization is

$$\hat{H} \approx \sum_l \sum_k \frac{E_k}{N} \underbrace{b_l^\dagger b_l}_{\hat{n}_l} + \sum_l \sum_k E_k e^{-ika} b_l^\dagger b_{l+1} + \sum_l \sum_k E_k e^{ika} b_{l+1}^\dagger b_l$$

⁴Note that for the terms with $n_l = 0$ the ket is not defined, but the prefactor corrects this by setting this term to zero.

To include **interactions** in the multi-particle Hamiltonian it is assumed that only particles which sit on the same lattice site interact.

Thus a term of the form

$$\sum_l \frac{U}{2} b_l^\dagger b_l^\dagger b_l b_l = \frac{U}{2} \hat{n}_l (\hat{n}_l - 1) \quad \text{using } [b_l, b_{l'}^\dagger] = \delta_{l,l'}$$

is added to the Hamiltonian. With

$$\frac{U}{2} n_l (n_l - 1) = \langle n_1 \dots n_l \dots n_L | \hat{V}_{int} | n_1 \dots n_l \dots n_L \rangle$$

and thus

$$U = \langle n_1 \dots n_l = 2 \dots n_L | \hat{V}_{int} | n_1 \dots n_l = 2 \dots n_L \rangle$$

being the amount of energy that is needed to put two particles in the same site. Thus the value of U is dependent on more specific details about the interaction process involved between the regarded particles. In optical lattice experiments it can be tuned all the way from repulsive to attractive via the lattice parameters. There the underlying forces are of type Van-der-Waals and the following expression depending on the s-wave scattering length a_s can be derived (see [Bis07])

$$U = \frac{2\pi\hbar^2 a_s}{m} \int d\vec{r} |w(\vec{r})|^4$$

Putting all this together the so-called Bose-Hubbard-Hamiltonian, i.e. the Hubbard-Hamiltonian for bosons is obtained

$$\hat{H} \approx \sum_l \left(\sum_k \left(E_k \left(\frac{1}{N} \hat{n}_l + e^{-ika} b_l^\dagger b_{l+1} + e^{ika} b_{l+1}^\dagger b_l \right) \right) + \frac{U}{2} n_l (n_l - 1) \right)$$

The original Hubbard model was derived for **fermions** where a very similar relation can be found which obeys the fact that only maximally two spin 1/2 fermions can sit on the same site and only if they are in different spin states. In addition to the interactions relevant for bosons also spin dependent interactions are possible, e.g. it may be necessary for a particle to change the spin to join another particle in one site.

Around these rather standard definitions for the Hubbard models, many similar models exist. There are, for example, specializations which take multiple particle species into account but also variations in the tight-binding approximation are possible. For example, next-nearest neighbor hopping elements could be included in the description. Another possibility is the use of a localized basis other than the Wannier basis. The generalized Wannier basis that was discussed in section 2.1.2 is yet another possibility. Such models will be referred

to as **Hubbard-like models**. The variation in the approximation and the used localized basis are relevant for this thesis.

For a homogeneous lattice, all the elements for the on-site energy, nearest neighbor hopping, next-nearest neighbor hopping and so on are each constant over all sites. Thus $\hat{H}_{l,l'}^{(\alpha)}$ is a Toeplitz matrix, i.e. a matrix with constant elements for each diagonal, for homogeneous lattices. In the **inhomogeneous lattices** treated with Hubbard-like models, this is no longer the case, i.e. there is a **site-dependency** for the on-site energies, hoppings and also the on-site interaction.

The on-site energy, hopping and on-site interaction for all the models are referred to as Hubbard parameters throughout this thesis.

2.5.1 Hubbard-like Model for Inhomogeneous Lattices

Every Hamiltonian can be expanded in a localized basis, just the way it was done with the periodic potential Hamiltonian above. This motivates a generalization of the Hubbard model. Whether such a model makes sense depends on the amount of matrix elements in the Hamiltonian that can be neglected in a tight binding-like fashion. In the case of a lattice with a small inhomogeneity, the description in a localized basis is expected to still be quite suitable.

Two localized bases turned up in the previous sections, the homogeneous lattice Wannier basis and the generalized Wannier basis for the inhomogeneous lattice system. Both can be used to express the inhomogeneous system Hamiltonian in.

For the Hamiltonian in the homogeneous system Wannier basis H_{l_0,l'_0} the matrix elements are calculated in the procedure explained above along the way. For the **Hamiltonian in the generalized Wannier basis** $H_{l,l'}$ the calculations have to proceed further to the point where the generalized Wannier functions are obtained. Then the elements of $H_{l,l'}$ can be calculated by continuing the above procedure using the overlaps found during the diagonalization of the band projected position operator

$$H_{l,l'} = \sum_E \langle l, \alpha | E, \bar{\alpha} \rangle E \langle E, \bar{\alpha} | l', \alpha \rangle$$

One feature that is already visible in the above representation is the **block diagonality** of $H_{l,l'}$ which it has in common with H_{hom} in the original Hubbard model. It is a trivial result from the fact that the generalized Wannier functions are constructed only from the eigenstates assigned to the same band. Contrary H_{l_0,l'_0} is not block diagonal, i.e. there, 'hopping' terms across bands are present.

Another property that sets these models apart from the original Hubbard model is the fact that the values on the diagonals are **not** constant, i.e. **site-independent** anymore. Every site has its own on-site energy and the hopping between sites also depends on what pair of sites is regarded. This has to be taken into account when approximations are made.

A very important difference between the two Wannier bases when used to make a Hubbard-like model is in the **on-site interaction**. If the homogeneous lattice Wannier basis is used, the on-site interaction will be the same as for the homogeneous lattice. If the inhomogeneous lattice Wannier basis is used, the

shape of the Wannier functions will correspond to the actual localized state in the inhomogeneous lattice.

2.6 Different Inhomogeneity Strengths

As was stated before, to calculate the eigenenergies and eigenstates of the lattice system with inhomogeneity, the complete Hamiltonian $\hat{H} = \hat{H}_{\text{lat}} + \hat{V}_{\text{inh}}$ has to be diagonalized. To calculate eigenenergies again but for a different inhomogeneity strength, the matrix elements don't actually have to be reevaluated. H_{lat} stays the same. \hat{V}_{inh} can be given a prefactor m_V

$$\begin{aligned}\hat{V}_{\text{inh}} &\rightarrow m_V \hat{V}_{\text{inh}} \\ \int |x\rangle V_{\text{inh}}(x)\langle x| dx &\rightarrow \int |x\rangle m_V V_{\text{inh}}(x)\langle x| dx \\ &= m_V \int |x\rangle V_{\text{inh}}(x)\langle x| dx\end{aligned}$$

The matrix elements for \hat{V}_{inh} only need to be evaluated once in the desired basis. To calculate the eigenenergies for a different trap strength, only a matrix addition and a multiplication with a scalar has to be done $\hat{H} = \hat{H}_{\text{lat}} + m_V \cdot \hat{V}_{\text{inh}}$ and the eigenvalue procedure has to be reapplied.

How the energy eigenvalues evolve with the inhomogeneity strength can be seen in Figure 2.6 where the energy eigenvalues of 4 bands are plotted for a harmonic trap potential.

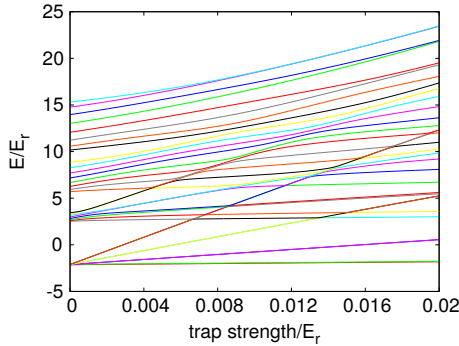


Figure 2.6: The evolution of the energy eigenvalues when the inhomogeneity, here a harmonic trap, is increased starting from $V_1 = 0E_r$. The lattice depth is $10E_r$.

2.6.1 Tracking the Energy Eigenvalues

Changing the inhomogeneity strength causes the energy eigenvalues to change. If the inhomogeneity strength is big enough, the eigenvalues will start to approach and seemingly cross each other. To still be able to assign different states to different bands based on their localization, it is necessary to track the energy eigenvalues. For this, it is beneficial to know how the values change when changing the inhomogeneity strength.

As discussed in the previous section, to find the eigenvalues for different inhomogeneity strength an eigenvalue problem of the following form has to be solved

$$(\hat{A} + c\hat{B})\vec{v}(c) = E(c)\vec{v}(c) \quad (2.12)$$

c corresponds to the inhomogeneity strength. The change of $E(c)$ is of interest so the derivative $\frac{\partial}{\partial c}$ is applied

$$\begin{aligned} \hat{B}\vec{v}(c) + (\hat{A} + c\hat{B})\frac{\partial}{\partial c}\vec{v}(c) &= \frac{\partial}{\partial c}E(c)\vec{v}(c) + E(c)\frac{\partial}{\partial c}\vec{v}(c) \\ \left(\frac{\partial}{\partial c}E(c) - \hat{B}\right)\vec{v}(c) &= \left(\hat{A} + c\hat{B} - E(c)\right)\frac{\partial}{\partial c}\vec{v}(c) \end{aligned}$$

$\vec{v}(c)$ is a unit vector. The derivative of a preserved unit vector is orthogonal to the vector itself, i.e. $\frac{\partial}{\partial c}\vec{v}(c)$ lives in the subspace that is spanned by the eigenvectors of $\hat{A} + c\hat{B}$ excluding $\vec{v}(c)$. So applying $\hat{A} + c\hat{B}$ on $\frac{\partial}{\partial c}\vec{v}(c)$ doesn't give contributions in the direction of $\vec{v}(c)$. Thus, to simplify the equation for $\frac{\partial}{\partial c}E(c)$ a projection onto $\vec{v}(c)$ is applied yielding

$$\frac{\partial}{\partial c}E(c) = \vec{v}^\dagger(c)\hat{B}\vec{v}(c) \quad (2.13)$$

\hat{B} is known and $\vec{v}(c)$ can be calculated from the eigenvalue problem (2.12). Equation (2.13) then yields the change of the eigenvalues in dependence of c . Applied to the inhomogeneous system this eigenvalue equation gives the **change of the eigenenergies in dependence of the inhomogeneity strength**.

2.6.2 Band Assigning

As discussed in section 2.4.2, all band information is lost when the inhomogeneous Hamiltonian is diagonalized. In this section different methods to assign these states to bands again are presented. In section 5.1.3 the results of these methods being applied to an actual inhomogeneous lattice system are tested.

To calculate generalized Wannier functions the band projection operator needs to be defined, see section 2.1.2. As long as a **band gap** remains open, (see the plot showing the eigenvalues as functions of the inhomogeneity strength, Figure 2.4), defining a band projector is easy. This is always true for small inhomogeneities. When no band gap can be identified, this is a challenge because there is no strict rule to do so. But even in systems where the band gaps have closed it is to some extent possible to assign the energy states to bands.

One way to motivate a certain choice is to demand that certain properties known about Wannier functions still hold. For example, a good localized basis is expected to have one localized state for every site for every band. **Using** different **measures** that act on the energy eigenstates, they are **grouped**. The band projector can then be defined using the previously mentioned grouping. If the correct measure is used the resulting band projector may fulfill the previously mentioned requirement for the generalized Wannier states. In section 2.6.4 some of the used measures are explained.

An alternative method to the “exclusive” band assigning is discussed in section A.5.1. Unfortunately this method has not been tested.

2.6.3 Avoided Crossings

When the individual lines that make up the energy eigenvalues are examined, the impression arises that the lines cross each other. Analytically it can be shown that the crossings are avoided on very small scales; it is a fundamental property of the system. So when zooming into one of these alleged crossings, a repelling effect between the lines should become visible. This is easier to see by looking at the derivative of the energy eigenvalues with respect to the inhomogeneity strength, see Figure 2.7. The repelling effect seems most pronounced when eigenvalues belonging to states localized at adjacent sites, cross, see the circles in the figure. In the derivatives, the avoidance is visible in a larger domain.

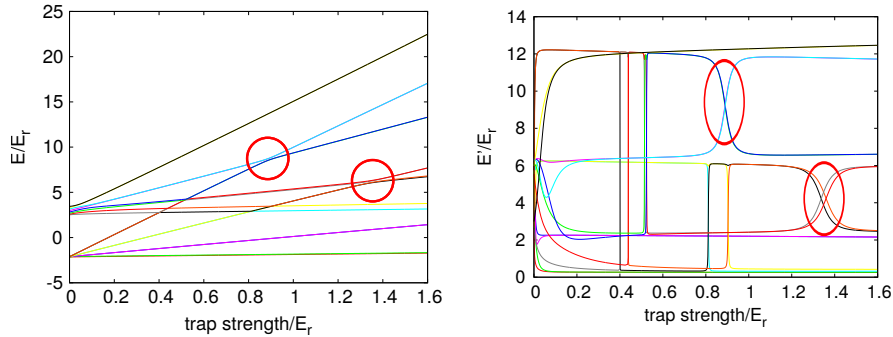


Figure 2.7: On the left, the evolution of the energy eigenvalues is shown again. On the right, the corresponding derivatives of the energy eigenvalues with the inhomogeneity strength are shown. There, the repelling effect at the avoided crossings is much more noticeable.

The assignment of the eigenstates to bands is still not very reasonable when assuming the crossings to be avoided so the other procedures are needed. These procedures allow **jumping over the avoided crossings** keeping the assignment of the states to certain bands despite non-existent band gaps. That’s what the previously mentioned measures are for.

At an avoided crossing *resonantly enhanced tunneling* can be observed, see [SZL⁺07].

2.6.4 Measures

Position

The eigenstates can be grouped according to the position where they localize. Using eigenstates each localized at a different position to define a band projector should allow the resulting generalized Wannier functions to each be localized at a different site, which is the requirement stated earlier.

Two measures for the position have been used: the expectation value of \hat{x} and $\sum_\alpha \hat{x}_\alpha$. They can be calculated efficiently, see section A.3. In inhomogeneous lattices the eigenstates localize, the stronger the inhomogeneity is. With a strong

enough inhomogeneity there will be one state localized per site, per band, except when there is a degeneracy or very close eigenvalues. With this information it should be a trivial task to assign every state to a band. In practice the procedure isn't this easy as will be shown in section 5.1.3, where the special case of the harmonic trapping potential is discussed.

First, the higher the energy/band, the stronger the inhomogeneity necessary to spark the localization and second, at the inhomogeneity strength where states have avoided crossings, the localization of the two seemingly crossing states, changes. At the avoided crossing it doesn't matter which state is assigned to which band. The unsatisfactory localization destroys the attempts to construct a nicely localized Wannier basis.

The plots in Figure 2.10 show both of the introduced measures \hat{x} and $\sum_{\alpha} \hat{x}_{\alpha}$. The latter measure is more discretized (see split-up at high inhomogeneity strength) and therefore more practical for the desired purpose. Both plots show how the localization changes when looking at energy sorted states.

Expectation of Band Projection Operator

Another technique to assign the inhomogeneous eigenstates to a band relies on the expectation value of the homogeneous system band projectors $\langle \hat{P}_{\alpha}^0 \rangle$. Given an inhomogeneous energy eigenstate $|\varphi_n\rangle$ the expectation of \hat{P}_{α}^0 can be calculated $\langle \hat{P}_{\alpha}^0 \rangle = \sum_k \langle \varphi_n | \varphi_{k,\alpha}^0 \rangle \langle \varphi_{k,\alpha}^0 | \varphi_n \rangle$ which can be taken as a measure of how much $|\varphi_n\rangle$ lies within band α . Its value will be high for a band in the homogeneous system whose states can reconstruct the regarded state well. Thus it seems reasonable to assign the state to the band whose projector has the highest expectation value. All of the expectations for different bands sum to 1.

$$\begin{aligned} \sum_{\alpha} \langle \hat{P}_{\alpha}^0 \rangle &= \langle \cdot | \sum_{k,\alpha} |\varphi_{k,\alpha}^0\rangle \langle \varphi_{k,\alpha}^0| \cdot \rangle \\ &= 1 \end{aligned}$$

This measure can be calculated very quickly because $\langle n | l_0, \alpha \rangle$ is already known from the diagonalization of \hat{H} in the unperturbed Wannier basis.

An example of how the expectation values for the different bands and states are visualized is given in Figure 2.10.

In this example it is visible that the high states in the first band are not lower in energy than the lowest state in the second band. Also it can be seen that the higher energy states can not easily be assigned to a certain band anymore because band edges are blurry.

2.6.5 Tracing the Bands

Another interesting representation can be obtained by subtracting the potential value of the position where a state is localized from the state's eigenvalue

$$\tilde{E} = E - V_{\text{trap}}(X(E))$$

At least for the lower bands in this representation the energy value lines for one band do not separate, see Figure 2.9.

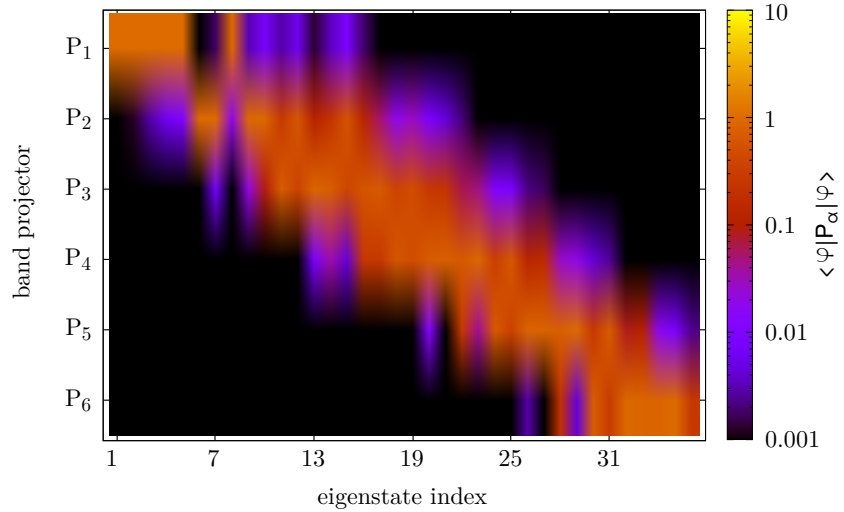


Figure 2.8: Example of the expectation values of different homogeneous system band projectors for different eigenstates. Most energy eigenstates can be clearly assigned to one band. This is not true anymore for the higher energy states.

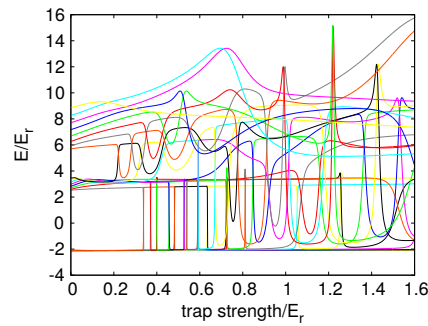


Figure 2.9: In this representation the local trap potential value is subtracted from the energy eigenvalues for every trap strength. This way, the obtained functions are almost constant, especially for the lower bands.

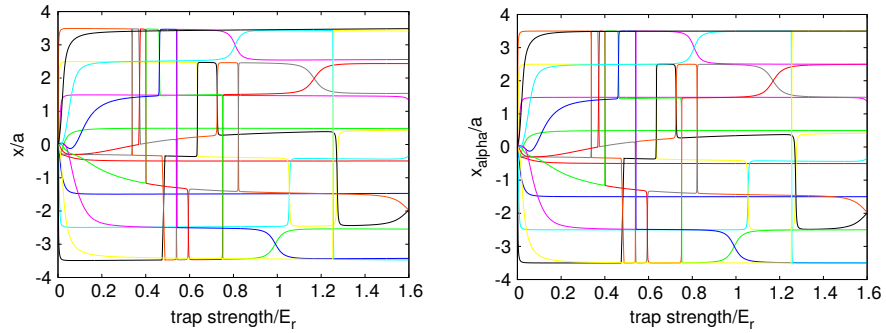


Figure 2.10: Two different measures for the localization. In the left, the expectation value of the position operator $\langle \hat{x} \rangle$ is shown. On the right, the expectation value of the sum of all the band projected position operators $\langle \sum_{\alpha} \hat{x}_{\alpha} \rangle$ is shown. The used system consists of 8 sites. The first two band eigenstates are examined for different trap strength.

2.7 Boundary Conditions

When only a spatially finite part of an infinite system is to be analyzed, the boundary conditions cannot be determined unless the infinite system is solved. This is impractical in most cases. But it can be motivated that in a system with localized eigenstates a simple **cut-off** can be applied to eigenstates that are localized outside the region of interest giving a small error on the partial system boundaries.

In Figure 2.11, a Hamiltonian in a localized basis is visualized. It extends to infinity in all directions. A spatially smaller subsystem (red/solid line frame) is to be analyzed. To get the eigenstates and eigenvalues of this system, the eigenvalue equations for the rows in the green/dashed frame have to be solved. Unfortunately, the elements outside the red frame are needed but inaccessible. Can neglecting them, i.e. taking them to be zero, be justified?

Let $|l_{in}\rangle$ be some state of the localized basis located inside the partial system and let $|l_{out}\rangle$ be located outside. Then $H_{l_{in},l_{out}} = \langle l_{in}|\hat{H}|l_{out}\rangle$ would be a matrix element inside the green but outside the red frame. If there is no eigenstate $|n\rangle$ in \hat{H} that has a **notable amplitude at both locations** at the same time, the matrix element $H_{l_{in},l_{out}} = \sum_n E_n \langle l_{in}|n\rangle\langle n|l_{out}\rangle$ will be small and thus negligible. If this is true for all combinations of l_{in} and l_{out} , all that remains is the red quadratic matrix for the Hamiltonian of the partial system. This can be solved.

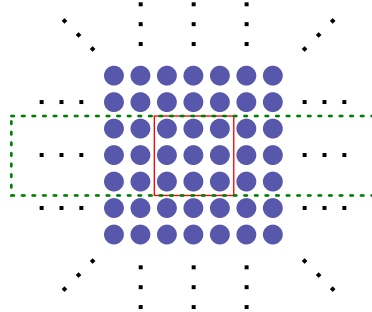


Figure 2.11: Schematic view of an infinite system Hamiltonian in a localized basis. The partial system in the red solid line frame is of interest.

The **error** can be further **qualified** if the approximate shape of the complete Hamiltonian is known. If, for instance, it is known that the Hamiltonian is tridiagonal in the regarded localized basis with off-diagonal terms small, then there is just one small element outside the red frame but inside the green frame at each edge of the system. This element $H_{l_{edge},l_{edge}+1} = \sum_{n_{edge}} E_n \langle l_{edge}|n_{edge}\rangle\langle n_{edge}|l_{edge}+1\rangle$ affects all the eigenstates localized at the edge $|n_{edge}\rangle$ with non-zero $\langle l_{edge}|n_{edge}\rangle$ and $\langle l_{edge+1}|n_{edge}\rangle$. Taking it to be zero should therefore cause a small error in $\langle n_{edge}|l_{edge}\rangle$ which is relevant for the partial system. This is in analogy to expanding the Hamiltonian in a not quite complete basis.

2.7.1 Periodic versus Non-Periodic Localized Basis

No matter if periodic or non-periodic boundary conditions are used, in either case there will be an error in the inhomogeneous Hamiltonian matrix elements due to the finite system size used. This error will be inherited throughout calculations:

$$\begin{aligned}
 & \langle l_0, \alpha_0 | \hat{H} | l'_0, \alpha'_0 \rangle \\
 \rightarrow & \langle \varphi | l_0, \alpha'_0 \rangle \\
 \rightarrow & \langle x | \varphi \rangle \\
 \rightarrow & \langle \varphi | \hat{x}_\alpha | \varphi' \rangle \\
 \rightarrow & \langle l | \varphi \rangle \\
 \rightarrow & \langle x | l \rangle
 \end{aligned}$$

When calculations are performed in a system whose eigenstates obey periodic boundary conditions, all derived bases are also periodic. This is the case in the implementation where the periodic Bloch basis in a finite system is used to obtain their also **periodic Wannier functions** in the finite system. This is a localized but periodic basis; non-periodic solutions cannot be obtained from such a basis. But the solutions to most systems are not expected to be periodic. So the Wannier functions in which arbitrary Hamiltonians are diagonalized, should ideally extend to infinity and should not be periodic.

One way out of this dilemma is to calculate the **Wannier basis in a larger finite system** and diagonalize the smaller system of interest in that basis, see section 3.3.1. This technique offers a localized basis which should be compatible with the method described in the previous section and thus allow for the truncation of the Hamiltonian in the localized basis. As mentioned in the previous section this causes an error.

To cope with this error in the non-periodic localized basis, **cutting off** the **edges** of the trap eigenstates $|\varphi\rangle$ was tested but didn't yield good results. Although cutting off the edges decreases the error in the eigenstates, the cropped eigenstates do not make up an orthogonal basis, which has been checked by calculating the overlap matrix $\langle l_0, \alpha_0 | l'_0, \alpha'_0 \rangle = \int_x \langle l_0, \alpha_0 | x \rangle \langle x | l'_0, \alpha'_0 \rangle dx$. Thus the diagonalization of the band projected position operator has to be done in the inaccurate basis of the trap eigenstates and again the error is being inherited throughout further calculations:

$$\begin{aligned}
 & \langle \varphi | \hat{x}_\alpha | \varphi' \rangle \\
 \rightarrow & \langle l | \varphi \rangle \\
 \rightarrow & \langle x | l \rangle
 \end{aligned}$$

Comparison of the errors suggested that using the periodic Wannier basis is beneficial. For the periodic and the non-periodic set of Wannier states the overlap matrices have been calculated to verify the shortcomings of the non-periodic set, when used as a basis. But as mentioned before, the periodic basis is also not ideal because it enforces periodic inhomogeneous eigenstates which is unrealistic for most cases.

Making the Wannier states **periodic enforces the same system size** for the homogeneous and inhomogeneous system, see section 3.3.1.

Chapter 3

Numerical Implementation

In order to calculate and investigate generalized Wannier functions, a computer program has been written. Except for some basic linear algebra and numerical routines, all of the code was developed from scratch for this thesis. This development process required most of the author's attention.

The programming language c++ was chosen for the implementation. Result data is written to text files with numbers given in a human readable representation. From these files, most of the plots were generated using *gnuplot* whose output vector graphics were then fine tuned using *inkscape*. The thesis itself was written using *latex*.

The **structure of the program** has been kept very simple. There is one major class called *inhLatticeSystem*. One object of this class is instantiated at the start of the program and the major calculation routine *calc()* is invoked. *calc()* executes many, mostly parameterless, methods within the class that complete the task of calculating all the interesting quantities for an inhomogeneous lattice system. The methods have descriptive names for the steps that lead to the generalized Wannier functions and beyond. These steps were outlined in section 2.1.2. In the next section, details on how these steps were implemented including optimizations, error estimates, debugging routines and complexity are given.

External libraries used in the implementation include *armadillo*, *GNU Scientific Library* (GSL) and “numerical recipes”. The differential equation propagation routine was initially implemented by hand using a Runge Kutta-solver with adaptive step size, later and for all of the results the Bulirsch-Stoer method from “numerical recipes” was used. The algorithms Romberg integration and *Ridders’ method* for finding roots were also taken from “numerical recipes”. The routines for matrix and vector handling, elementary linear algebra arithmetic and solving eigenvalue problems were taken from the armadillo library. The Brent minimization algorithm was provided by GSL.

A class to treat **discretized functions** was adopted from U. Bissbort but heavily modified.

3.1 Propagation

Most numerical differential equation solvers only support real numbers and first order differential equations. So, in order to propagate the second order complex differential equation for the infinite homogeneous system (2.1), it has to be **converted** into a system of real first order **differential equations**. This is done in section A.1.

Also, the propagation cannot go all the way to infinity. To get the homogeneous system Wannier functions in a finite system, it doesn't have to. To solve this issue the amount of homogeneous system eigenstate solutions has to be **discretized** and only the solutions that are periodic within a given real space interval have to be taken into account. This can be achieved by propagating only for certain quasi momenta k with $\varphi_{k,\alpha} = u_{k,\alpha} e^{ikx}$.

The u 's have the same periodicity as the lattice a . If e^{ikx} has the same or a multiple m of the periodicity a then φ will also have that periodicity $l = m a$. So, if the quasi momenta are chosen $k = \frac{2\pi}{m}n$ with $n \in \mathcal{N}$ and $-\frac{m}{2} \leq n < \frac{m}{2}$, only m solutions with at least periodicity l are obtained. Obviously, the amount of energy eigenvalues obtained in this way will also be finite. Just like the amount of states (energy and Wannier), it is the same as the amount of sites m in the system.

When the Wannier functions are calculated with either definition they also adopt this **periodicity**. This can be problematic because using them as a basis then means that only periodic functions can be constructed from them, see also section 2.7.1. So implicitly periodic boundary conditions are enforced.

When the definition for the generalized Wannier functions is used, it can be shown analytically that the matrix elements of the band projected position operator are defined up to a common diverging factor in the infinite homogeneous system, see section A.2. This factor only influences the eigenvalues but not the eigenstates because they are normalized.

In the current implementation, the *Bulirsch Stoer* differential equation solver is used. Previously, a differential equation solver was part of the implementation, see section 3.7.3.

3.1.1 Extraction of Energy Eigenstates from Bulirsch Stoer Solver

The Bulirsch Stoer Differential equation solver doesn't return the propagated function on an **equidistantly spaced grid**. Unfortunately, the class that handles discretized functions is only able to do arithmetics on functions defined on an equidistantly spaced grid. That's why the functions coming from the differential equation solver is interpolated to an equidistantly spaced grid before arithmetics are performed.

3.1.2 Spline Interpolation

The library that handles discretized functions usually interpolates linearly between the tabulated points. When enabled it can also interpolate using splines. To enable this option, a call to `prepare_for_spline_interpolation()` has to be issued, after the function is defined and whenever it is changed. Then all the function values for the requested points are calculated using splines. This takes

more time than using linear rather than spline interpolation. Tests indicated that using linear interpolation with a high amount of points ($\approx 160/\text{site}$) is beneficial in terms of performance given the same level of accuracy.

3.2 Multiple Root Finding

In order to find energy eigenvalues using the real space propagation methods explained in section 2.3 multiple roots of a function, that is evaluated by propagating an ordinary differential equation, need to be determined. Such a functions for the case of a finite lattice is shown in Figure 3.1. Sadly no numerical library to fulfill such a task could be found, so the functionality was implemented by hand and put into a class called *multipleRootFinder*. This class relies itself on a single root finding procedure provided by the “numerical recipes” library called Ridder’s method and also on the Brent minimization algorithm from GSL. The procedure of finding the infinite lattice roots has been optimized extensively. These optimizations are explained in the following.

In a previous version an own implementation of a root finder was used, see section 3.7.3.

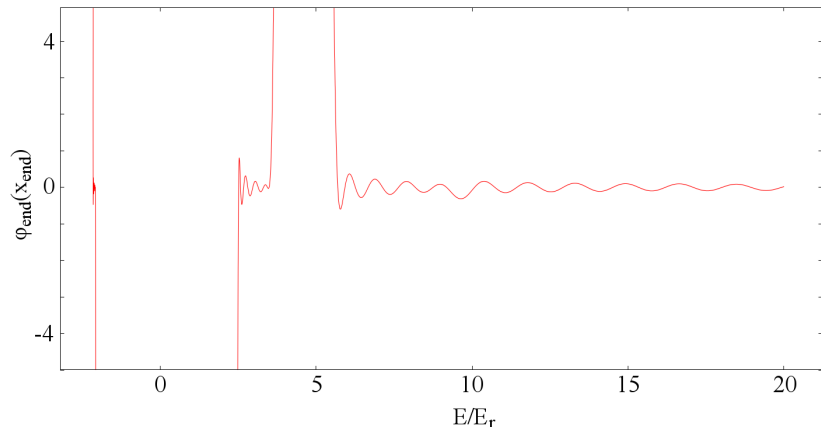


Figure 3.1: The function value at the end of the propagation for different energies in the case of a lattice in a infinitely deep well. Every root of this function corresponds to an actual energy eigenvalue. There are multiple roots for one band. Outside a band the function diverges from 0 exponentially.

3.2.1 Fast Homogeneous System Eigenvalues

The procedure that calculates the eigenvalues of the homogeneous Hamiltonian has been optimized in three ways. These optimizations speed up the calculation by a factor of over 100 especially for high amounts of lattice sites. On top of the speed gain, the method seems to be more robust in numerically challenging cases.

A drawback of the optimization is that it **specializes** the code for sine-like potentials which the previous code version was able to handle arbitrary periodic potentials.

Optimization 1: Faster Root Finding for $k = 0, \pi$

In order to find the energy eigenvalues, roots have to be found of a function which is costly to evaluate (evaluation involves propagation of an ODE). The roots of this function used to be searched for, by calculating points on a closely spaced grid. Whenever two consecutive grid points lay on opposing sides of the x-axis a root had been found.

Unfortunately for $k = 0$ and $k = \pi$ the grid has to be chosen very dense in order to still be able to find the roots, as seen in Figure 3.2. For these k -values, it is much easier to **search for minima or maxima**, which usually lie close to the desired roots. Thus the spacing of the grid can be chosen much larger and less points of the functions have to be evaluated. An example calculation showed that the amount of points to be evaluated can be reduced to a fifth for the same amount of roots found.

Optimization 2: Bracket around Intermediate k -values

Once the energy eigenvalues have been calculated for $k = 0$ and $k = \pi$ in a band, a bracketing interval for all other k -values in that band is also known, since the dispersion relation for a sine lattice has its maxima and minima at either points $k = 0$ or $k = \pi$ (for every band shuffled) see Figure 3.3. This interval contains the desired root and is needed by the external root finding procedure.

This optimization restricts the code's validity to sine-like potentials for the homogeneous lattice.

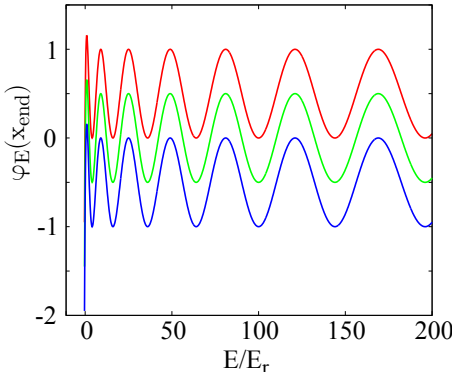


Figure 3.2: The function of E whose roots have to be found for the infinitely large lattice. The different curves are for different quasi momenta $k = 0, \pi/2, \pi$. Every root belongs to a different band, as opposed to the case found in the well.

Optimization 3: Just one Arm of Dispersion Relation

The dispersion relation for sine potentials is symmetric. Thus we don't need to calculate the energy for values $k = k_a$ and $k = -k_a$ because they are the same. When the calculation is performed with many k -values, this optimization reduces the effort by a half.

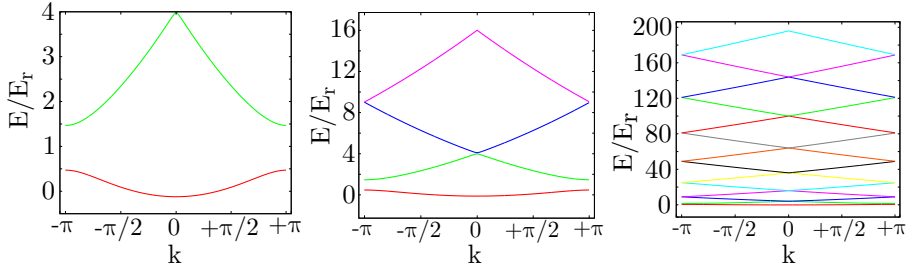


Figure 3.3: Dispersion relation for 2, 4 and 14 bands using 256 sites and a lattice depth of $2 E_r$

3.3 Wannier Functions

In the most recent implementation, the **common definition** is used to obtain Wannier functions **for the homogeneous lattice**. For the simple 1D-sine potential this is faster than using the generalized definition. Using all the calculated homogeneous eigenfunctions, one centered Wannier function is calculated. This function is translated to all of the available lattice sites in the inhomogeneous lattice system which can have a different amount of lattice sites than the homogeneous lattice system.

Using the **generalized definition** causes the implementation to be slower. All the matrix elements for the band projected position operator have to be calculated via integration, then the eigenvalue problem has to be solved. The calculation of the matrix elements can be sped up, but this has not been implemented. The procedure is explained in section A.2.1. A non-trivial side note is that when using the generalized definition for the Wannier states, exactly the set of Wannier states that are localized in the regarded real space area (defined by the periodically chosen Bloch states) are obtained.

The previously mentioned procedure can be sped up even further using the exact diagonalization procedure, see section A.5, where the matrix elements of the band projection operator can be expressed in terms of the Fourier coefficients of the u -functions.

3.3.1 Different System Size for the Homogeneous and the Inhomogeneous System

The size of the homogeneous system whose Wannier functions are used to diagonalize the complete inhomogeneous Hamiltonian in, can be chosen differently from the homogeneous system if the basis that is used to diagonalize the inhomogeneous Hamiltonian in is non-periodic. If only low bands are taken into account, the homogeneous system can be chosen smaller as long as the Wannier functions converge to 0 inside the system. Also, sometimes there is a benefit in choosing the homogeneous system larger than the inhomogeneous system in cases where the Wannier states do not converge but a non-periodic basis is desired.

3.3.2 Spread of the Homogeneous Wannier Functions

To check how fast the Wannier functions decay with the distance from the sites where they are localized, the Wannier functions for the first few bands have been examined, see Figure 3.7 and Figure 3.8. The variance of the Wannier functions as a function of the band index was plotted in Figure 3.4.

For the first 4 bands an **exponential growth** in the **variance** with the band index can be seen. These calculations were performed with 256 sites (40 points per site) and a lattice depth of $10E_r$. Unfortunately, a systematic behaviour cannot be seen after the 5th band. This could be due to limited accuracy in the calculation, but different tests couldn't resolve this. The same results were obtained using the foreign implementation.

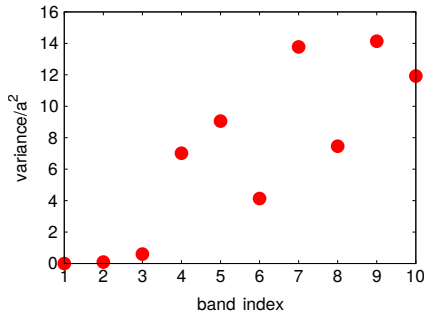


Figure 3.4: The variance of the Wannier functions as a function of the band index. For the first 4 bands the variance grows exponentially.

3.4 Homogeneous System Results

The homogeneous system energy eigenvalues obtained via the propagation can be plotted versus the quasi momentum k . The dispersion relation ensues, see Figure 3.5

Due to the discretization explained in section 3.1, there are **only points** in the dispersion relation. Specifically, there are as many points as there are sites in the calculation. In an infinite lattice, these points connect to form lines. These lines mark energy intervals in which the system is in energy eigenstates. These energy intervals are called the bands. Energy intervals without energy eigenstates are called band gaps.

Starting from the band with the lowest energy eigenstates each band is given an index $\in \mathcal{N}$. The size of the interval of a band increases with its band index while the size of the band gap interval decreases.

The **eigenstates** for a homogeneous lattice are also called the Bloch states. They extend over the whole system. In Figure 3.6 the influence of different system parameters on the eigenstates is visualized.

In real space the eigenstates consist of a fast oscillating part and an envelope. The amount of oscillations in the fast oscillating part is determined by the band index. The amount of oscillations of the envelope changes within a band and depends on the quasi momentum of the state. This can also be seen when reversing the common definition for Wannier functions

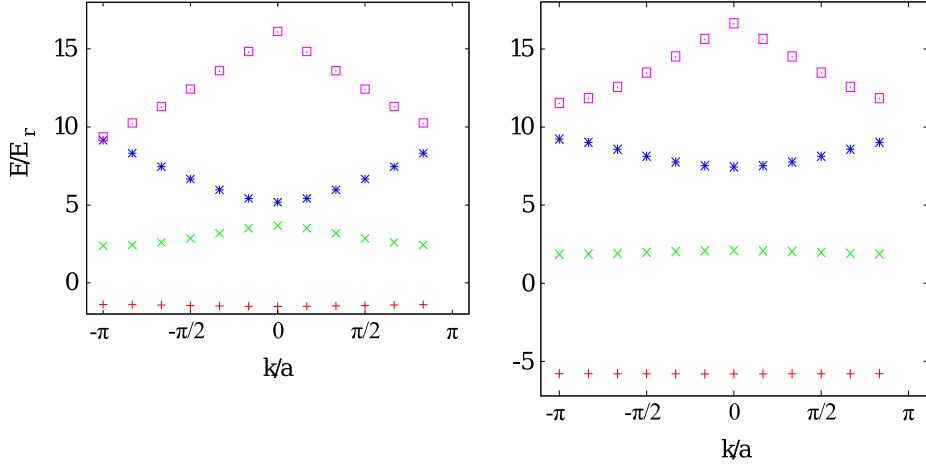


Figure 3.5: Dispersion relations for lattices each consisting of a single sine function with a lattice depth of $8E_r$ (left) and $20E_r$ (right). The width of the bands increases with the band index, while the width of the band gaps decreases with the band index for each of the presented lattice depth. The higher the lattice depth is, the smaller is the band width and the higher is the band gap width.

$$\varphi_{k,\alpha}(x) = \frac{1}{\sqrt{N}} \sum_l e^{ikla} w_{l,\alpha}(x)$$

The Wannier functions can be chosen real. The normalized complex prefactor represents the slowly oscillating envelope.

The homogeneous Wannier functions are shown in Figure 3.7. There are as many Wannier functions per band as there are sites and each function is localized on a different site. The spread of the Wannier functions generally increases with the band index, as elaborated in section 3.3.2, as does the amount of their oscillations.

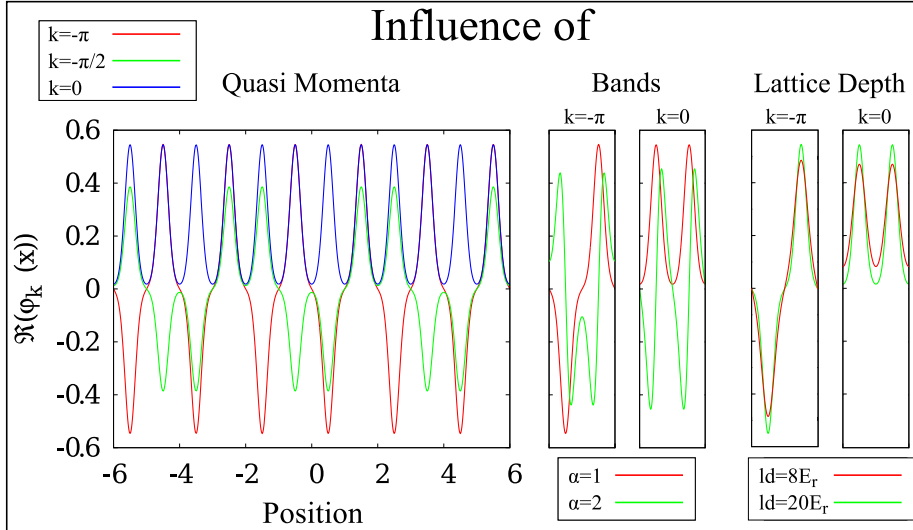


Figure 3.6: Real part of Bloch states of sine function potential compared for different quasi momenta ($k = -\pi, -\pi/2$ and 0), bands (first and second) and lattice depth ($ld = 8E_r$ and $20E_r$). The different quasi momenta influence the envelope of the Bloch functions. For $k = 0$ the envelope is constant while for $k = -\pi$ the envelope oscillates with twice of the lattice potential periodicity. Higher band Bloch functions have a more complex oscillatory behaviour. A higher lattice depth increases the peak amplitude (without affecting the normalization).

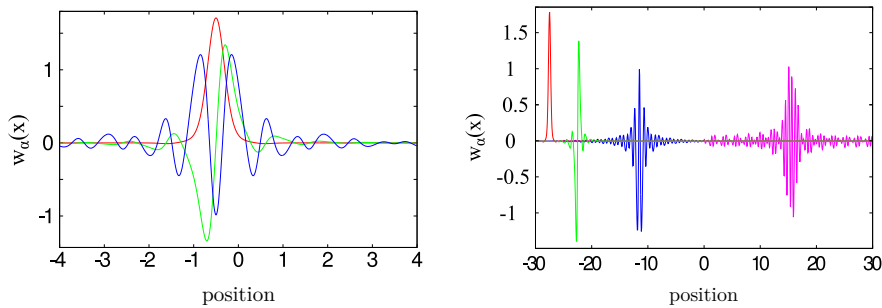


Figure 3.7: On the left the homogeneous system Wannier functions of the first three bands localized at the site at position -0.5 are shown. On the right the first through fourth band homogeneous Wannier functions are shown shifted apart. (1. band red, 2. band green, 3. band blue, 4. band purple) The growing spread with the band index is very noticeable.

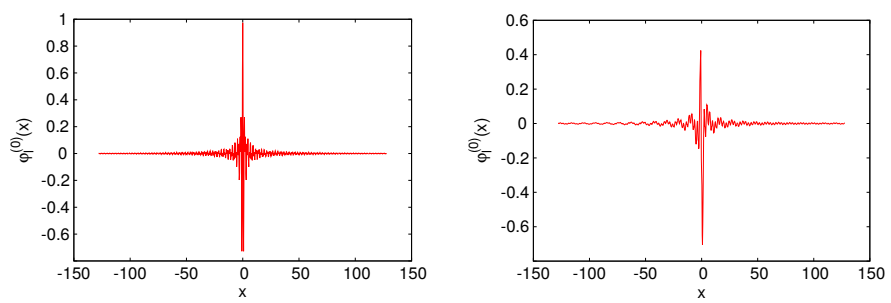


Figure 3.8: The Wannier functions for bands 7 and 8. They are extended over many sites.

3.5 Diagonalization of Complete System Hamiltonian

3.5.1 Basis for Diagonalizing the complete Hamiltonian

Both of the methods explained in section 2.4 have been implemented and the eigenstates gained with the two methods have been compared using their overlaps to verify their consistency. Due to the many advantages of the Wannier basis, namely the diagonal-like structure of the Hamiltonian and the possibility to limit the integration length in the calculation of the matrix elements, each of which are explained in the following two sections, support for the first method of calculating the complete system Hamiltonian in the basis of the homogeneous system eigenstates, has been discontinued.

3.5.2 Cut-off for Off-site Elements

When calculating $\langle l, \alpha' | \hat{H} | l', \bar{\alpha}' \rangle_0$, elements decrease exponentially with $\Delta l = l - l'$ if the inhomogeneity is not too big. After some Δl , it is convenient to make a cut-off to reduce calculation effort. The procedure that calculates these elements has been optimized in that respect. It was verified that it yields the same results as the procedure calculating all elements.

3.5.3 Restricting Integration Length

When calculating the elements of \hat{H} in the homogeneous system Wannier basis, an integration over the entire system has to be computed. Fortunately Wannier functions are localized which means that the integration can be restricted to the interval where the integrand function and thus each Wannier function is not exponentially close to zero.

After the centered Wannier function (one for every band) is calculated from the homogeneous system eigenstates, a cut-off is applied to the region where the Wannier function is close to zero. When the system Hamiltonian is diagonalized in the homogeneous Wannier basis, only the areas where the two Wannier functions and the potential have significant overlap are integrated. For low bands in which the Wannier functions have a small spread, this particularly reduces the computation effort, see section 3.3.2.

The calculation of these matrix elements requires a big fraction of the processing time taken by the whole program, see section 3.7.2. So optimizing this calculation promises to allow for the calculation of larger systems. A test conducted using 5 bands indicated that this optimizations can easily speed up calculations by a factor of two. During this test, the “cropping” has still been done very much in favor of the accuracy and less in favor of the execution time. By changing this or using fewer bands the execution can be accelerated even further.

3.6 Verification

3.6.1 Comparison with Foreign Implementation

Another implementation was provided by U. Bissbort where the lattice with a harmonic trap was solved using the method explained in section 2.3.2. This implementation has been used to verify the results obtained in the local implementation. The homogeneous system eigenfunctions and homogeneous system Wannier functions were compared using overlaps. The inhomogeneous system eigenvalues and eigenfunctions were only compared visually. In all of the comparisons, the lattice depth has been set to $10E_r$.

The overlaps $\langle s, \alpha | s', \alpha \rangle$ were calculated between the normalized states in the same bands of the different implementations s, s' . Only one state per band was used for this; the ground state for the energy eigenstates and the centered state for the Wannier functions.

The results of the comparison of the **homogeneous eigenstates** are shown on the left side of Figure 3.9, where the overlap between the states of the two implementations is plotted. In this calculation, only 2 sites were used in order to allow for a higher accuracy in the grid (400 points per site) and also for higher bands.

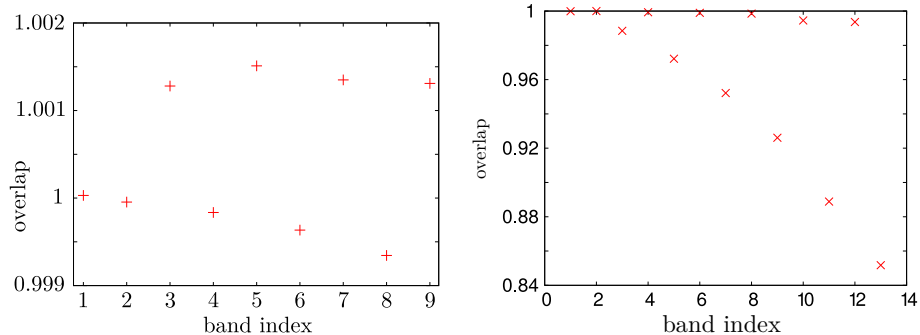


Figure 3.9: The overlap between the homogeneous system eigenstates (left) and the homogeneous system Wannier states (right) of the same bands for the two implementations. Ideally the overlap should be 1. The discrepancies are expected to come from numerical inaccuracies in either of the two implementations.

There are small deviations probably due to numerical inaccuracies. The overlap for normalized states cannot be larger than 1.

On the right side of Figure 3.9 the **homogeneous Wannier states** have been compared. In this calculation, 128 sites have been used with a grid of 40 points per site.

For higher bands, the error in the homogeneous Wannier states becomes non-negligible.

Finally, the eigenvalues and eigenfunctions for the system consisting of a lattice, with a harmonic trap symmetrically superimposed, were compared. Due to time constraints, this was only done visually without calculating overlaps.

The eigenvalues match very well with less than a 1 percent error but this error increases for higher energy states. The first 8 eigenfunctions calculated with both implementations are shown in Figure 3.10.

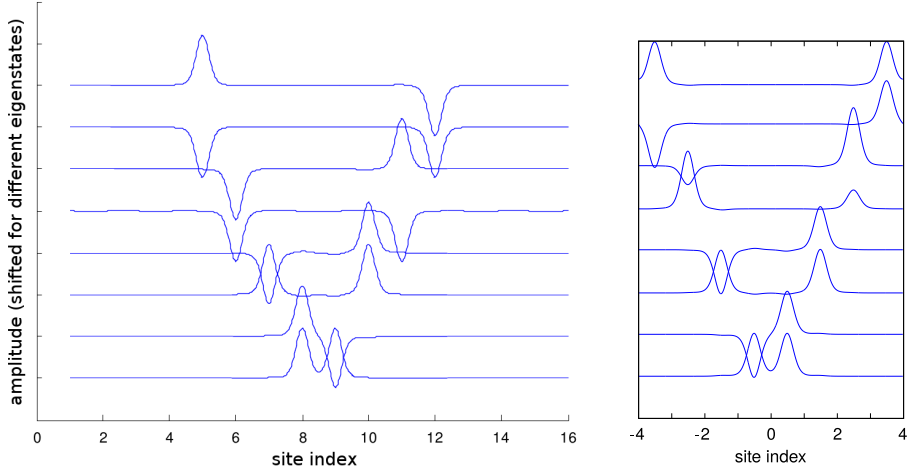


Figure 3.10: Foreign (left) and local (right) implementation eigenfunctions of a lattice with a harmonic trap. Due to the degeneracy the states do not match exactly which is to be expected. The implementations use different offsets for the site index.

Due to the degeneracy of pairs of eigenvalues in this system, the eigenfunctions may differ. But a superposition of two eigenstates that are localized at the same sites needs to be able to construct both of the eigenfunctions from the other implementation that are localized on the same sites. This is the case.

3.6.2 Determining Calculation Inaccuracies

If $\varphi^{(\text{calc})}$ was an exact energy eigenstate solution for the system, it should of course fulfill the stationary Schrödinger equation (eigenvalue equation for \hat{H}). It can be easily evaluated because the Hamiltonian is originally given in real space and $\varphi^{(\text{calc})}$ is usually obtained in real space or can be calculated from overlaps with other states given in real space.

Unfortunately, $\varphi^{(\text{calc})}$ will usually not be exact due to numerical and analytical inaccuracies (Hilbert space cut-off). Thus, there should be small deviations from the equality when the calculated state and its eigenvalue $E^{(\text{calc})}$ is plugged into the Schrödinger equation. This deviation is position dependent:

$$\text{Sdev}(x) = (\hat{H} - E^{(\text{calc})})\varphi^{(\text{calc})}(x)$$

When looking at $\text{Sdev}(x)$ locally at one x , it should be clear that $\hat{H}\varphi^{(\text{calc})}$ should yield some position dependent quantity which is of course not precisely eigenvalue times eigenvector. However, this quantity can be split into one position independent part E' which is common to all local relations and a normalized

position dependent part $\varphi'(x)$. If E' is taken to be the calculated eigenvalue $E^{(\text{calc})}$ (note that this assumption might conflict with the normalization of $\varphi'(x)$) the equation becomes

$$\text{Sdev}(x) = E^{(\text{calc})}(\varphi'(x) - \varphi^{(\text{calc})}(x))$$

$\text{posError}(x) = \varphi'(x) - \varphi^{(\text{calc})}(x)$ can be interpreted as the error in $\varphi^{(\text{calc})}$ although it is not the deviation from the exact state $\varphi^{(\text{err})} = \varphi^{(\text{calc})} - \varphi$. However, it should be of the same order. So

$$\text{posError}(x) = (\hat{H}/E^{(\text{calc})} - 1)\varphi^{(\text{calc})}(x) \quad (3.1)$$

which can be evaluated.

Though this argument isn't anything close to an actual proof, the experience of working with $\text{posError}(x)$ numerically shows that it can be used as a measure of the inaccuracy.

With (3.1) given the overall error in a whole state shall be defined through the L^2 -norm

$$\text{stateErr} = \sqrt{\int_x |\text{posError}(x)|^2 dx}$$

The error per band shall be defined as the average error per state in that band

$$\text{bandErr}_\alpha = \sum_n \text{stateErr}_{n,\alpha} / N$$

α : the band for which the errors are averaged

n : the eigenstate index

N : number of states per band

When processing $\text{Sdev}(x)$ further also the following expression can be derived

$$\text{Sdev}(x) = -E^{(\text{err})}\varphi^{(\text{calc})}(x) + (\hat{H} - E)\varphi^{(\text{err})}(x)$$

This equation shows more clearly that there are actually two errors contained in Sdev and thus in posError .

With some further work a more accurate result for the eigenenergy E might be gained.

The calculated $\varphi^{(\text{calc})}$ as well as the exact φ are normalized. $\varphi^{(\text{err})} = \varphi^{(\text{calc})} - \varphi$ is assumed to be small. Thus $\varphi^{(\text{err})}$ should be almost orthogonal to φ and $\varphi^{(\text{calc})}$ as visualized in Figure 3.11.

Furthermore, applying \hat{H} to $\varphi^{(\text{err})}$ should deliver a function that is still orthogonal to φ because \hat{H} cannot map a state without components in φ direction to a state that has components in φ direction.

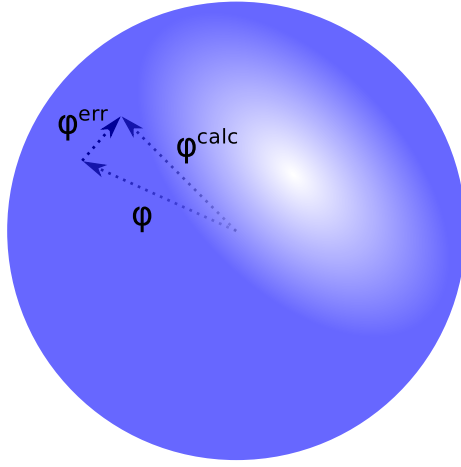


Figure 3.11: Approximate orthogonality between the functions $\varphi^{(\text{err})}$ and φ , $\varphi^{(\text{calc})}$ in a schematic 3d view. The sphere represents the Hilbert space.

$$\int_x \left[\hat{H} \varphi^{(\text{err})}(x) \right] \varphi^*(x) dx \approx 0$$

$$\int_x \left[\hat{H} \varphi^{(\text{err})}(x) \right] \varphi^{(\text{calc})*}(x) dx \approx 0$$

$E^{(\text{err})}$ can now be calculated individually by projecting the expression for Sdev onto $\varphi^{(\text{calc})}$

$$\int_x \text{Sdev}(x) \varphi^{(\text{calc})*}(x) dx = \int_x -E^{(\text{err})} \varphi(x)^{(\text{calc})} \varphi^{(\text{calc})*}(x) dx$$

$$+ \int_x \left[(\hat{H} - E) \varphi^{(\text{err})}(x) \right] \varphi^{(\text{calc})*}(x) dx$$

$$E^{(\text{err})} \approx - \int_x \text{Sdev}(x) \varphi^{(\text{calc})*}(x) dx$$

Even $\varphi^{(\text{err})}$ can now be determined by solving the following differential equation

$$(\hat{H} - E) \varphi^{(\text{calc})}(x) \approx (\hat{H} - E) \varphi^{(\text{err})}(x)$$

The expression on the left side can be evaluated. On the right side there is a differential expression of $\varphi^{(\text{err})}$.

Although the upper procedure should make it possible to get more accurate values for E and $\varphi(x)$ the performed calculations use posError for simplicity as the measure for the error.

Application to Implementation

`posError` has been used extensively to determine errors and inaccuracies in the calculation. Together with `stateErr` and `bandErr`, it is calculated in the implementation for the homogeneous and the inhomogeneous system eigenstates, indicating whenever a normalization or a call to `prepare_for_spline_interpolation()` has been forgotten.

Giving the error in every position, `posError` is also helpful in determining the quality of a given basis. Using a non-periodic basis, as described in section 2.7, leads to a higher error at the system edges where the basis is insufficiently complete, see Figure 3.12. This is more pronounced in higher bands because there the homogeneous Wannier states, which were used to diagonalize the complete Hamiltonian in, have a wider spread.

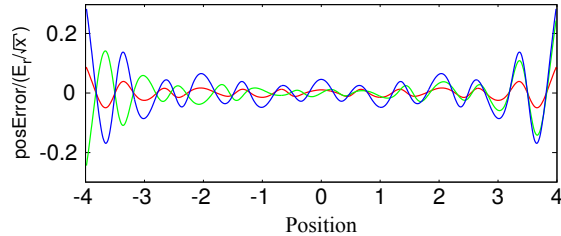


Figure 3.12: Position error in the eigenstates of a lattice with harmonic trap in the third band. At the system boundaries the error is higher which is related to the non-periodic basis used in this calculation.

In section 3.6.2, a test was performed to see how well the non-periodic Wannier basis can reconstruct a function that is localized close to the edge of the system.

Using the periodic Wannier basis caused the calculation of the trap eigenstates to be more accurate. With a trap strength of $0.00814147E_r$ and 16 sites, 6 bands, 160 points per site and a lattice depth of $10E_r$, the band errors (`bandErr`) are as follows

	band 1	band 2	band 3
lattice only	0.00280665	0.00606663	0.0108373
with trap	0.016677	0.0074954	0.0182714
	band 4	band 5	band 6
lattice only	0.0254046	0.0589841	0.124103
with trap	0.0473781	0.11036	0.224321

Gaussian in Wannier Basis

A normalized centered Gaussian has been expanded in the homogeneous Wannier basis. The reconstruction of that Gaussian by the Wannier basis using differing amounts of bands can be seen in Figure 3.13. The overlaps between the original and the reconstructed Gaussian, using different amounts of bands, are given in the tables below:

2 bands	0.73767
3 bands	0.99776
4 bands	0.998763
5 bands	0.999943

The above procedure has been repeated for a Gaussian shifted to the edge of the system, see Figure 3.14. The overlaps are

2 bands	0.73335
3 bands	0.984307
4 bands	0.985664
5 bands	0.989306

The graphs and the overlaps show that the Gaussian located at the system edge can't be reconstructed as well as the centered Gaussian in the non-periodic Wannier basis.

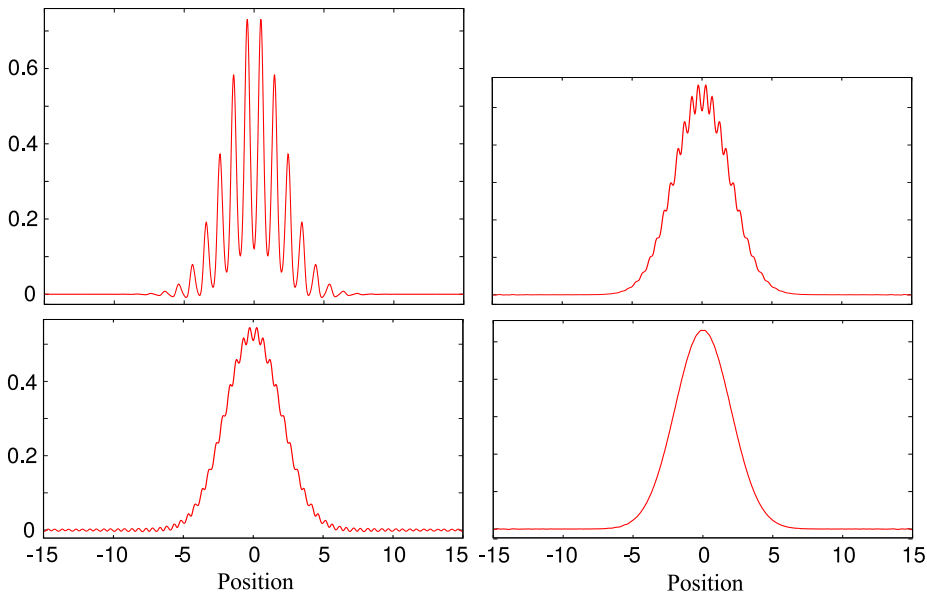


Figure 3.13: Gaussian function expressed by superposition of Wannier functions using 2 (top left), 3 (top right), 4 (bottom left) and 5 (bottom right) bands. A moderate amount of homogeneous Wannier functions is able to reconstruct the Gaussian function.

3.6.3 Limits

In the system consisting of a lattice with a harmonic trap, the results to the individual systems are known. Setting the strength of either constituent in the implementation to zero should yield the known result for the other system to which it can be compared. This way the correct working of the implementation in the regarded regime can be tested.

In the case of zero trap strength, obviously the homogeneous eigenstates should be obtained again. More interesting is the case of zero lattice strength.

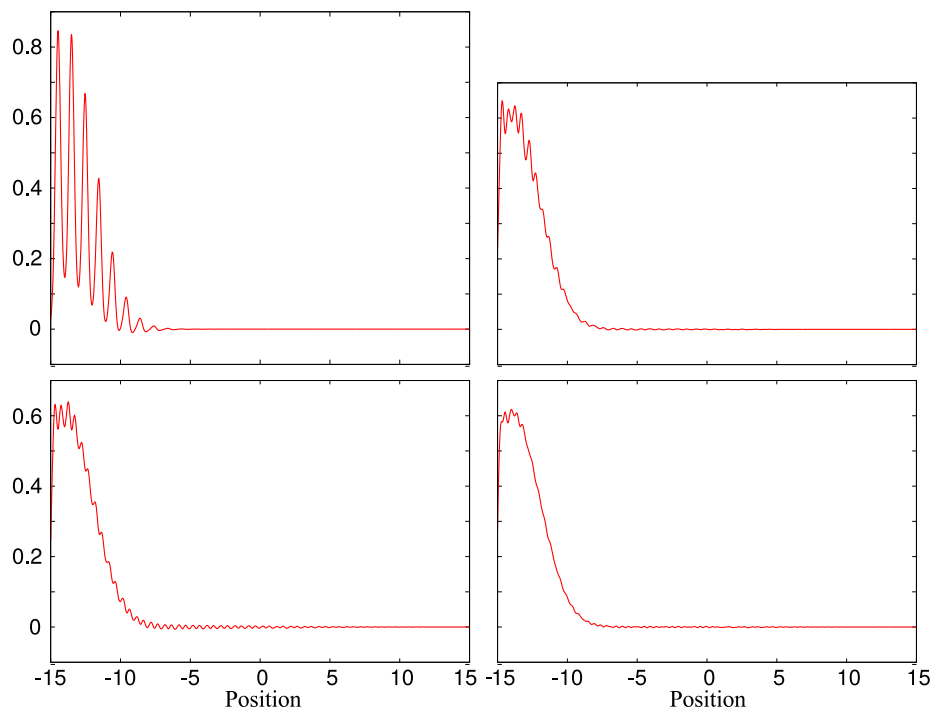


Figure 3.14: Shifted Gaussian expressed by superposition of Wannier functions using 2 (top left), 3 (top right), 4 (bottom left) and 5 (bottom right) bands. The insufficient completeness of the Wannier basis is pronounced at the system edge.

Harmonic Trap without Lattice

When the lattice is turned off, the eigenstates of the system should be the eigenstates of the trap i.e. eigenstates of the harmonic oscillator. In Figure 3.15, the first five states calculated in this way are shown.

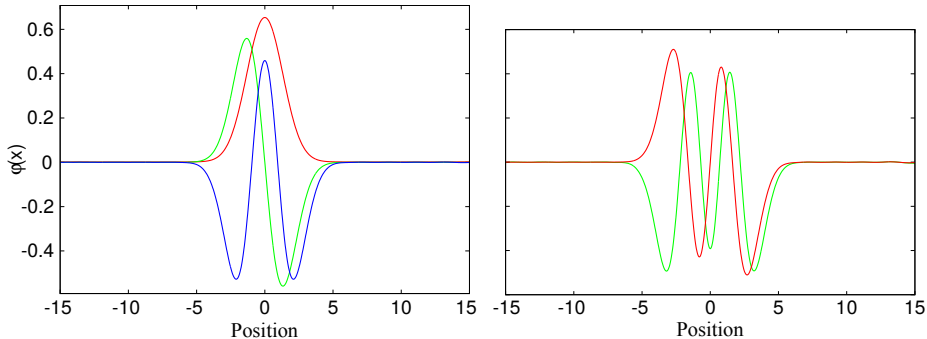


Figure 3.15: The harmonic trap eigenfunctions (no lattice). On the left, the ground state (red), first (green) and second (blue) excited eigenstates are shown. On the right, the third (red) and fourth (green) eigenstates are shown. When the lattice is turned off, the harmonic trap eigenstates should be obtained. They can also be calculated using a known analytical expression which allows for comparison.

Additionally, the states are calculated using the analytical solution of the harmonic oscillator. The overlap between the calculated and analytically determined states is a good measure for how well the eigenfunction calculation works. In the following, this overlap is shown

```

1.00 0 0 0 0 0 0 0 0 0
0 1.00 0 0 0 0 0 0 0 0
0 0 1.00 0 0 0 0 0 0 0
0 0 0 1.00 0 0 0 0 0 0
0 0 0 0 1.00 0 0 0 0 0
0 0 0 0 0 1.00 0 0 0 0
0 0 0 0 0 0 0.99 0 0 0
0 0 0 0 0 0 0 0.99 0 0
0 0 0 0 0 0 0 0 0.97 0
0 0 0 0 0 0 0 0 0 0.98

```

Although only 5 bands were used in the homogeneous system Wannier basis, the harmonic oscillator states are reproduced well beyond the 5th band.

3.6.4 Validity Checks

The implementation of the desired functionality is very prone to error. To verify that the results which were computed using multiple chained error-prone tasks is still related to reality, several validity checks can be performed:

- all overlap matrices need to be unitary

- calculate inh eigenfunctions from inh Wannier functions and compare with original eigenfunctions
- overlap between different homogeneous and inhomogeneous eigenfunctions and Wannier functions needs to be zero (orthogonality)
- eigenvalue equations need to hold for all calculated eigenvalues and vectors
- all $u(k, x)$ need to be periodic with the same periodicity as the lattice
- all $\varphi(k, x)$ need to be periodic with periodicity $\frac{2\pi}{\Delta k}$

3.7 Performance

3.7.1 Complexity of Operations

As illustrated in the last two chapters, there are many different computations that have to be performed by the implemented program. In the following, the most time consuming of these computations are listed. Additionally, the approximate computation time needed in proportion to the input parameters is shown. Input parameters are the number of sites (s), number of bands (b), number of points per site (pps). Different optimizations may reduce the computation time, as noted.

- calculation of matrix elements via integration
 - inhomogeneous system Hamiltonian in homogeneous system Wannier basis $\sim s^3 b^2 pps$ ($s^2 b^2$ matrix elements, $s pps$ integration length, optimized by matrix cut-off (section 3.5.2), restriction of integration length (section 3.5.3) and hermiticity)
 - band projected position operator in inhomogeneous system eigenstates $\sim s^3 b pps$ ($s^2 b$ block-diagonal matrix elements, $s pps$ integration length, optimized using hermiticity)
- propagation of differential equation
 - homogeneous system eigenfunctions $\sim s^2 b pps$ ($s b$ eigenstates, $s pps$ propagation length)
- eigenvalue problem
 - inhomogeneous system Hamiltonian in homogeneous system Wannier basis, depends on external diagonalization algorithm, matrix has $s^2 b^2$ elements (optimized by matrix cut-off)
 - band projected position operator in inhomogeneous system eigenstates, depends on external diagonalization algorithm, matrix has $s^2 b$ block-diagonal elements

Note for Matrix Elements

The calculation of the matrix elements for \hat{H} in the Wannier basis has to perform on the order of $s^2 b^2$ integrations. This is in contrast to the calculation of x_α in the energy eigenbasis where the matrix is block diagonal and thus takes only on the order of $s^2 b$ integrations. The first integration can be further optimized through the use of the two referenced methods. In this way the integration for \hat{H} can be a lot faster than the integration for x_α depending strongly on the amount of bands taken into account.

3.7.2 Execution Speed and Program Output

The program notifies the user via its text output, whenever it is done with one procedure and starts the next procedure. This is done by printing the name of a procedure as soon as it starts executing and by printing the time it needed to execute after the procedure has finished. In the following, an example of this output is shown

```
calculating H0eigenstates ... -50.04s
calculating x_alpha0 in H0 basis ... -2.23s
calculating HOWannier0Overlap ... -0.01s
calculating Wannier0 functions ... -0.2s
calculating H in Wannier0 basis ... -181.34s
calculating WOHOOverlap ... -0.03s
calculating Heigenfunctions ... -0.76s
calculating x_alpha in H basis ... -150.72s
calculating Wannier functions ... -0.209984s
```

3.7.3 Own Implementations of Numerical Routines

Most of the numerical procedures used in the code have been implemented by hand before an external library has been used. An overview of the versions obtained in this way, is given by Figure 3.16.

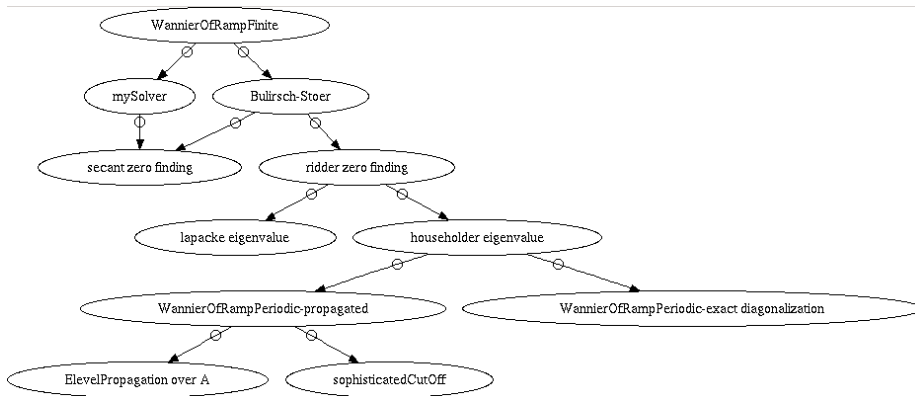


Figure 3.16: The code versions gained by implementing numerical routines by hand. Later the implementation was changed to use more sophisticated external libraries.

Prior to using the Bulirsch-Stoer differential equation solver from “numerical recipes”, the implementation had its own differential equation solver with an adaptive step size Runge-Kutta method called *mySolver*. The Bulirsch-Stoer solver, which picks the sampling points in a beneficial way, is faster.

Previously, the program used Ridder’s method for finding single function roots an own implementation utilizing a secant method which doesn’t rely on a bracketed root was used. Ridder’s method proved faster and more reliable.

Initially, the program used the eigenvalue procedure dsyev from Lapack and another eigenvalue procedure from “numerical recipes” relying on the Householder method. Later the armadillo library was included in the project which covers many linear algebra routines. The armadillo eigenvalue procedure relies on Lapack.

The eigenvalue solver from “numerical recipes” using the Householder method and the solver dsyev from Lapack have been compared in terms of performance. Both solvers act on symmetric matrices. The conclusion, drawn from the results seen below, is that Lapack is faster for larger matrices.

- 10x10 matrices: Householder faster than Lapack by factor 3
- 100x100 matrices: Householder and Lapack equally fast
- 1000x1000 matrices: Lapack faster than Householder by factor 5

3.8 Units

The basic units used in the implementation are the recoil energy E_r , the lattice constant (periodicity) a and the reduced Planck constant \hbar .

Usually a and m is given yielding $E_r = \frac{\hbar^2 k_L^2}{2m} = \frac{\hbar^2 \pi^2}{2ma^2}$ and the system is determined.

Where non-basic units are given in the thesis the special case of ^{87}Rb atoms and a lattice constant of $a = 1064\text{nm}$ is assumed.

$$m = m(^{87}\text{Rb}) = 1.443160769 * 10^{-25}\text{kg}$$

$$\rightarrow E_r = \frac{(1.05457173 * 10^{-34}\text{kg} \frac{\text{m}^2}{\text{s}})^2 * 3.1415926535^2}{2 * 1.443160769 * 10^{-25}\text{kg} * (1064 * 10^{-9}\text{m})^2} = 3.359108480 * 10^{-31}\text{kg} \frac{\text{m}^2}{\text{s}^2}$$

In the implementation the basic units mentioned above are set to 1.
Thus for the mass which is used to define the recoil energy

$$m = \frac{\hbar^2 \pi^2}{2E_r a^2}$$

$$\rightarrow \text{kg} = \frac{\pi^2}{2 * 1.443160769 * 10^{-25}} = 3.419440375 * 10^{25}$$

holds. Also

$$\text{meter: } m = 1 / (1064 * 10^{-9}) = 9.39849624 * 10^5$$

$$E_r / \hbar = \frac{3.359108480 * 10^{-31}\text{kg} \frac{\text{m}^2}{\text{s}^2}}{1.05457173 * 10^{-34}\text{kg} \frac{\text{m}^2}{\text{s}}} = 3185.2821 \frac{1}{\text{s}}$$

$$\text{second: } s = 3185.2821$$

Where applicable, i.e. where the interaction energy U is calculated, also the scattering length of ^{87}Rb atoms is assumed $a_s = 100.40 a_0$ with a_0 being the Bohr radius, see [EOD⁺12].

Chapter 4

Results for a Lattice in a Well

A lattice of finite size with infinitely high walls at its edges was studied. To solve this system, the procedure explained in section 2.3.1 has been utilized. So in this system, as opposed to the other systems studied, the homogeneous lattice eigenstates were not calculated in advance.

The function whose roots need to be determined in order to find the energy eigenvalues looks like the one shown in Figure 3.1. Remarkably this function yields all of the system energy eigenvalues, unlike the case in the infinite system, where the quasi momentum is introduced and discretized.

In this system, the common definition for calculating Wannier states cannot be used, because the Bloch theorem doesn't hold and no quasi momentum is undefined. The generalized definition for Wannier states resolves this issue effortlessly.

In Figure 4.1, the results for a lattice in a well consisting of 9 sites and a lattice depth of $10E_r$ are shown. From the differential equation it is known that the eigenfunction solutions can be chosen to be solely real.

The eigenstates and Wannier states look similar to the infinite lattice states, except that they are non-periodic. Despite this they form a complete basis. For this reason this system can be used to determine the influence of a periodic basis as it relies on a non-periodic basis itself.

Due to the finite lattice size, the system is inhomogeneous. Thus, the Wannier functions are not translational invariant anymore. The walls of the well represent the inhomogeneity, so the deviations from the infinite lattice Wannier functions are expected to be highest at the walls and lowest in the well center. To visualize the invariance, all the Wannier functions were subtracted by the Wannier function localized in the well center. This is shown in Figure 4.2.

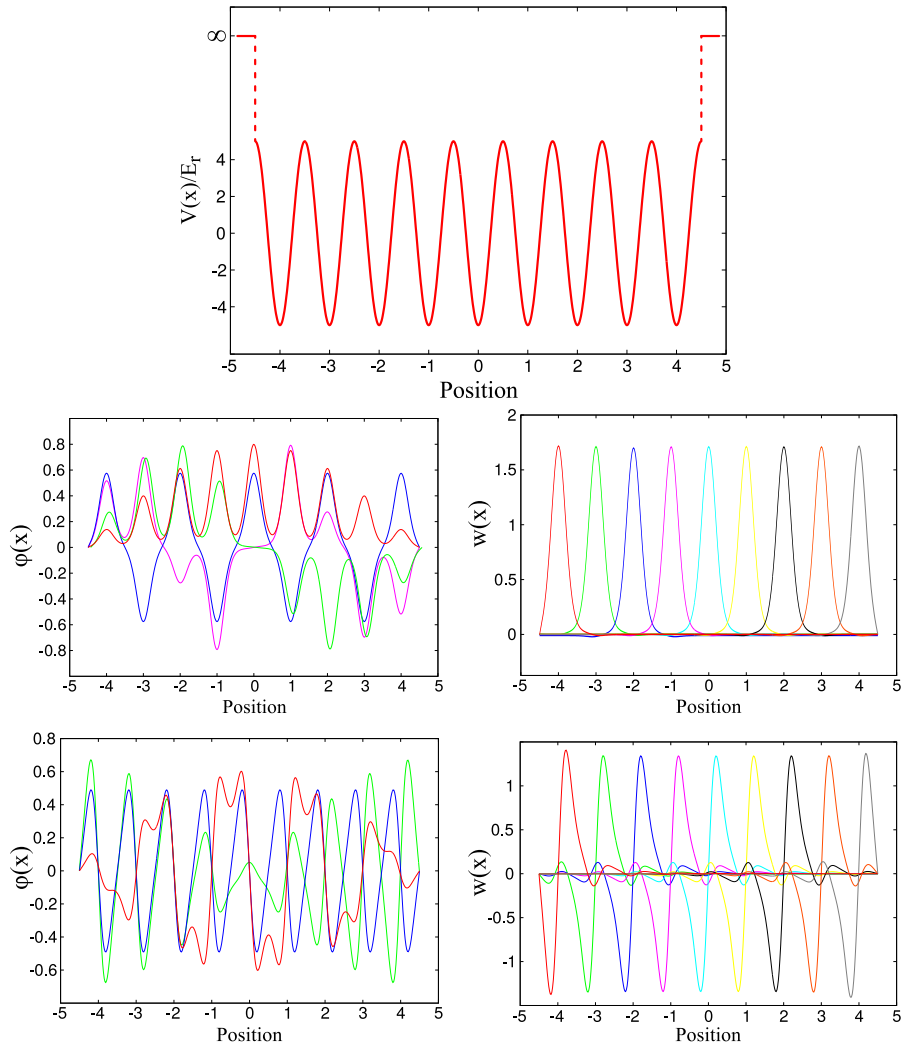


Figure 4.1: In the top, the potential of a lattice in an infinite well consisting of 9 sites is shown. Below, the first band eigenstates (left) and Wannier states (right) are shown. In the bottom row, the respective second band states are shown.

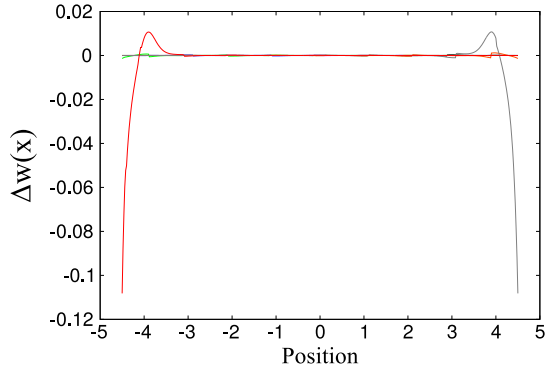


Figure 4.2: The remainder of the Wannier functions when subtracted by the most centered Wannier function. This visualizes that the translation invariance is lost in this system, mainly for the Wannier functions located at the system edges.

4.1 Additional Linear Potential

To the previously used lattice within a well, a linear potential is added. This corresponds to an accelerated optical lattice in which *Bloch oscillations* can be observed, see [KH91]. The eigenstates form the *Wannier-Stark Ladder*.

The slope of the linear potential is $0.4E_r$ per lattice site. The results for this system are shown in Figure 4.3. The additional linear potential caused the energy eigenstates to localize at the locations of the lattice sites¹. Also in this case with two inhomogeneities, the generalized definition for Wannier states can be applied easily.

In Figure 4.4 the behaviour of the energy eigenvalues with the slope of the linear potential has been examined. The eigenvalues of the first two bands are shown versus the slope ranging from 0 to $1E_r$ per site. Avoided crossings can be observed.

¹Choosing a high linear potential slope and a high system size causes the calculation to become numerically unstable. A cut-off routine was implemented to cope with this situation but user intervention may still be required.

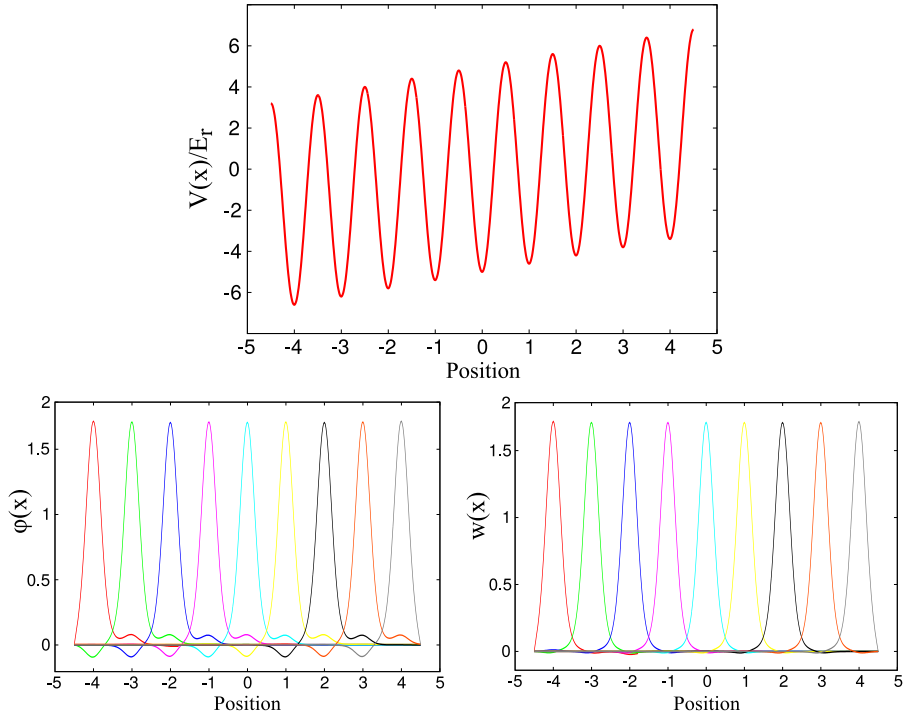


Figure 4.3: In the top, the potential for a system consisting of a lattice in a well with an additional linear potential is shown. Below are the energy eigenstates (left) and the Wannier states (right). The energy eigenstates are localized to a single site each and look almost identical to the Wannier functions.

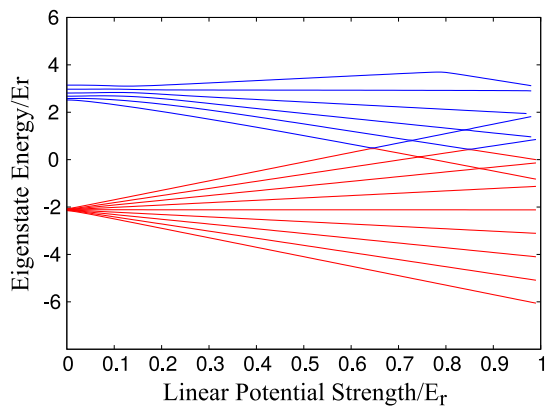


Figure 4.4: E levels as function of the linear potential slope

4.2 Conclusion

Generalized Wannier states have been calculated for an inhomogeneous lattice system consisting of a lattice in a well with infinitely high walls and also with an additional linear potential. Thereby, the strength of the generalized definition was demonstrated, as the common definition cannot be applied in this case.

Unfortunately Hubbard parameters haven't been calculated and the band assignment techniques developed later weren't applied to this system. It should be easy to include these features in a follow-up version of the implementation.

Chapter 5

Results for a Lattice in a Harmonic Trap

When ultracold atoms are prepared in an optical lattice there usually is an additional trapping potential used in addition to the lattice potential to confine the atoms in a certain region. Frequently, dipole traps are employed for this purpose which create a harmonic oscillator potential

$$V_{trap}(x) = V_1 \frac{x^2}{a^2}$$

In this chapter such a harmonic trap is taken to be the inhomogeneity in a lattice potential. First, some of the general properties of the system will be discussed using a small 6 site system as reference. The eigenstates, Wannier states, band assigning procedures and Hubbard parameters will be discussed exemplary. Finally, larger, more realistic systems are investigated.

As mentioned in section 3.8 the **unit system** that is used in the simulations assumes $\hbar = 1$, $a = 1$ and $E_r = 1$. From this it follows that $s = 3185.1821$ (s=second) for a system with ^{87}Rb atoms and a lattice constant of $a = 1064\text{nm}$. With this it is possible to calculate the actual trap frequency in Hz in an experiment from the inhomogeneity strength in E_r . In the table below, the trap strength V_1 in E_r is shown for two different lattice constants a and two trap strengths in Hz.

system parameters		
lattice constant	$a=1064\text{nm}$	
particle mass	$m(^{87}\text{Rb})$	
scattering length	100.40 a_0	

V_1/E_r	$a = 812\text{nm}$	$a = 1064\text{nm}$
$V_1/\text{Hz} = 50$	0.00814147	0.0240019
$V_1/\text{Hz} = 100$	0.0325659	0.0960075

To find the eigenstates of the system the **procedure** along the right red dashed path using the common definition for the Wannier states as illustrated in Figure 2.1 is used. Here, the results of the calculations for these systems are discussed.

In [HQ04] the same system is investigated. Limiting cases in the vicinity and away from the trap center are regarded. The energy eigenfunctions and the

density of states are calculated. The dynamics, initiated by a sudden lattice shift in this system, are investigated in [SH07].

5.1 Qualitative Behaviour Portrayed in a Small System

In the following, a small system consisting of only 6 sites is analyzed. This ought to give a qualitative understanding of the system's behaviour. During this calculation 12 bands have been included. The higher bands are important for the high trap strengths only.

system parameters	
sites	6
lattice depth	$10E_r$

5.1.1 Eigenstates and Wannier States for Shallow Trap

To start off the eigenstates and generalized Wannier states have been determined for different inhomogeneity strengths. The result is shown in Figure 5.1. There are three rows each of which reflect a system with a different trap strength V_1 , starting with no trap at all in the top, to a moderate trap strength in the bottom. The systems in these plots have no avoided crossings between the first and second band, see Figure 5.4, and are thus referred to as being shallow traps. On the left side all of the first band Wannier functions and the two most centered Wannier functions are shown inside the system potential. The **height of each state** reflects its energy expectation value (on-site energy). The amplitude of the states is just schematically shown, i.e. no actual scale for their probability density is given.

system parameters	
trap strength	$0, .03, .4E_r$
trap shift	$.3a$

On the right side of the figure, the four most leftward first band Wannier functions and four similarly localized first band eigenfunctions are shown individually. Also, the second band most centered Wannier functions and energy eigenfunctions are shown.

The Wannier functions in the three systems look very similar for each band. Neither the potential value at the site where they are located nor the trap strength in general have a visible influence on the **Wannier function shape**. The **on-site** energy of the Wannier functions reflects the potential strength at the site where the state is localized. Second band states have a higher on-site energy. While the first band states hardly overlap visibly, the greater spread of the second band states causes them to overlap significantly. Of course, this visible overlap is not to be confused with the actual overlap integral $\langle l, \alpha | l', \alpha' \rangle = \delta_{l,l'} \delta_{\alpha,\alpha'}$ which is zero for different states.

The energy eigenfunctions shown in the right are spread out over the entire system when the trap potential is zero, but just a small trap strength is sufficient for them to start **localizing**, as can be seen in the middle plot. This effect is less strong in the center of the trap where the trap potential changes slowly, thus in the middle plot even the first band centered states are still more extended. In the bottom plot, all the first band eigenstates are localized. In the limit of a high trap strength, the energy eigenstates will resemble the Wannier states.

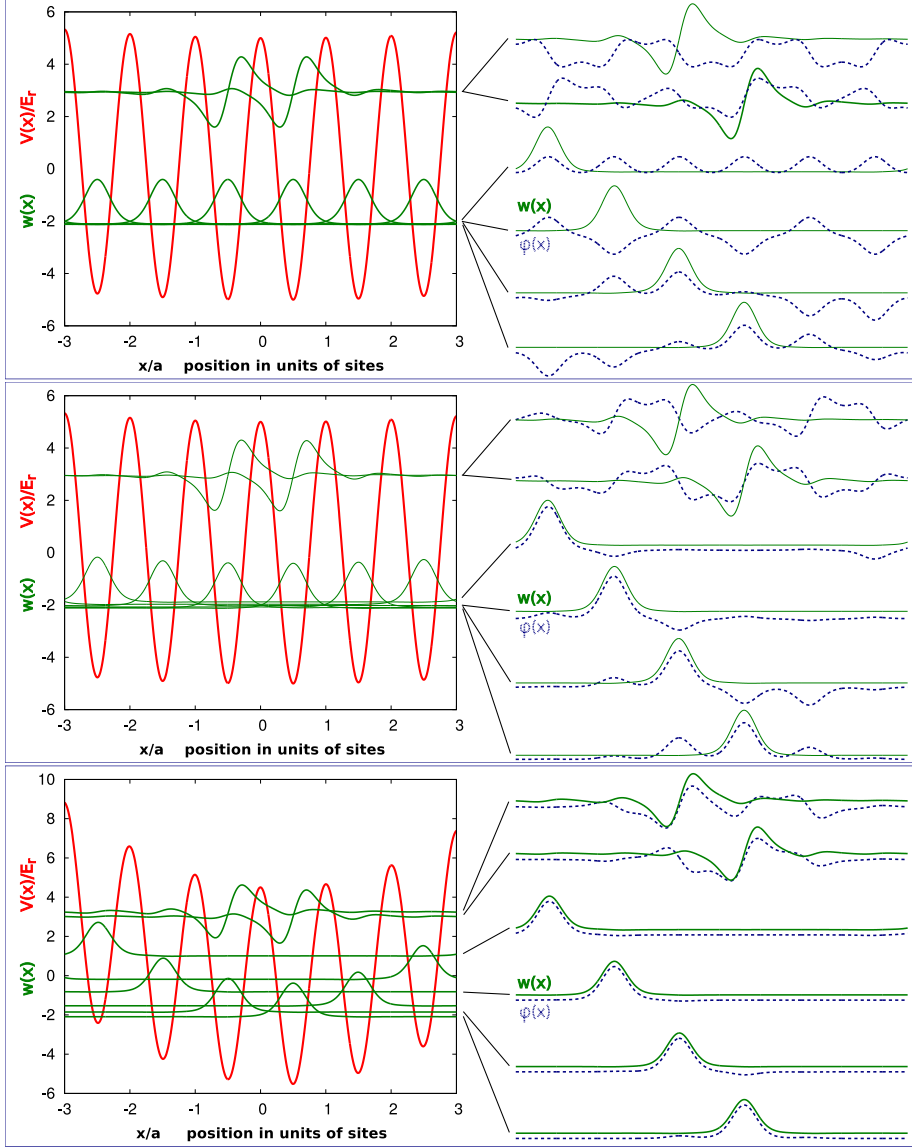


Figure 5.1: Overall potential $V(x)$, generalized Wannier functions $w(x)$ and energy eigenfunctions $\varphi(x)$ for $V_1 = 0E_r$ (top), $V_1 = .03E_r$ (middle) and $V_1 = .4E_r$ (bottom). The homogeneous lattice depth is $V_0 = 10E_r$. On the left side, all of the first band and the second band most centered Wannier functions are shown with their height offset reflecting their on-site energy. On the right side, some of the Wannier functions are shown, again separated, along with some energy eigenfunctions that have similar localization.

The second band states localize less quickly for increasing trap strength. Even in the bottom plot they are not quite localized and still differ a lot from the Wannier states. This is not the case anymore for the second band states located at the system edge which aren't shown in the plots.

Both the Wannier states and the energy eigenstates are **periodic** which is a consequence of the finite system size, see section 3.1 and section 2.7. This is not true for the potential which has a different amplitude at the system edges, see bottom plot.

There is a slight shift between the lattice and the trap potential. This shift is introduced to avoid degeneracies, as will be discussed now.

Degeneracy

When the trap potential and the lattice potential are exactly aligned in a point of symmetry, degeneracies appear. When the states are degenerate in this system, they are localized partly in opposite sites from the origin with equal potential, see Figure 5.2. The position expectation value will be zero and thus cannot be used to assign states to bands. To circumvent this, a **slight shift** between the lattice and the trap can be introduced which eliminates the degeneracy. This was used in all of the analyses presented here. Another method to still get a sense of the localization is to use the absolute value of the position operator or to use the spatial variance instead.

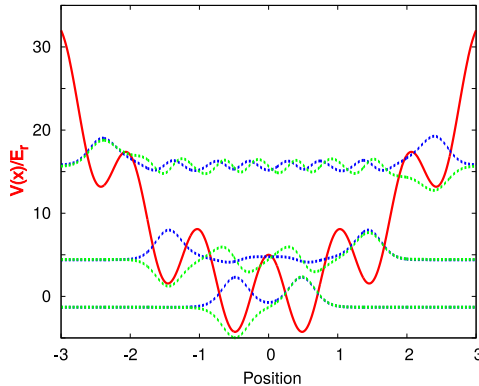


Figure 5.2: Degenerate energy eigenfunctions are observed when the lattice and the harmonic trap are exactly aligned in their points of symmetry.

5.1.2 Hubbard Parameters for a Shallow Trap

For the three lattice strengths discussed in the last section, the Hubbard parameters using the homogeneous system Wannier basis and the generalized Wannier basis were calculated. The results for the first two bands are shown in Figure 5.3. Only the first band on-site interaction is shown.

system parameters	
trap strength	3.E_r
trap shift	0 a

In the **top row**, the trap is turned off. Thus, the two plots for the Hubbard parameters in the homogeneous and inhomogeneous Wannier basis are the same. Also, there is absolutely no site-dependency in the on-site interaction, because the Wannier functions strictly obey translation symmetry in the homogeneous system.

Turning the trap on, to a very **weak strength**, hardly changes the Hubbard parameters. In the homogeneous Wannier basis, terms, that couple different homogeneous system bands appear. In the inhomogeneous system basis, the Hamiltonian is of course diagonal. The on-site interaction now possesses a very weak site-dependency on the order of $10^{-6}E_r$, but without obvious structure. This is probably due to numerical inaccuracies.

This is different if the trap strength is increased to some notable value as shown in the **bottom plot**. Here, the on-site interaction seems to resemble the harmonic trapping potential with a site-dependence on the order of $10^{-5}E_r$. The small magnitude of the on-site interaction resembles the fact that the Wannier functions in Figure 5.1 did not change their shape visibly.

Also, the on-site energy displays a notable site-dependency in both bases as do the inter-band terms in the homogeneous system basis. In the second band, the hopping has a notable site-dependency and off-diagonal terms become non-negligible. This is due to an avoided crossing with a third band state, see top middle plot in Figure 5.4.

As long as no second band excitations play a role in the system, it can be described very well using the generalized Wannier basis. A **tight binding-like** approximation can be applied leaving only the on-site energy, the nearest neighbor hopping and the on-site interaction in a Hubbard-like model.

5.1.3 Avoided Crossing

When the trap strength is increased further, the energies of the lowest energy state from the second band and the highest energy state from the first band approach each other. In Figure 5.5, these two states are shown for trap strengths before, on top of and after an avoided crossing, see Figure 5.4. The situation encountered before and after the avoided crossing seems intuitive, i.e. at some point the first band state localized at the system edge will become higher in energy than the second band state localized in the trap center. Less intuitive is the situation on top of the avoided crossing. The states show a behaviour similar to degenerate states because they are localized at two sites at once. Additionally, they have notable first and second band Wannier function contributions at once.

Some **methods to assign states to bands** were explained in section 2.6.2. The methods using the position expectation value and the band projector expectation value were applied in this system. The results are shown in the middle and right column in Figure 5.5. In the center, the position expectation value of the first 4 band eigenstates is plotted against their corresponding energy eigenvalues. As mentioned in section 2.6.2 each band is expected to have one state localized at each site. The plots show that this is only true for the lower bands. The higher band states localize around the trap center. Before the avoided crossing, the method can be used to assign the states of the first two bands. On top of the avoided crossing the first band seems to be missing the highest energy state which is not localized at the system edge anymore. Also, for the

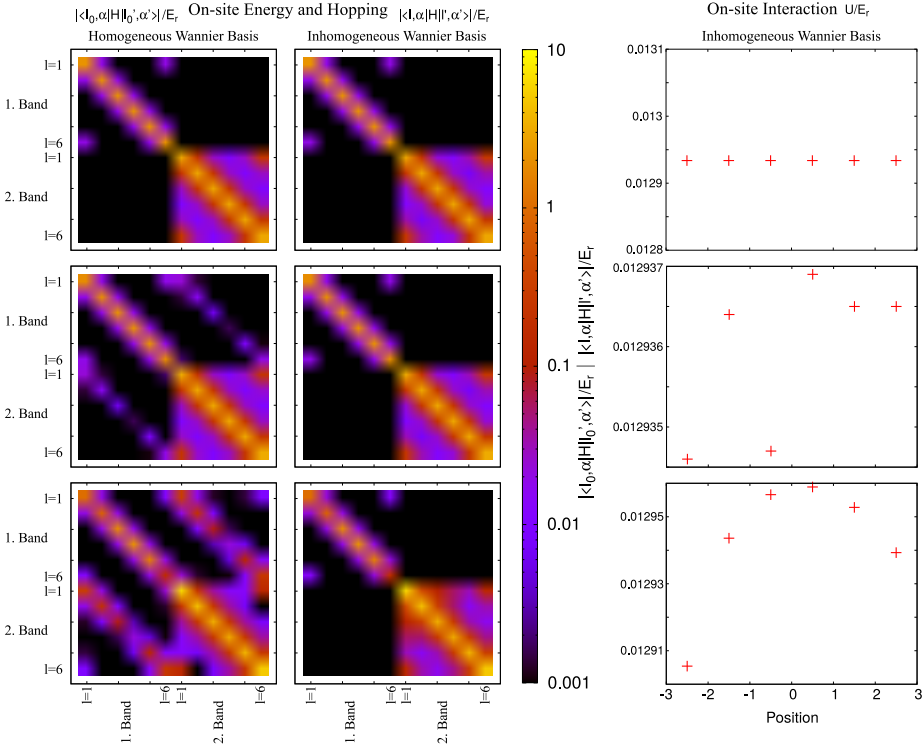


Figure 5.3: The Hubbard parameters for systems with trap strengths of $0E_r$, $.03E_r$ and $.4E_r$. In the left column the elements $|\langle l_0, \alpha | \hat{H} / E_r | l'_0, \alpha' \rangle|$ are shown. In the center the elements $|\langle l, \alpha | \hat{H} / E_r | l', \alpha' \rangle|$ are shown.

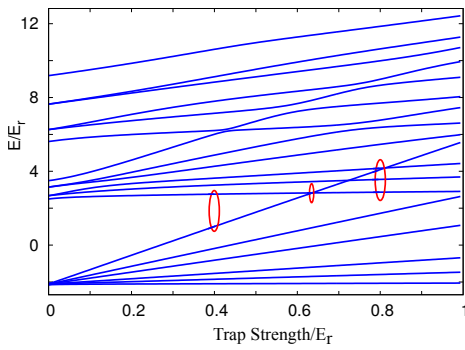


Figure 5.4: The energy eigenvalues for different trap strengths. Marked are the trap strengths before, on top of and after an avoided crossing. These three cases are further analyzed.

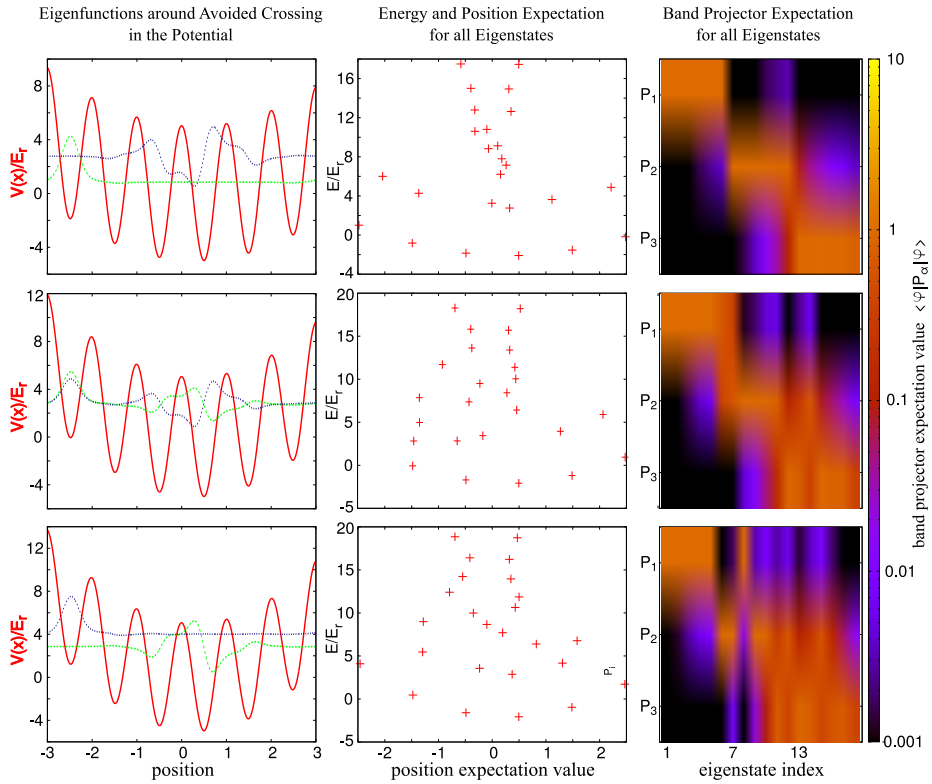


Figure 5.5: The highest energy first band eigenstate and the lowest energy second band eigenstate before (top plot $V_1 = 0.4E_r$), on top of (middle plot $V_1 = 0.6355E_r$) and after (bottom plot $V_1 = 0.8E_r$) an avoided crossing. The distribution of the position expectation values versus the energy of the eigenstates and the expectation values of the homogeneous system band projection operators in the first few complete system eigenstates is also shown.

second band the assignment is not clear. After the avoided crossing the first band states can be selected clearly but the second band states cannot.

In the right column the **expectation value of the homogeneous system band projection operators** is shown for the lowest 18 eigenstates. The same conclusions are drawn. Assignment to the first band is clear before and after the avoided crossing. For the second band only, the assignment before the crossing is clear.

It becomes clear that assigning states to bands at an avoided crossing is not very reasonable.

5.1.4 Hubbard Parameters at Avoided Crossing

In Figure 5.6, Hubbard parameters for the first 4 bands are shown for the two lower systems in Figure 5.5, i.e. for trap strengths of $V_1 = 0.6355E_r$ and $0.8E_r$. The matrices displayed in the upper row in Figure 5.6 are the Hamiltonians for the system **at the avoided crossing**. In the left the homogeneous system Wannier basis was used. There are notable contributions from matrix elements across bands. These cannot be neglected in a decent description. Despite these off-block-diagonal terms the hopping does decrease quickly with increasing Δl . A Hubbard-like model with a tight-binding-like approximation could give a decent description if the off-block-diagonal terms were taken into account.

On the right, where the generalized Wannier basis with band assignment following the eigenenergies' order was used, things are different. The Hamiltonian is block diagonal, but the hopping terms have notable far-off-diagonal elements. The tight binding approximation can't be applied here, anymore. The **on-site interaction** for the first band Wannier function on the left system edge will be erroneous because the first band assumption used in the derivation of the on-site interaction is not applicable. Perhaps a Hubbard-like model without on-site interaction could still rely on the generalized Wannier basis.

The lower two plots show the Hamiltonian in two different generalized Wannier bases for the system **after the avoided crossing**. The two bases have different band projectors. In the left plot, the states were assigned to bands using the order of the eigenvalues. This choice doesn't include any states localized at the most leftward site, see bottom plot in Figure 5.5. Despite being block diagonal the result isn't very satisfying because many hopping terms need to be included in the description. This is different in the right plot, where first band terms are almost tridiagonal. This is due to a different band assignment using the expectation value of the first homogeneous band projector seen in the bottom right plot in Figure 5.5. The sixth eigenstate can clearly be assigned to the second homogeneous band and the eighth eigenstate to the first homogeneous band. This example shows that a great benefit can be drawn from a proper band assignment.

5.1.5 Strong Trap

In the last analysis of the small 6 site system, the trap strength is increased even further to $V_1 = 3E_r$. Figure 5.7 shows the results. The **potential**, together with the first band **states** and one second band state, is shown in the upper left plot. At these high inhomogeneity strengths, the energy eigenstates and Wannier states look the same. The lowest energy second band state is now

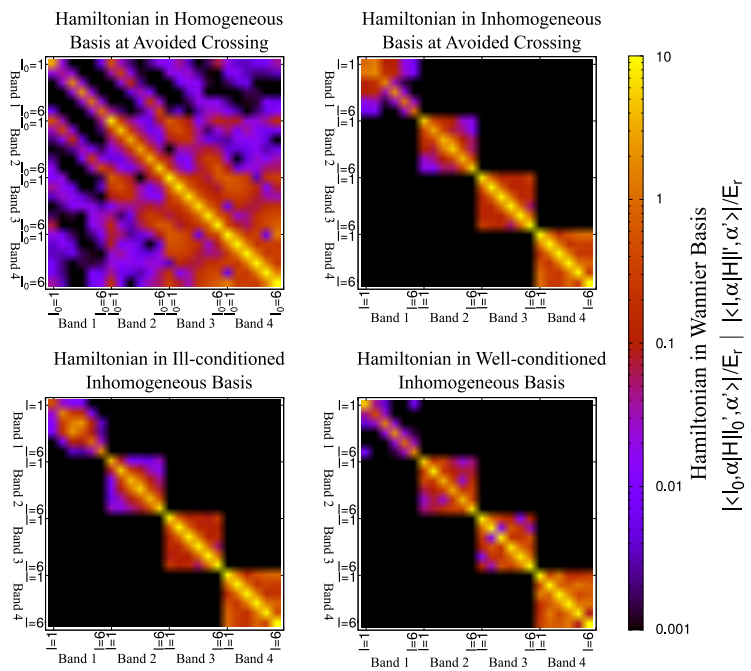


Figure 5.6: The upper two matrices represent the system at the avoided crossing ($V_1 = 0.6335E_r$) and the lower two matrices represent the system after the avoided crossing ($V_1 = 0.8E_r$). In the ill-conditioned case the band assigning was done naively using simply the order of the energy eigenvalues.

lower in energy than the three highest first band states. The first band energy eigenstates localized on the system edge contain a small fraction of an extended state.

In the upper centered plot, the **evolution of the energy eigenvalues** up to a trap strength of $3E_r$ can be seen. There are numerous avoided crossings for the first band edge states. On close inspection, the repulsive effect is visible for avoided crossings at high trap strengths. It is notable that the higher band states don't possess the same divergent characteristic as the lower band eigenvalues, which is a result of their insufficient localization. They only seem to be aware of the harmonic trap, but not aware of the lattice. Another feature visible in the plot is the disappearance of gaps between higher bands.

The **expectation values** of the first 8 **homogeneous band projection operators** for the first 48 states are shown in the upper right plot. Only the states for the first band can be selected clearly, the other states have contributions in many different homogeneous bands.

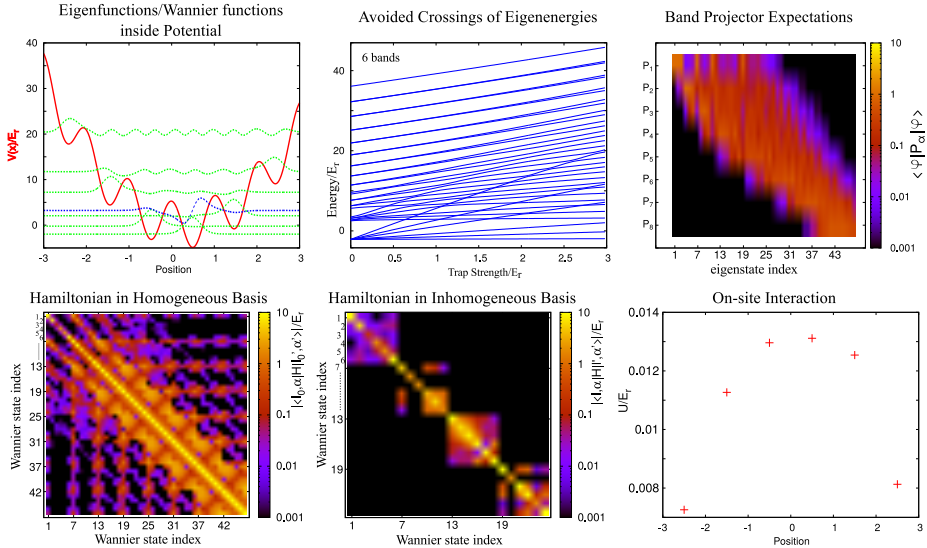


Figure 5.7: The analysis of a system consisting of 6 sites and a strong harmonic trap. There are many avoided crossings but the band assignment works decently for the first band.

In the bottom row, the Hubbard parameters are shown. The left plot depicts the **Hamiltonian in the homogeneous lattice Wannier basis**, showing 8 bands. For all the states in the first band, there are major couplings to higher bands. This is even more pronounced for the leftmost highest energy state which is close to an avoided crossing, see upper centered plot. This state has contributions up to the eighth band and beyond.

The bottom center plot uses the **generalized Wannier basis**. Of course the Hamiltonian is block diagonal; additionally the Hamiltonian has only small long-range hopping terms. This is very promising and should allow for a description using a Hubbard-like model. This is not true for the second band. Only few hopping terms are non-zero, this is expected to result from an insufficient band assignment, where less than six states were selected for the second band, see

top right plot.

The **on-site interaction** for the first band is shown in the bottom right plot. It reflects the shape of the harmonic trapping potential. The order of the site-dependency is by a factor of 10^2 greater than in the shallow trap. This shows that the Wannier functions are now far from being translationally symmetric. This was already visible in the top left plot, where the higher states have some extended component.

Even in the highly inhomogeneous regime regarded here, it is possible to describe this system using a Hubbard-like model. This shows the strength of the generalized definition of Wannier functions.

5.2 Realistic Systems

This section aims at giving some statements applicable to real systems. Therefore, the system **size** is increased. Two systems with 26 sites, one with a shallow and another one with a strong trap, and a system with 100 sites are analyzed.

5.2.1 Shallow Trap

In a shallow trap, the trap strength V_1 is weak enough so that no avoided crossings appear in the first band eigenvalues yet. For 26 sites, the eigenvalues for such a potential for different inhomogeneity strengths are shown in Figure 5.8. The first avoided crossing between the first and second band eigenvalues is at an inhomogeneity strength of about $V_1 = 0.028E_r$. Using ^{87}Rb atoms in a 1024nm lattice, a trap strength of $V_1 = 0.0240019E_r$ corresponds to a trap frequency of 50Hz. Thus, such a system is not expected to contain an avoided crossing between the first and second band yet and qualifies as an example of a shallow trap.

system parameters	
sites	26
lattice depth	$10E_r$
trap strength	$.0240019E_r = 50\text{Hz}$
trap shift	.3 a

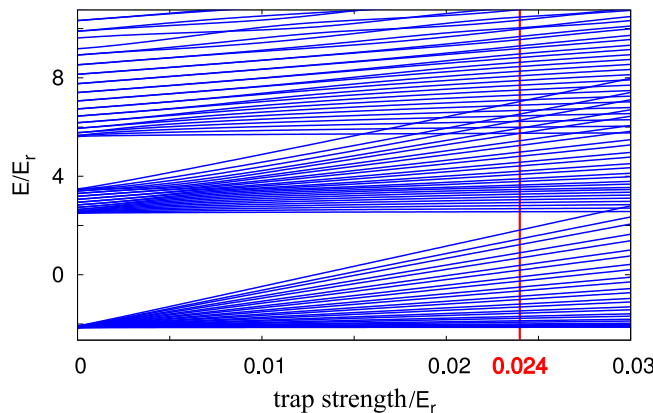


Figure 5.8: Energy eigenvalue dependence on the trap strength for the 26 site system. At $V_1 = 0.0240019E_r$ there are no avoided crossings with the first band, yet.

All data obtained for the system are shown in Figure 5.9. In the top left, the **potential** can be seen with 4 energy states and 4 Wannier **states**. For the first and second band, each, one Wannier and one energy state localized in the center and one localized close to the system edge is shown. The energy states in the center are again somewhat delocalized, just as the second band energy state close to the edge. The Wannier states are all localized.

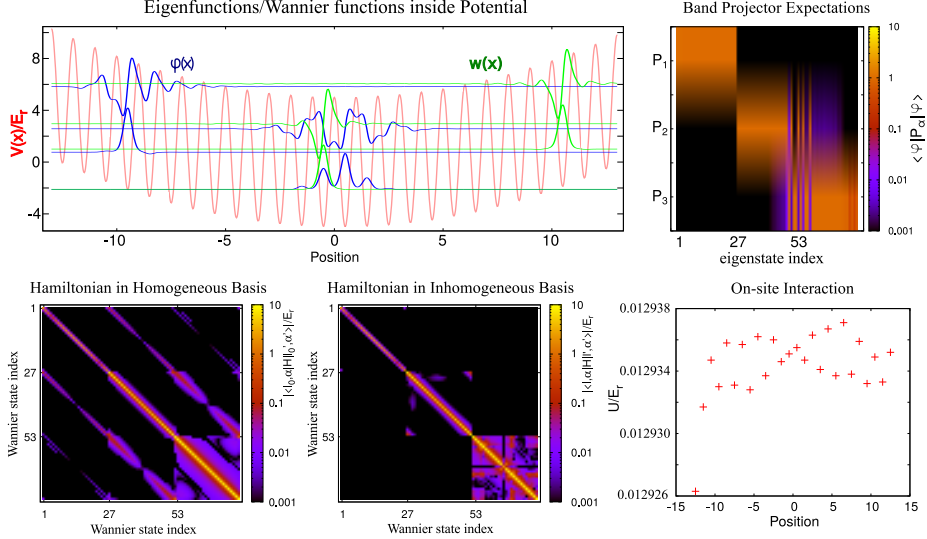


Figure 5.9: The analysis of the shallow trap with 26 sites. Clearly there are no avoided crossings in this system, as can be seen in the expectation values of the band projectors.

The plot on the right side shows that **band assigning** is not an issue in this system. As expected, there is no avoided crossing in the first band and even in the second band, states can be assigned to bands clearly.

The **Hubbard parameters** can be found in the second row. The off-diagonal terms are small for both bases. The homogeneous system Wannier basis still requires notable coupling elements between the first and the second band states in a Hubbard-like model. The generalized Wannier basis is the better choice for a Hubbard-like model. Even the second band can be described in this basis but more hopping terms have to be taken into account. To include a **second band on-site interaction**, new considerations would have to be made¹. The first band on-site interaction is shown in the lower right. Its site-dependency doesn't reflect the potential shape and is of very small order (10^{-5}).

The on-site energy, nearest neighbor and next-nearest neighbor hopping in the generalized Wannier basis are also shown as **graphs** in Figure 5.10. They all resemble the shape of the potential.

5.2.2 Strong Trap

¹The on-site interaction term used in the calculations was derived using the lowest band approximation and the s-wave scattering length.

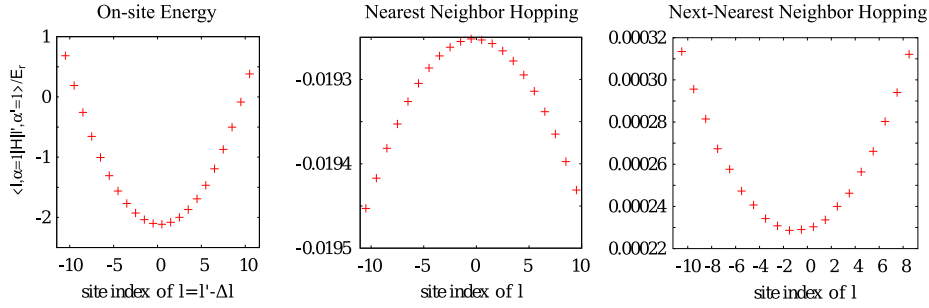


Figure 5.10: On-site energy, nearest neighbor hopping and next-nearest neighbor hopping for the shallow trap containing 26 sites. The shape of the harmonic trap is reflected in every plot.

The trap strength of the system with 26 sites is increased to a trap frequency of 100Hz. The results are shown in Figure 5.11. This causes the centered eigenstates to be more localized than in the previous system. Second band states are not shown because the band assignment no longer works reliably for the second band, see upper right plot. There are many **avoided crossings**.

system parameters	
sites	26
lattice depth	10E _r
trap strength	.0960075E _r = 100Hz
trap shift	.3 a

The Hamiltonian is remarkably close to being diagonal despite the high trap strength. Second band effects are visible in the left plot. The **generalized Wannier basis** should allow for an efficient first band description of the system with very few hopping terms. The site-dependency of the **on-site interaction** resembles the shape of the trapping potential. Over all sites, it changes on the order of 10^{-4} .

The on-site energy, nearest neighbor and next-nearest neighbor hopping in the generalized Wannier basis are also shown as graphs in Figure 5.12. They all resemble the shape of the potential.

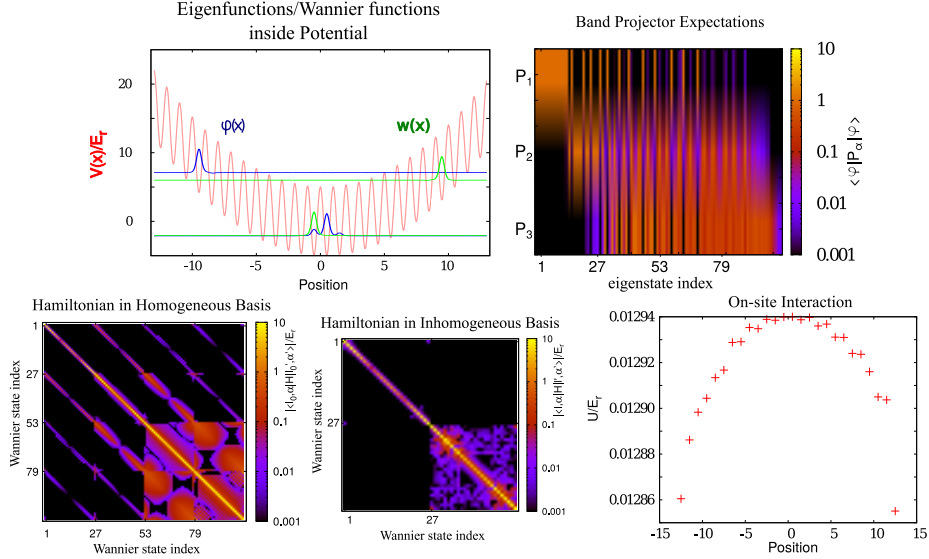


Figure 5.11: A system containing 26 sites and a strong trap. Even though there are many avoided crossings, the first band can clearly be chosen. The on-site interaction roughly resembles the shape of the trap. The left plot of the Hamiltonian in the homogeneous system Wannier basis shows four bands to inform of the off-block-diagonal elements. The middle plot of the Hamiltonian in the inhomogeneous Wannier basis is enlarged showing only two bands to allow for a better inspection of the off-diagonal hopping elements.

5.2.3 Large System

The last system to be analyzed consists of 100 sites. The eigenstates localized on the system edges are much higher in energy than the ones in the center due to the system size. Thus there are many **avoided crossings**. Given a low temperature, excitations into the states localized at the edge are unlikely. Again, the generalized Wannier functions allow for an **efficient single-band description**; on some sites including next-nearest neighbor hopping terms should improve accuracy. The **on-site interaction** reflects the shape of the potential with a site-dependency on the order of 10^{-4} . Two insufficiently assignable states interrupt this pattern.

system parameters	
sites	100
lattice depth	$10E_r$
trap strength	.03E_r
trap shift	.3a

The on-site energy, nearest neighbor and next-nearest neighbor hopping in the generalized Wannier basis is also shown as **graphs** in Figure 5.12. They roughly resemble the shape of the potential, but at the site of the two insufficiently assignable states the regularity is disturbed.

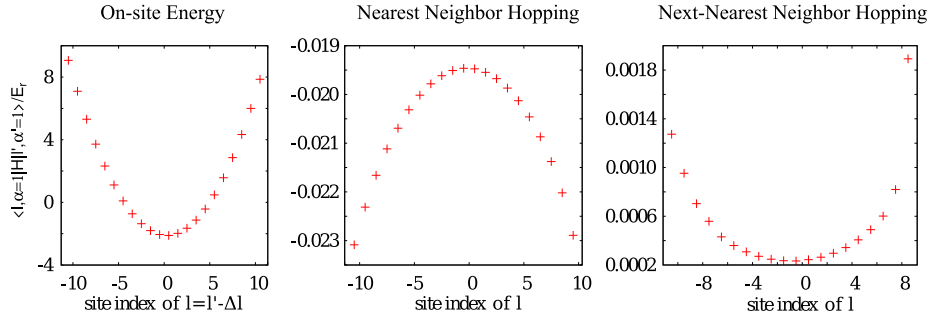


Figure 5.12: On-site energy, nearest neighbor hopping and next-nearest neighbor hopping for the strong trap containing 26 sites. Despite the avoided crossings the harmonic trap potential shape is reproduced.

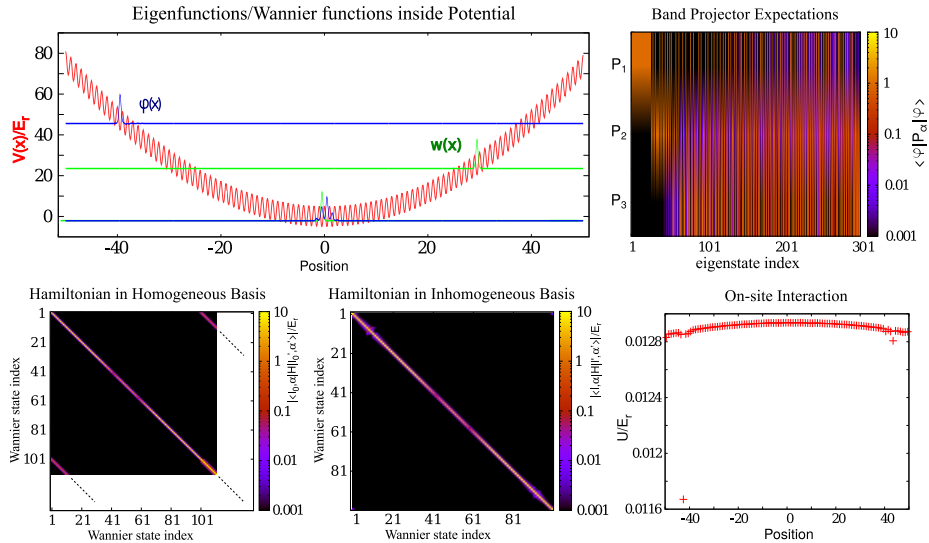


Figure 5.13: A system containing 100 sites and a strong trap. Two states could not be assigned to the first band clearly, which explains the irregularities at position -42 and +42.

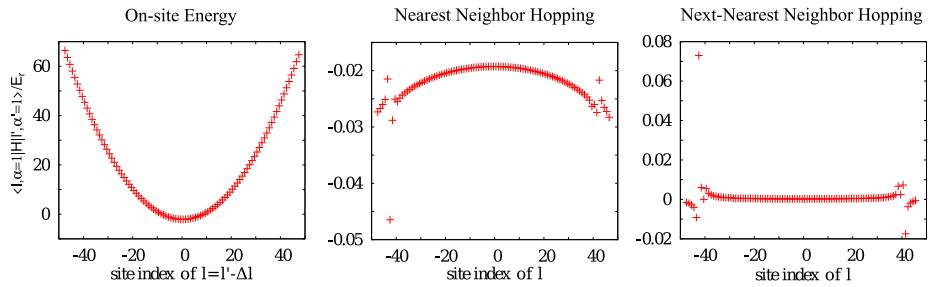


Figure 5.14: On-site energy, nearest neighbor hopping and next-nearest neighbor hopping for the large system containing 100 sites. The irregularities are due to avoided crossings. The shape of the potential is reproduced.

5.3 Conclusion

The code implemented for this thesis is able to predict properties of lattice systems under the influence of a harmonic trapping potential. The Hubbard parameters for the system in the homogeneous lattice Wannier basis and in the inhomogeneous lattice (generalized) Wannier basis can be calculated and the **feasibility** of different **tight binding**-like approximations can be evaluated. The site-dependencies in the Hubbard parameters due to the introduction of the inhomogeneity are reproduced. While the homogeneous Wannier basis often has to take off-block-diagonal terms into account, the generalized Wannier basis often allows for a single-band description.

Generalizing the description of the on-site interaction to include second band effects would pose a nice extension of this work.

Chapter 6

Results for a Lattice with Quasi-Disorder

A potential that can be easily implemented by today's optical lattice experiments is that of incommensurate lattices, see [GTVG97]. This is simply a superposition of two ordinary lattice potentials but with an irrational ratio of periodicities α and different amplitudes between them.

$$V(x) = \frac{V_0}{2} \cos(2k_L x) + \frac{V_1}{2} \cos(2\alpha k_L x)$$

These systems qualify as examples of quasi disorder. This is because the periodicity of the overall potential is on the order of the smallest common integer multiple of 1 and α . This can be arbitrarily large. True disorder in a lattice which can be generated in today's experiments using a speckle laser still have a slightly different behavior in which the disorder seems to be of a higher quality, i.e. more random.

The **calculation** is performed in accordance with the calculation for the harmonic trap system, i.e. first the eigenstates of one of the lattices are determined. Then the overall Hamiltonian is diagonalized in the Wannier basis of the primary lattice.

This **chapter** is split in two parts. In section 6.1 a general analysis for generalized Wannier functions in an incommensurate lattice system is performed. In section 6.2 the localization of the energy eigenstate is investigated. This section is closely connected to a paper written by Biddle et al. in [BWP⁺09]. The results found in that paper are to be reproduced and similarly to the paper different approximations are tested in a model benchmarking.

Throughout the text a **distinction** between the primary **Hubbard parameters** and the generalized Hubbard parameters will be made. The first refers to the complete system Hamiltonian and the on-site interaction in the Wannier basis obtained from the primary lattice while the second refers to the complete system Hamiltonian and the on-site interaction in the generalized Wannier basis that takes both lattices into account.

6.1 General Analysis for Incommensurate Lattices

In this section some general properties and results for incommensurate lattices will be discussed.

6.1.1 Energy Eigenvalues

For the complete system the Bloch theorem no longer holds, so no quasi momentum can be assigned and thus no dispersion relation can be calculated. But consideration of the energy eigenvalues is still worthwhile especially when taking the strength of the secondary lattice into account.

In Figure 6.1 the energy eigenvalues for the complete system are shown in dependence of the secondary lattice strength. The primary lattice strength is kept constant at $10E_r$. Similar to the result gained in the trap system, the bands start to broaden when the inhomogeneity is turned on. Eventually the band gaps close and the energy eigenstates cannot be assigned to primary lattice bands anymore. And, as in the case of the harmonic trap, crossings are avoided.

Going to high secondary lattice strength **new bands** seem to form. This seems logical because there the primary lattice strength can be regarded as small when compared to the secondary lattice strength and thus the secondary lattice determines the band structure. In the calculation 30 primary lattice sites have been used and the factor in the secondary lattice periodicity is $\frac{2}{\sqrt{5}-1}$. From this the amount of secondary lattice sites can be estimated to be around 18. In Figure 6.1 this value is confirmed even though the first band gap is not quite as clearly pronounced as the second one (it is between the red lines).

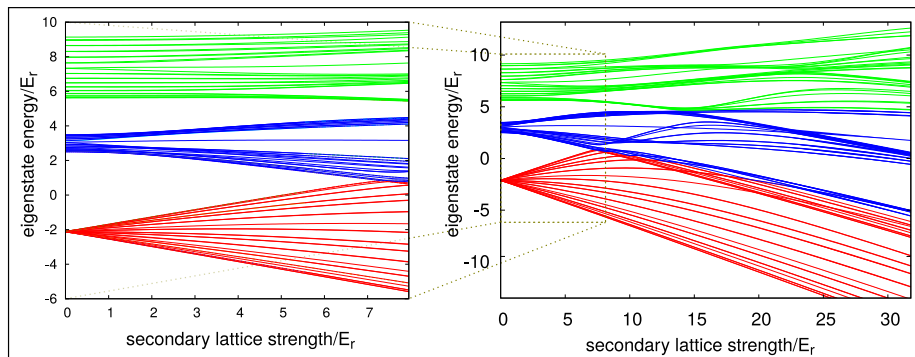


Figure 6.1: Energy eigenvalues for two incommensurate lattices in dependence on the secondary lattice strength. Initially, for low inhomogeneity strength, 3 bands with 30 states each are visible. For high inhomogeneity strength new bands form with 18 states each. The first secondary lattice band gap can be found among the red lines while the second band band gap is more pronounced.

From an experimental point of view, the observed behavior seems very promising. It should allow for the creation of **arbitrary energy values** in the eigenvalue spectrum and thus allow for things like switching absorption on and off or inducing emission. If the ratio of periodicity is not chosen to be a

completely irrational number, but instead for instance the number 2, this corresponds to a lattice with sites of alternating high and low on-site energies. As a result every band is split in two with a gap in between.

6.1.2 Energy and Wannier States

In order to give some insight into the general properties, a small system with just six sites has been analyzed. The results of this analysis can be found in Figure 6.2 where the potential $V(x)$, the generalized Wannier functions $w(x)$ and the eigenstates $\varphi(x)$ are shown for three different configurations. For all the configurations the primary lattice potential amplitude is set to $10E_r$. The secondary lattice potential is set to three different values $0E_r$, $1E_r$ and $6E_r$ each is shown in its own row.

The **on-site energy** for each of the Wannier states is visualized as the height of the base line of the state inside the potential. For example the Wannier states in the system configuration with the secondary lattice turned off in the first row all have the same on-site energy around $-2E_r$. When the secondary lattice is turned on, the states localized at different sites also have different on-site energies. The depth of the potential at a site clearly determines the on-site energy of the state that is localized there.

The amplitudes of the states are just schematically shown, i.e. no actual scale for their probability density is given. The **localization** of the energy eigenstates is strongly affected by the amplitude of the secondary lattice. If the secondary potential is turned off, all the states are spread out over the whole lattice which can be seen in the first row. When the secondary potential is turned on and the on-site energies for the different lattice sites start to differ, the eigenstates localize almost immediately. An intermediate case can be found in the second row where the secondary potential amplitude is set to $1E_r$. Two states on the far left are still localized around two sites at once where the on-site energy is almost identical.

Another nice visualization of the localization can be seen in Figure 6.3. Here the expectation value of the position operator is plotted as a function of the secondary lattice strength. The plot shows that just a very small inhomogeneity is enough for the states to center around a certain position but it doesn't show the localization. With low secondary lattice strength the behaviour is quite complex.

Another feature that can be observed in the plot is the **site-dependence** of the generalized Wannier functions particularly by looking at the lower plot with high secondary lattice strength. Unlike the Wannier states of a homogeneous lattice, these states have no translational symmetry but instead exhibit a slightly different shape depending on which site they are localized in. The Wannier state with the highest on-site energy seems to have a greater spread than, for example, the Wannier state with the lowest on-site energy.

In the case of a strong secondary lattice intensity the energy eigenstates become almost identical with the generalized Wannier states. This can also nicely be seen in the overlap matrix that is gained from the diagonalization of the band projected position operator x_α in the energy eigenbasis.

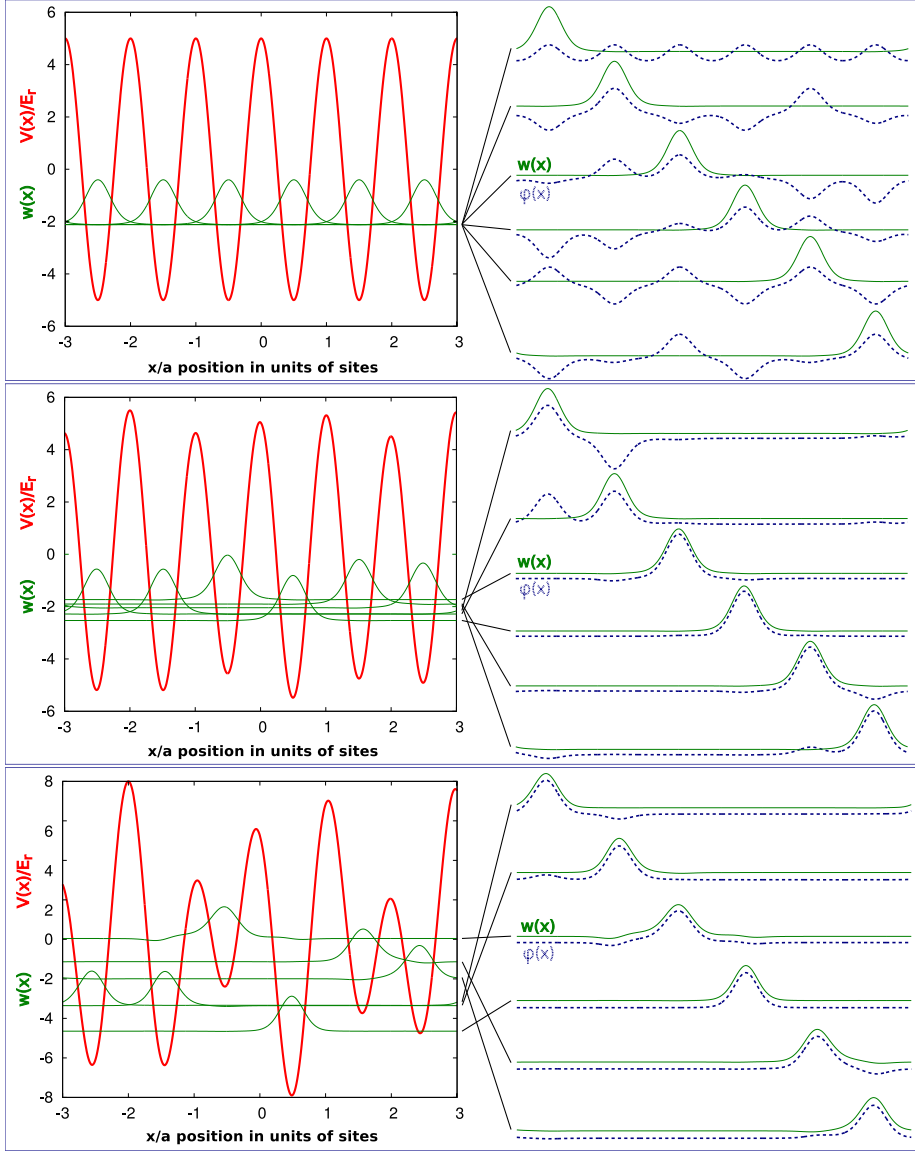


Figure 6.2: Overall potential $V(x)$, generalized Wannier functions $w(x)$ and energy eigenfunctions $\varphi(x)$ for $V_1 = 0E_r$ (top), $V_1 = 1E_r$ (middle) and $V_1 = 6E_r$ (bottom). The primary lattice potential amplitude is $V_0 = 10E_r$. The localization of the energy eigenstates can be observed. The on-site energies resemble the potential values at the corresponding sites.

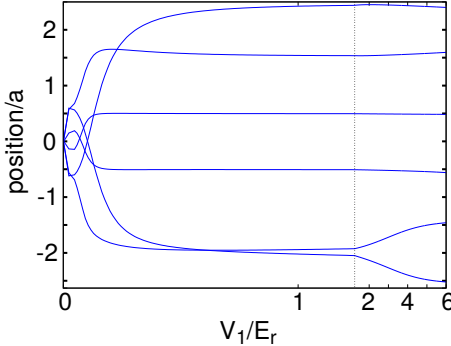


Figure 6.3: Position expectation value of energy eigenstates as a function of the secondary lattice strength. The first band states localize for very low secondary lattice strength.

6.1.3 On-site Energy, Hopping and On-site Interaction

Every localized **basis** may be suitable for a **Hubbard model** formulation. The characteristic Hubbard model parameters on-site energy, hopping and on-site interaction are dependent on this basis. When the Wannier basis of the primary lattice in the incommensurate lattice system is used to diagonalize the complete system Hamiltonian, the elements for a Hubbard model using the primary lattice Wannier basis are already known.

Using this primary lattice Wannier basis for the Hubbard model brings some unfavorable consequences because the complete system Hamiltonian is not block diagonal in it. This may mean that a single-band description is not suitable in this model because second band effects caused by the superposition with the secondary lattice are not taken into account.

This can be seen in Figure 6.4 where the complete system Hamiltonian is plotted in the primary lattice Wannier basis and in the generalized Wannier basis. In the primary lattice Wannier basis terms across bands are clearly not negligible. Even if only the first band behavior is of interest the higher bands have to be included in the diagonalization. This is different if the generalized Wannier basis is used in which the Hamiltonian is block diagonal as can be seen in the plots.

In the lower part of Figure 6.4 the on-site energy and hopping terms gained from the generalized Wannier basis are **related to** the complete system **potential**. For the on-site energy it is clear how it relates to the potential values at each site.

How is the hopping influenced by the potential? The potential values in between the sites seem to determine the nearest-neighbor hopping. This can be justified by looking at the mathematical expression of this matrix element: The overlap of two adjacent Wannier functions which ought to be located in between the two lattice sites is weighted with the potential. The next-nearest neighbor hopping is already very weak. At the very top the single n^6 hopping element can be seen. The non-negligible value of this element is an artifact caused by the use of the periodic Wannier basis, see section 2.7.

The **dependence** of the nearest neighbor hopping on the **site index** seems to be without any order as can be seen in a plot for a larger system with 30

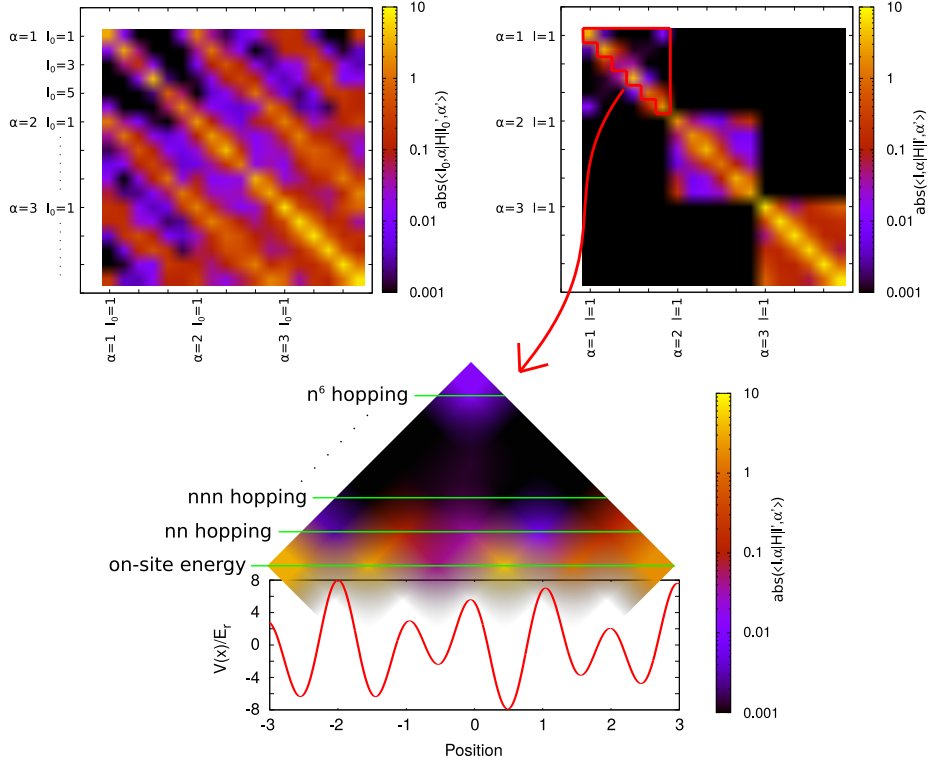


Figure 6.4: The complete system Hamiltonian in the primary lattice Wannier basis (top-left) and in the generalized Wannier basis (top-right). In the lower part the entries are related to the potential. It should be noted that the absolute values are plotted. That is the reason why the on-site energies may be falsely interpreted as being higher in a lower site. The on-site energies are all negative except for the one at the site on position -0.5 . The nearest-neighbor hoppings are all negative.

sites in Figure 6.5. Apparently the disorder in the potential manifests itself in the hopping as well. The same is true for the on-site interaction which is also shown. In order to still provide some qualitative statement some statistics have been done in the next section.

For the calculation of the on-site interaction the scattering length of ^{87}Rb atoms was used.

6.1.4 Statistics for Hubbard Model Parameters

Histograms for the Hubbard model parameters were calculated. To accomplish this a system with 30 sites was solved repetitively but with a random shift between the primary and secondary lattice potential each time. The values for the on-site energy, hopping and on-site interaction were sorted in the histograms for every program run.

Along with the histograms, the mean and standard deviation were calculated. Figure 6.6 shows some averaged values for the system Hamiltonian in the

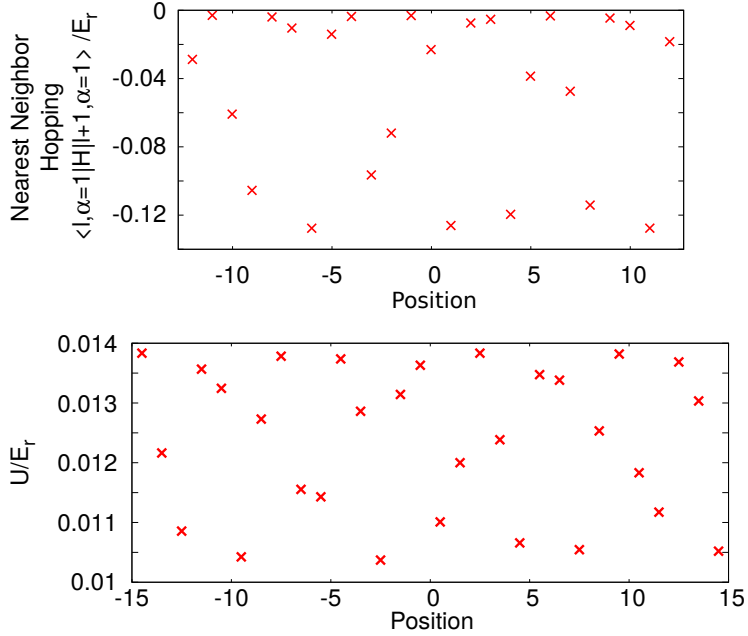


Figure 6.5: Nearest neighbor hopping and on-site interaction for the first band. The disorder of the potential manifests itself in the Hubbard parameters. No regularities in the site-dependency is observable.

primary lattice Wannier basis $\langle l_0, \alpha | \hat{H} | l'_0, \alpha' \rangle$.

On the left side the values for the on-site energy, nearest and next-nearest neighbor hopping are shown for systems with secondary lattice strength $V_1 = 1E_r$ and $V_1 = 6E_r$ in the first band ($\alpha = 1$).

It is most notable that the **mean** values of the model parameters are the same for the different secondary lattice strength, the secondary lattice doesn't seem to influence the mean. Also the values decrease exponentially with Δl . This is also the behavior expected from a single lattice where the terms have no site-dependence. Thus the conclusion is that the secondary lattice does not influence the mean value of the Hubbard model parameters.

This is of course different for the **standard deviation**. If the secondary lattice is present, the parameters will have a site-dependency. See Figure 6.4 as an example. The standard deviation for the small inhomogeneity ($V_1 = 1E_r$) is much lower than for the high inhomogeneity ($V_1 = 6E_r$) where it is of the same order as the mean itself.

On the right hand side of Figure 6.6 the matrix elements for **inter-band hopping** are plotted. Just like for the single lattice the mean value is zero. The standard deviation has a similar behavior to the intra-band hopping in that it increases with the inhomogeneity strength and it is smaller for elements with higher Δl .

From the above it should be clear that an **approximation** which relies only on the mean values of the Hubbard parameters and thus neglects their site-dependency should yield the results for the primary lattice. A tight binding approximation alone would neglect the inter-band hopping which might have

notable site-dependent contributions and the intra-band n^m -hopping ($m > 2$) which is only significant for low lattice amplitudes.

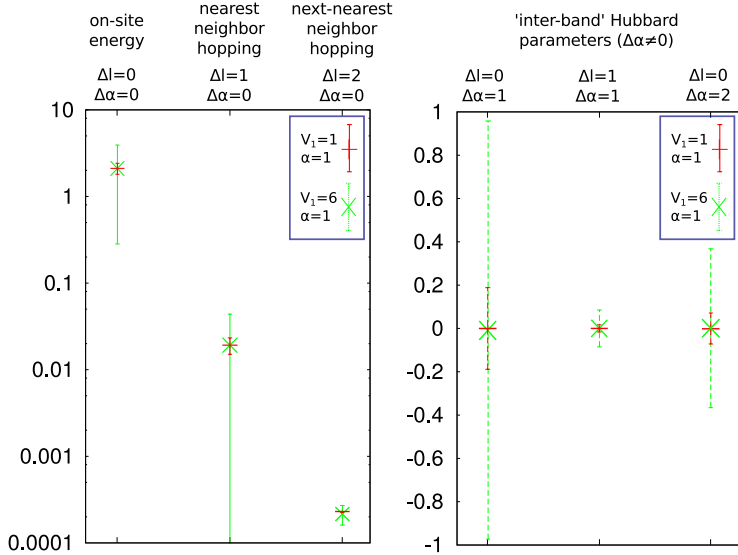


Figure 6.6: Mean and standard deviation of Hubbard parameters in the primary lattice Wannier basis for systems with different secondary lattice strengths (primary lattice strength $V_1 = 1E_r, 6E_r$). The variances reflect the site-dependency of the Hubbard parameters. The mean for the elements with $\Delta\alpha = 0$ vanishes just like in the homogeneous case, but the site-dependency causes a variance around this 0 mean.

The previous analysis has been repeated using the **generalized Wannier basis**. The results are shown in Figure 6.7. The display of the intra-band values was skipped because they are all zero. Instead, another dataset for the hopping in the second band is shown.

The fact that the **mean** values for the different secondary lattice strength in the first band do not coincide anymore is most striking. The higher secondary lattice strength causes the mean to be closer to zero. This is much more pronounced for higher Δl . For the Hubbard parameters in the second band the same exponential suppression with Δl as in the first band can be seen. Just as in the primary lattice Wannier basis a higher inhomogeneity causes a greater **standard deviation** relative to the mean.

In Figure 6.8 the histograms for the generalized Hubbard parameters, whose mean and standard deviation was shown in Figure 6.7, can be seen. Common to most of them is a half-pipe like **shape** (starting from the mean close to the middle going to the edge values become disproportionately high). This is similar to the frequency distribution of the range of a sine function. That seems logical because the depth of the lattice sites is expected to be distributed according to the shape of the secondary lattice which is a sine function.

As mentioned before, the spread in the histogram of the systems with higher secondary lattice strength is greater, especially when compared to the mean

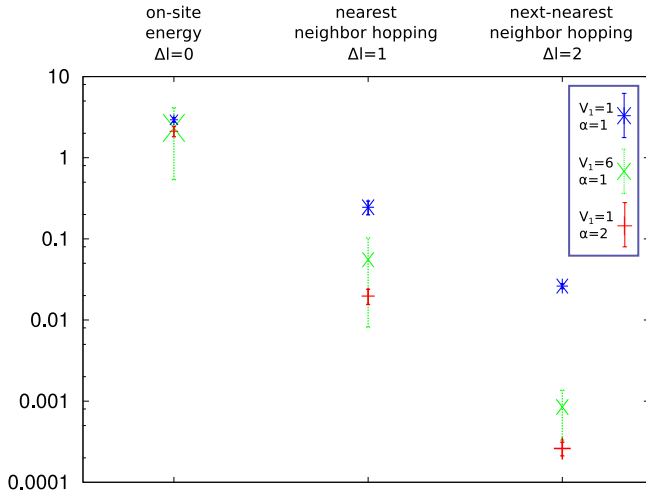


Figure 6.7: Mean and standard deviation of Hubbard parameters in generalized Wannier basis for systems with different secondary lattice strength (V_1) and bands (α). Higher inhomogeneities and bands have higher site-dependencies.

value. The means for different secondary lattice strength do not coincide.

For the next-nearest neighbor hopping, the shape is somewhat deformed. This is due to numerical **inaccuracies** which become a greater influence when the results become small relative to the input quantities. Furthermore most of the histograms have scattered entries outside the half-pipe region. This is due to inaccurate values coming from states that are located around the system's edge, where the periodic basis causes higher errors in the states.

In Figure 6.9 the mean, standard deviation and the entire histograms for the **on-site interaction** are plotted. For higher secondary lattice strength, the mean on-site interaction decreases while the standard deviation increases significantly. This could already be motivated in the display of the generalized Wannier functions in Figure 6.2 where the increase in the secondary lattice strength caused some Wannier functions to have higher variances and thus lower on-site interactions. This behavior is very site-dependent causing the standard deviation in the on-site interaction to be high.

The histograms have the same half-pipe like shape for the on-site interaction as was encountered for the on-site energy and hopping.

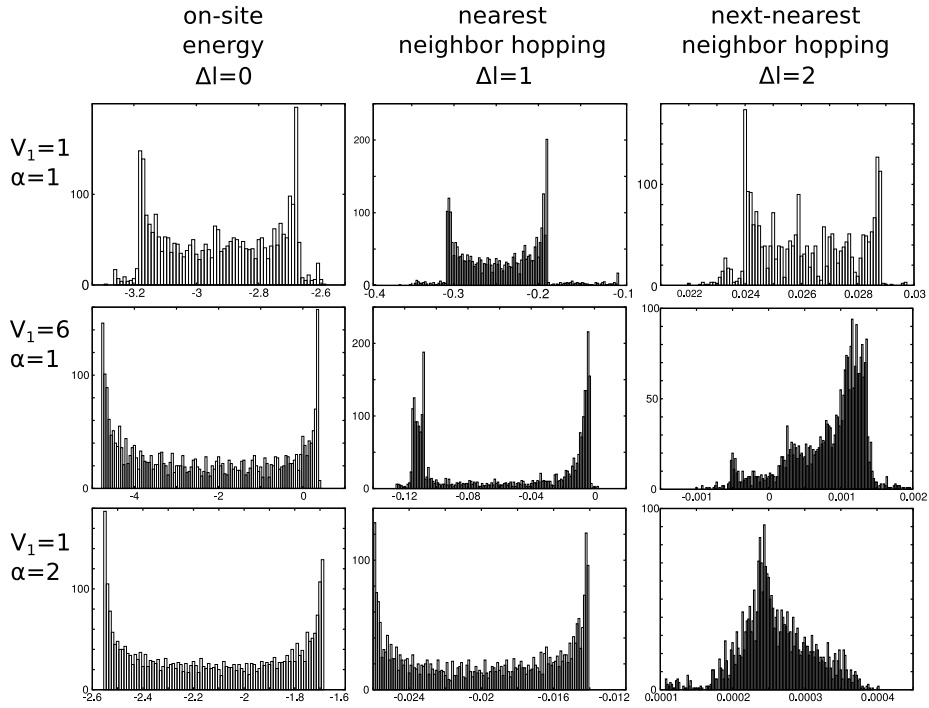


Figure 6.8: Histograms of on-site energy and hopping for systems with different secondary lattice strength (V_1) and bands (b)

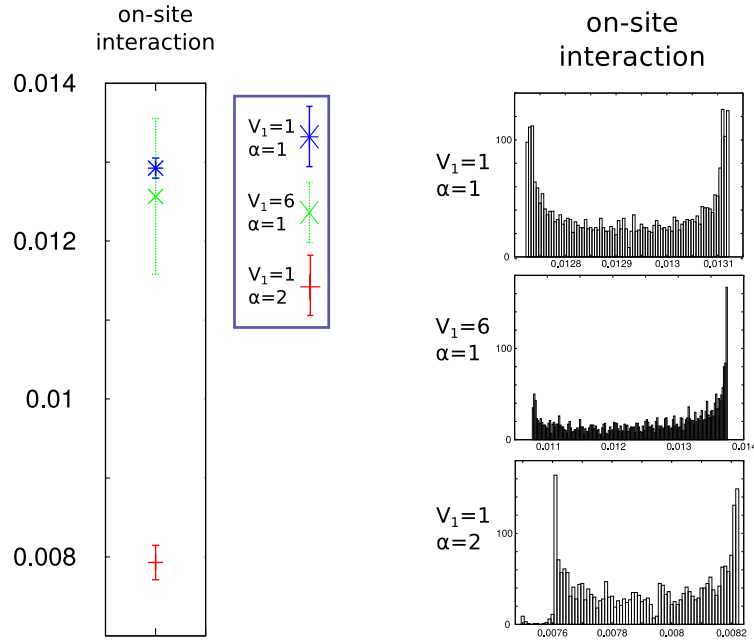


Figure 6.9: The mean values and histograms for the on-site interaction for systems with different secondary lattice strength (V_1) and bands (b)

6.2 Localization in Incommensurate Lattices

In [BWP⁺09] the transition from extended to localized states in incommensurate lattice systems has been investigated by Biddle et al. In this section of the thesis a very similar investigation is performed in which many of the **results** gained in the **paper** are to be **reproduced** utilizing the “inhomogeneous lattice”-code implemented for this thesis.

The paper can be split in **two parts**, each employing a separate technique to solve for the system’s eigenstates. Similarly, this section is split in two parts. In each, the method used will be explained and compared to the local implementation before the results will be presented and compared.

As discussed in the previous section the eigenstates start to localize when the secondary lattice in the incommensurate lattice system is turned on. In order to distinguish between extended and localized states a new measure the so-called *inverse participation ratio* short IPR is introduced for every eigenstate i

$$\text{IPR}^{(i)} = \frac{\sum_n |u_n^{(i)}|^4}{\left(\sum_n |u_n^{(i)}|^2\right)^2} \quad (6.1)$$

with $u_n^{(i)} = \langle l_n | \varphi_i \rangle$ being the overlap between a localized basis state and the energy eigenstates. Note that the denominator would be 1 if the localized basis states were normalized, would constitute a complete basis and the energy eigenstate would also be normalized. Then the numerator expression is maximal when an eigenstate is located only at one site (localized state) and minimal if the state is spread out over the entire lattice. This explains why the IPR is a good **measure for the localization**. The localized basis used in the calculation of the IPR is different in the two parts of the paper. Thus further details are given in the corresponding sections of this chapter.

6.2.1 Extended Aubry-André Model

In the first part of [BWP⁺09] the incommensurate lattice system is analyzed using an Aubry-André model which includes next-nearest neighbor hopping elements.

The Aubry-André model is a **Hubbard-like model** in that it relies on a localized basis. For the calculation of the on-site energy, this basis is taken to consist of Gaussian functions, each localized at a different lattice site. The diagonal elements of the Hamiltonian (on-site energies) are then calculated using the real space Hamiltonian and the real space Gaussian functions. The nearest neighbor hopping terms are adopted from the primary lattice and thus, **unlike** the **on-site energies, site-independent**. Further, off-diagonal hopping elements and higher band contributions are taken to be zero. **No interaction** term is taken into account. This completes the Aubry-André model.

Biddle et al. extended the Aubry-André model by also including **next-nearest neighbor hopping** elements. These elements are assigned the same site-independent value t_2 for every calculation. The results for several such calculations are shown on the left hand side of Figure 6.10. It shows the inverse participation ratio (IPR) of different first band eigenstates for different inhomogeneities (here V , see [BWP⁺09]) and next-nearest neighbor hopping (t_2). Here,

the **IPR** is calculated by first diagonalizing the Hamiltonian **obtained from the Hubbard parameters** and then taking the resulting overlap elements as the $u_n^{(i)}$ in (6.1).

For low values of t_2 a straight line the so-called **Aubry-André duality point** at $V \approx 2t_1$ can be made out that separates the extended from the localized states. In this regime the eigenstate number doesn't influence the value of the potential, at which the corresponding state starts to localize. This is different for high t_2 where the localization threshold in V depends on the eigenstate number (=eigenstate index). It jumps to higher values discontinuously at certain eigenstate numbers which causes a staircase like structure made up of several so-called mobility edges.

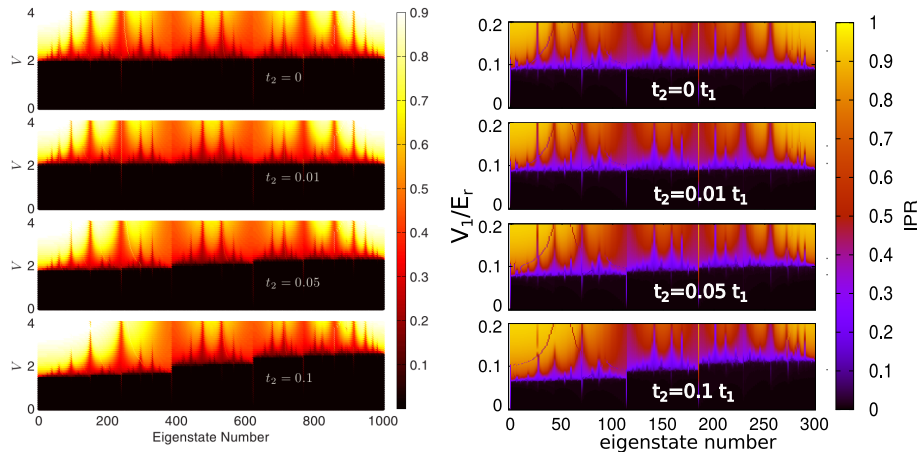


Figure 6.10: On the left side the original plot Fig. 1. from [BWP⁺09] is shown where only Hubbard parameters are used as a starting point for the calculation. On the right side the reproduced version using Wannier functions for the calculation of the site-dependent on-site energy and nearest neighbor hopping is shown. The values for t_2 and V are in units of t_1 in [BWP⁺09].

In order to qualitatively reproduce these results, a system of 300 sites and a primary lattice strength of $V_0 = 10E_r$ was used. Opposed to [BWP⁺09] where quantities closely related to the Hubbard-like model (V, t) are used as a starting point, here the quantities of the real space potential (V_0, V_1) are used which then yield the Hubbard parameters. This poses an **additional challenge** in reproducing the results as Biddle et al. were free to choose t_2 arbitrarily; for the reproduced case a potential would have to be found where t_2 attains the desired value.¹ This is circumvented by simply setting t_2 to the desired value later in the calculation after the Hubbard parameters have been calculated from the real space potential. The actual t_2 that results from solving the real space potential for given V_0, V_1 is very small and thus closely resembles the case plotted in the very top in Figure 6.10.

For the $u_n^{(i)}$ in the local calculation of the IPR, the overlap elements between the eigenstates and the primary lattice Wannier basis have been used which correspond to the elements Biddle et al. obtained by diagonalizing the Hamiltonian

¹In both cases it is questionable if the values still correspond to an incommensurate lattice.

constructed from the Hubbard parameters.

Further notes:

- Just like the calculation in the paper only a single-band description was used although the implementation was tested to work with at least 6 bands for 30 sites as well.
- Biddle et al. were able to simulate systems up to a size of 40,000 sites. This is impossible with the local implementation because the Hubbard parameters need to be calculated first which uses real space integration of the primary lattice Wannier states which are determined from the primary lattice energy eigenstates. For 40,000 sites this is far too memory and performance demanding. Here, another implementation using the direct diagonalization procedure discussed in section A.5 could be useful.
- The local implementation uses site-dependent nearest-neighbor hoppings which take the secondary lattice contribution into account. Biddle et al. instead use the site-independent primary lattice nearest neighbor hopping.
- This calculation doesn't take advantage of generalized Wannier functions.

6.2.2 Discretized Real Space Schrödinger Equation

In the second part of [BWP⁺⁰⁹] the real space Schrödinger equation is discretized and diagonalized. Although this approach is unfavorable in terms of numerical efficiency, it helps with some considerations. No tight binding approximation is made, which is helpful when choosing an appropriate ratio between t_1 and t_2 , and higher band effects in the primary lattice induced by the secondary lattice are taken into account. With this approach Biddle et al. show that **mobility edges** appear in real incommensurate lattice systems in cases where the primary lattice strength is small. To calculate the IPR Biddle et al. choose $u_n^{(i)}$ in (6.1) to be the overlaps between the energy and position eigenstates.

Along with the effort to reproduce the results gained in [BWP⁺⁰⁹], the following analysis is also testing the **effect of different approximations**. While Biddle et al. could skip the considerations mentioned in the previous paragraph the local implementation has to include them because it uses a Hubbard-like model in any case. In the following section, the approximations tested in the local implementation are explained. The influence of the approximations on the eigenstates at the Aubry-André duality point is investigated for 2 scenarios from [BWP⁺⁰⁹] (Fig. 3.(b) and Fig. 4(b) shown and explained later). For the latter and a third scenario (Fig. 5.) also the IPR will be calculated using the different approximations for the primary lattice and generalized Wannier basis. Finally, these results are shown next to and compared with the results obtained by Biddle et al.

Approximations

Until now, the calculations made with the implementation were exact in the sense that the full Hamiltonian was diagonalized in a complete basis. The only inaccuracies come from the finite precision numerics and from the higher band

cut-off in the Wannier basis. In a Hubbard model many more terms of the Hamiltonian in the localized basis are usually neglected.

In this section an investigation is performed to see how the approximations done in Hubbard-like models affect the resulting eigenstates and the inverse participation ratio. The tests are done for the primary lattice Wannier basis as well as the generalized Wannier basis. The states are calculated with four different levels of accuracy determined by the amount of Hamiltonian matrix elements taken into account. This is visualized in Figure 6.11.

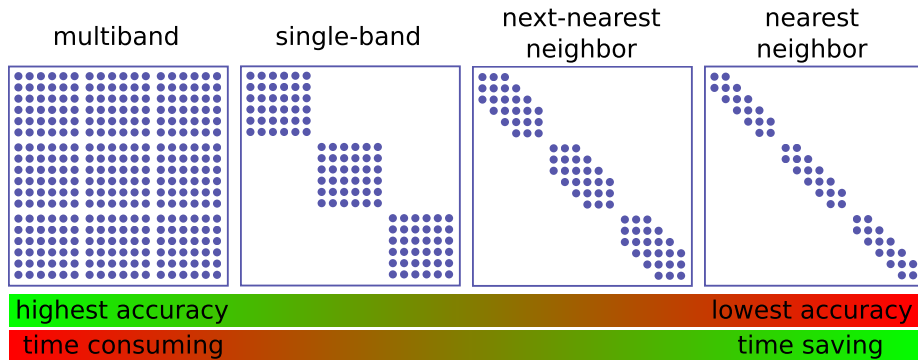


Figure 6.11: Schematic view of a Hamiltonian in a localized basis with 6 states per band and 3 bands. The dots represent elements that are to be calculated while the empty regions are taken to be zero.

Eigenstates at the Aubry-André Duality Point ([BWP⁺09] Fig. 3./4.)

For this analysis, the strength of the secondary lattice has been chosen such that the system is in the Aubry-André duality point which is at

$$V_1 = \frac{16}{\sqrt{\pi}} \exp \left(\sqrt{V_0/E_r} \left(\frac{\alpha^2}{V_0/E_r} - 2 \right) \right) (V_0/E_r)^{3/4} E_r$$

In accordance with [BWP⁺09] Fig. 3.(b) the primary lattice strength is chosen to be $V_0 = 30E_r$ and the incommensurate ratio $\alpha = \pi/2$. Thus the Aubry-André duality point is at $V_1 = 0.00317374E_r$

Figure 6.12 shows the matrix elements of the Hamiltonian when calculated in the primary lattice and generalized Wannier basis (only first two bands). Most notable is that the off-diagonals are tiny, so applying the **tight binding** approximation does not change the system solutions noticeably. This seems plausible when looking at the lattice potentials. The primary lattice is very strong which justifies the tight binding approximation. The secondary lattice is very weak thus second band effects are unlikely to be caused by it which is why generalized Wannier functions don't bring an advantage in this calculation.

In conclusion, for [BWP⁺09] Fig. 3. it is safe to use either basis and neglect next-nearest neighbor hopping and maybe even nearest neighbor hopping in the first band.

Next, the scenario in [BWP⁺09] Fig. 4. is investigated. The primary lattice strength is $V_0 = 2E_r$ and the incommensurate ratio $\alpha = (\sqrt{5} - 1)/2$.

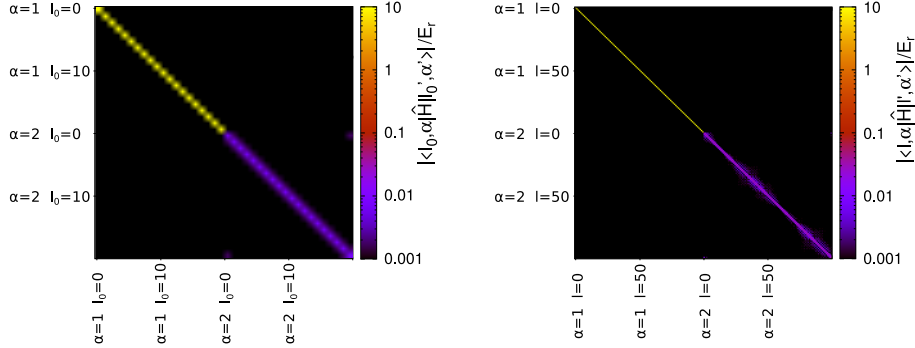


Figure 6.12: Hamiltonian in the primary lattice Wannier basis (left) and generalized Wannier basis (right) for a system with $V_0 = 30E_r$ and $V_1 = 0.00317374E_r$

The Aubry-André duality point is at $V_1 = 1.17556E_r$. In Figure 6.13 the corresponding matrix is shown. It is very notable that the **off-diagonal elements** are much **greater** in this case when compared to the scenario from [BWP⁺09] Fig. 3. This is plausible since the lattice strength is generally lower which interferes with the tight binding approximation. Also, now the two lattice potentials are of the same order which explains higher off-diagonal terms at least in the primary lattice basis. This poses the question of how many off-diagonal elements can be neglected.

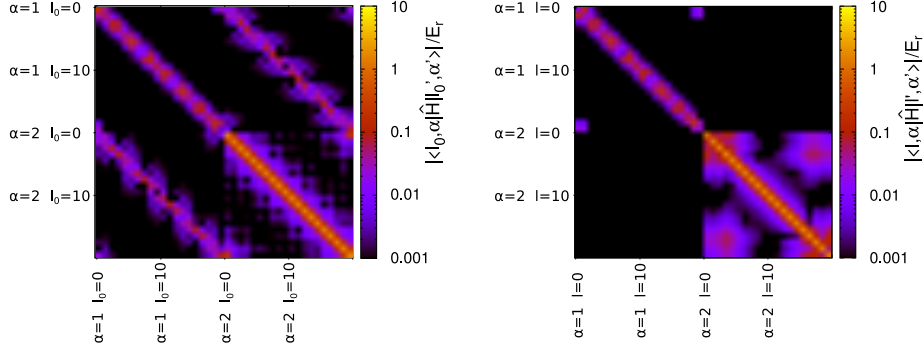


Figure 6.13: Hamiltonian in primary lattice Wannier basis (left) and generalized Wannier basis (right) for system with $V_0 = 2E_r$ and $V_1 = 1.17556E_r$

With the Hamiltonian matrix elements given in the primary lattice Wannier basis and the generalized Wannier basis, the **eigenstates** in both bases have been computed using differing amounts of matrix elements as shown in Figure 6.11. The resulting overlap between the Wannier states in both bases and the energy eigenstates can be seen in Figure 6.14.

As expected, there are differences in the overlap matrices due to the approximation made, but most of these differences are just in the weak elements. For the primary lattice Wannier basis from the 12th (0-indexed) eigenstates onwards there seems to be a slight **change in the ordering** of the localization. For the generalized Wannier basis the multi-band and single-band overlaps are exactly the same. This is expected because the Hamiltonian is block diagonal

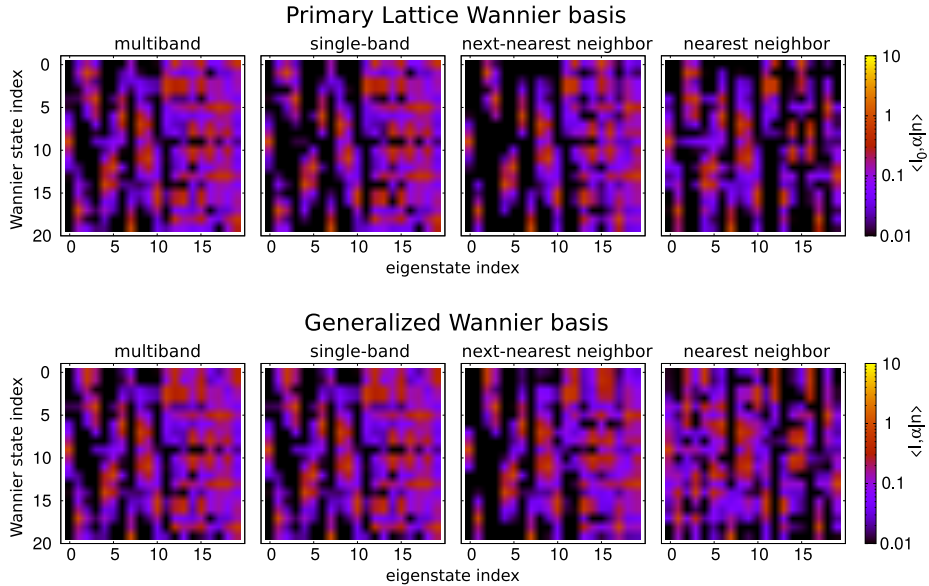


Figure 6.14: Overlap between primary lattice (top)/generalized (bottom) Wannier states and complete system energy eigenstates using different degrees of approximation

in the generalized Wannier basis. For the higher approximations the order of the states is changed which indicates changes in the eigenenergies.

Given the high magnitude of the secondary lattice in the scenario from [BWP⁺09] Fig. 4 it is also advisable to check if **avoided crossings** in the energy eigenvalues occur before calculating generalized Wannier states. This has been done for both of the previous scenarios. Despite the high inhomogeneity and low primary lattice strength there are no avoided crossings yet as shown in Figure 6.15. Therefore, generalized Wannier functions can safely be calculated without concern about band assigning.

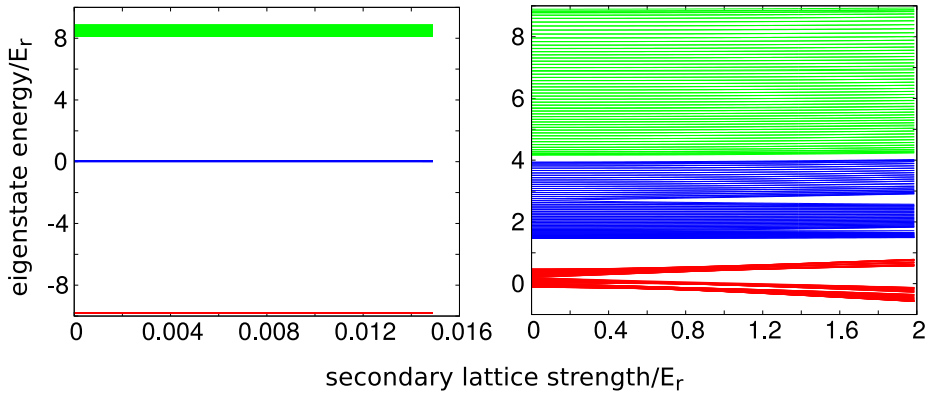


Figure 6.15: Energy eigenvalues for both given scenarios.

IPR in two Bases (see Fig. 4. in [BWP⁺09])

The IPR as shown in [BWP⁺09] Fig. 4. has been calculated using both Wannier bases and the different levels of accuracy discussed before. The results are shown in Figure 6.16 and Figure 6.18. Remarkably, a similar result like the one in Figure 6.10 is obtained. Given this real incommensurate lattice scenario neglecting next-nearest neighbor elements causes the **mobility edges** to disappear. By including all of the elements in the first band, more structure appears (eigenstates are sorted by energy). This is especially true in the high energy regions. This structure is confirmed by the original plot from Biddle et al. obtained in their real space analysis see Figure 6.17. Thus it can be hypothesized that in this non-tight-binding regime, taking elements beyond the next-nearest neighbor hoppings into account changes the result qualitatively i.e. more mobility edges appear.

The IPR diagrams obtained using the generalized energy basis look quite similar to the ones where the primary lattice Wannier basis was used. Very noticeable are the **horizontal lines** that appear when hopping elements are neglected. Closer investigations showed that these lines are formed by all elements at certain constant secondary lattice strengths for which the off-diagonal matrix elements in the Hamiltonian have notable contributions caused by approximate periodicity in the potential and thus insufficient incommensurability.

As expected, the plots for multi-band and single-band are the same and very similar to the multi-band plot for the primary lattice Wannier basis. Thus, using the **generalized Wannier basis** can provide advantages when a single-band description is desired. But for every approximation the amount of mobility edges seems to be the same as in the analysis with the primary lattice Wannier basis. Thus it can be concluded that the generalized Wannier basis doesn't give an advantage in predicting mobility edges in the present configuration.

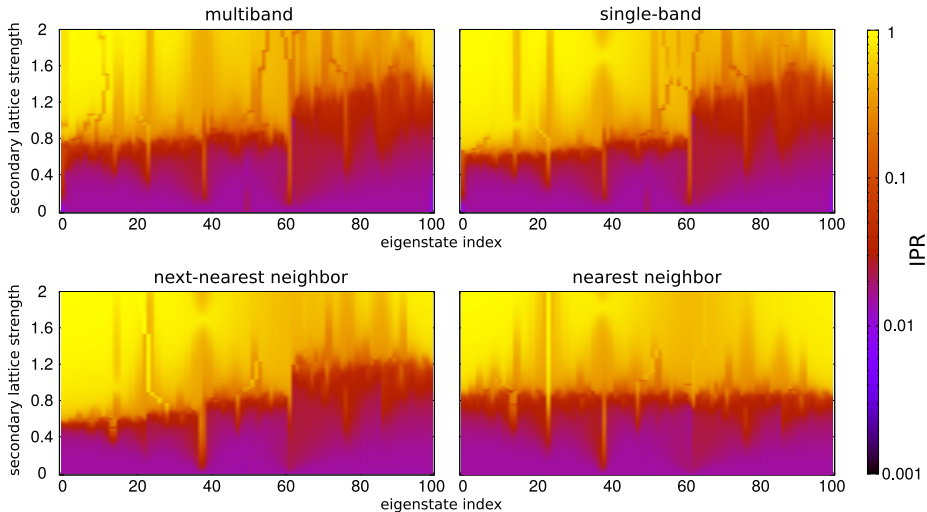


Figure 6.16: The inverse participation ratio for a system with primary lattice strength of $2E_r$ using the primary lattice Wannier basis with different levels of accuracy

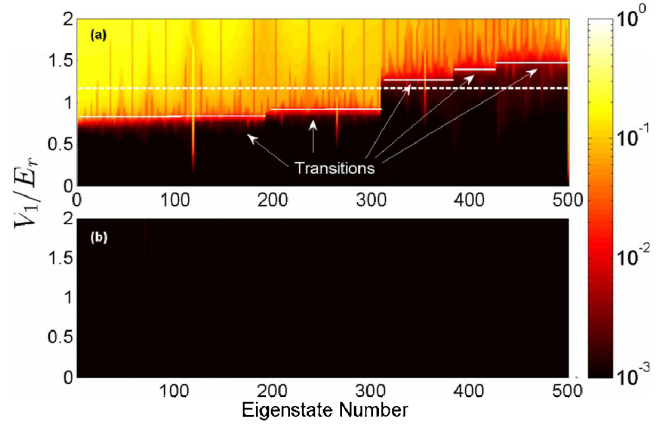


Figure 6.17: The inverse participation ratio for a system with primary lattice strength of $2E_r$ as obtained by Biddle et al. shown in [BWP⁺09] Fig. 4.

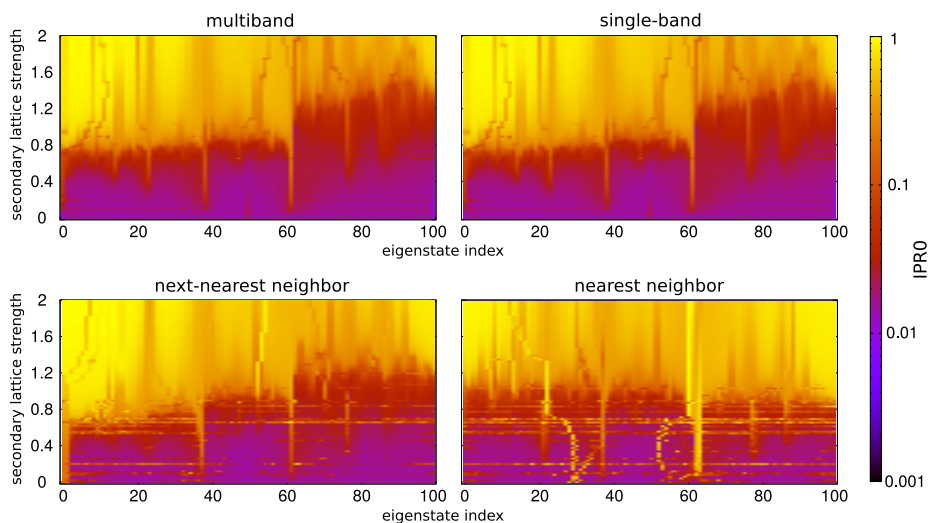


Figure 6.18: The inverse participation ratio for a system with primary lattice strength of $2E_r$ using the generalized Wannier basis with different levels of accuracy

Groundstate IPR for Different Potential Strengths and Periodicity Ratios

In Figure 6.19 which is taken from [BWP⁺09] Fig. 5. it is shown how the IPR behaves in dependence on the complete system potential amplitude ($V_0 = V_1$) and the periodicity ratio α . This plot was attempted to be reproduced using the primary lattice Wannier basis to ensure the absence of avoided crossings in the energy eigenvalues. The different kinds of approximations which were discussed previously, were applied. Unfortunately, the reproduced plots which are shown in Figure 6.19 differ considerably from the original plot by Biddle et al. Strangely, the plot with the **lowest accuracy matches** the plot by Biddle et al. most closely which can only be a coincidence as the real space analysis as done by Biddle et al. is expected to give the most accurate results.

Further notes:

- the analysis for [BWP⁺09] Fig. 5. has been calculated on the “LOEWE-CSC” supercomputer
- for the IPR the Wannier and the real space basis have been tested
- also a non-periodic basis was used in the hopes of producing a better match
- Biddle et al. don’t state what boundary conditions were used in their analysis

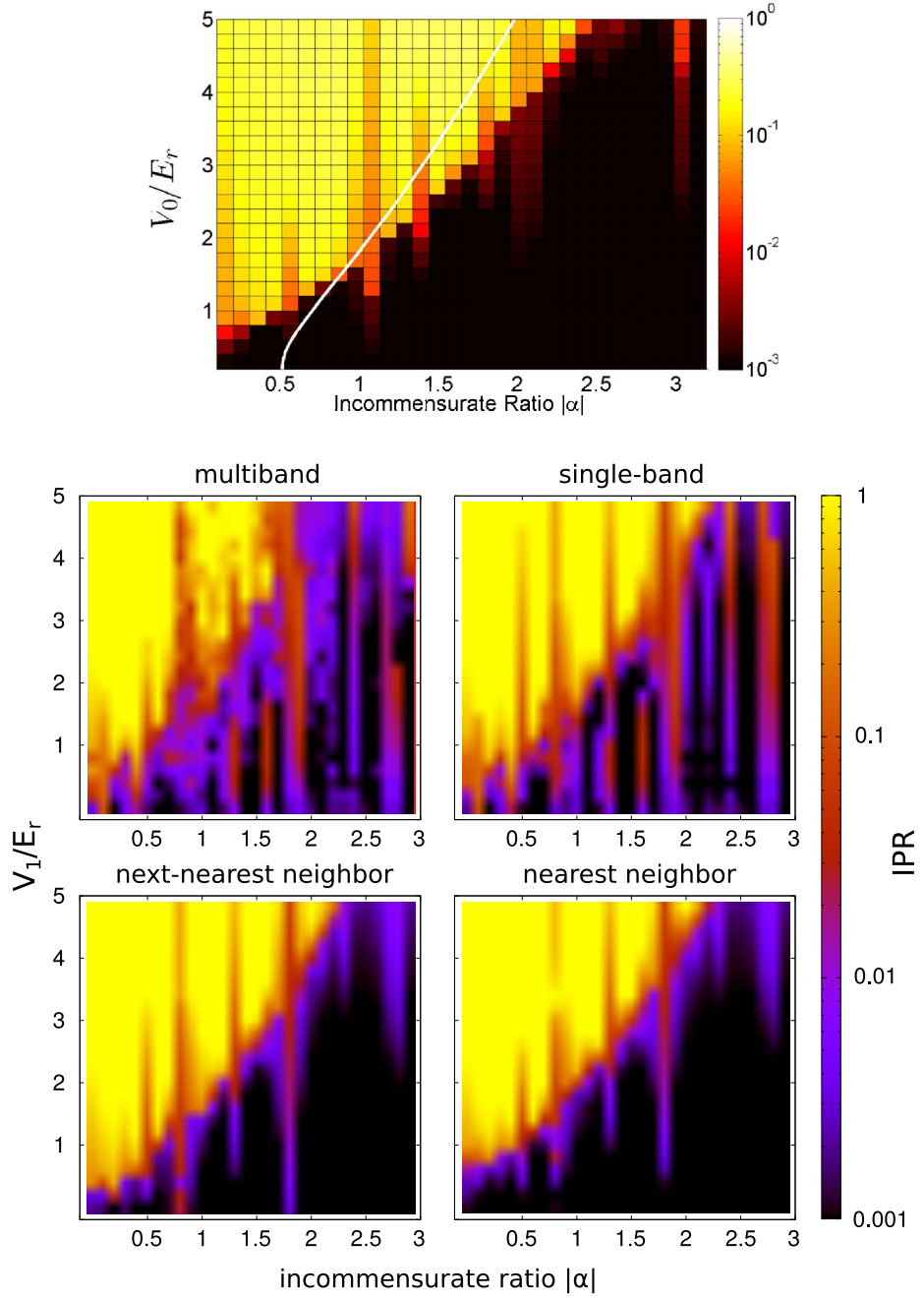


Figure 6.19: In the top single plot the IPR for the groundstate with different overall potential strengths ($V_0 = V_1$) and periodicity ratios as obtained by Biddle et al. in [BWP⁺09] Fig. 5. is shown. The bottom four plots show the reproduced scenario using different amounts of accuracy.

6.3 Conclusion

Incommensurate lattices represent systems that can be described well using Hubbard models. Even in regimes where a tight binding approximation is not suitable anymore (low primary lattice strength) valid results can be obtained. When optimizing a calculation it needs to be checked what elements of the Hamiltonian expressed in a localized basis can be neglected. If a single-band description is desired, the **generalized Wannier basis** can simplify calculations. In any case the matrix elements become site-dependent. For the prediction of **mobility edges**, the generalized Wannier basis does not offer advantages.

Results obtained by Biddle et al. could be reproduced with the generalized Wannier basis offering slight advantages over the primary lattice Wannier basis where a single-band description without tight binding approximation is desired.

Further notes:

- all comparisons with the data in the paper are merely done by subjective evaluation of the plots. The cases cannot be reconstructed exactly because not all the system parameters for the simulations done in the paper are known (e.g. latticeShift).

Chapter 7

Outlook

A **program** to calculate generalized Wannier functions and the corresponding Hubbard parameters for inhomogeneous lattice systems in one dimension has been developed. Three **model systems** have been investigated and documented in this thesis, two of which (Lattice in a Harmonic Trap, Quasi Disorder) are of relevance for current research in optical lattice systems.

It was shown that with **generalized Wannier functions** single-band descriptions can be applied to systems where common Wannier functions call for a multi-band treatment. In a Hubbard-like model, utilizing the generalized Wannier basis, calculations can therefore be simplified allowing for the treatment of even more complex systems.

Many **extensions** to the currently existing program are possible but couldn't be implemented due to time constraints. The most promising path to proceed with the implementation is, in the eyes of the author, a switch to the **exact diagonalization** procedure. Thereby, the path to treat **more** than single **dimension** problems is cleared. A promising application is the graphene system which demands a two dimensional description¹. A derivation of an **on-site interaction** relation covering **multiple bands** could offer insight for higher temperature regimes, in which higher band excitations are also possible.

The current implementation can also be used to further investigate **different systems**. Three interesting examples are a lattice system with **alternating on-site potential**, speckle disorder or the introduction of an impurity in a lattice.

For the first example, the quasi disorder code simply needs to be invoked with a periodicity ratio of two. For **speckle disorder**, which can be implemented in an experiment easily, randomness needs to be inserted into the potential. Last, in addition to each of the previously mentioned potentials a localized **impurity** can be used. This can be another particle in one site which causes a local interaction. This fixed particle can be described to be in a Wannier state. The potential caused by this particle is then given by the spatial density of the fixed particle times a prefactor which causes the interaction to be either attractive or repulsive.

Further experimenting with the **band assignment** seems promising. The procedure explained in section A.5.1 would be a possible starting point.

¹Such an analysis has already been performed in [UJM⁺13]. More system are given in [WS13]

Finally, this implementation can be used to provide **Hubbard parameters for other calculations** based on Hubbard models, from which multi-particle stationary states involving **interactions** can be obtained. **Dynamics** can also be studied. For instance, in [DZS⁺03] a dynamical Gutzwiller approach is used to investigate the transition to special system phases with unique properties.

Appendix A

Derivations and non-implemented material

A.1 Conversion of Effective Schrödinger Equation to Real-Valued First Order DGL

The equation $\left(V_{lat} + \frac{-\hbar^2}{2m}(ik + \frac{\partial}{\partial x})^2\right) u_{k,\beta}(x) = E_{k,\beta} u_{k,\beta}(x)$ is to be converted into a system of real first order differential equations

$$\begin{aligned}
& \left(V_{lat} + \frac{-\hbar^2}{2m} \underbrace{(ik + \frac{\partial}{\partial x})^2}_{(-k^2 + 2ik\frac{\partial}{\partial x} + \frac{\partial^2}{\partial x^2})} \right) \underbrace{u_{k,\beta}(x)}_{\Re(u_{k,\beta}(x)) + i\Im(u_{k,\beta}(x))} = E_{k,\beta} u_{k,\beta}(x) \\
& \left(V_{lat} + \frac{-\hbar^2}{2m} (-k^2 + 2ik\frac{\partial}{\partial x} + \frac{\partial^2}{\partial x^2}) \right) (\Re(u_{k,\beta}(x)) + i\Im(u_{k,\beta}(x))) \\
& \quad = E_{k,\beta} \Re(u_{k,\beta}(x)) + iE_{k,\beta} \Im(u_{k,\beta}(x)) \\
& \left(V_{lat} + \frac{\hbar^2 k^2}{2m} - \frac{ik\hbar^2}{m} \frac{\partial}{\partial x} - \frac{\hbar^2}{2m} \frac{\partial^2}{\partial x^2} \right) (\Re(u_{k,\beta}(x)) + i\Im(u_{k,\beta}(x))) \\
& \quad = E_{k,\beta} \Re(u_{k,\beta}(x)) + iE_{k,\beta} \Im(u_{k,\beta}(x)) \\
& \left(V_{lat} + \frac{\hbar^2 k^2}{2m} - \frac{\hbar^2}{2m} \frac{\partial^2}{\partial x^2} \right) \Re(u_{k,\beta}(x)) - \frac{ik\hbar^2}{m} \frac{\partial}{\partial x} i\Im(u_{k,\beta}(x)) + \\
& \quad + \left(V_{lat} + \frac{\hbar^2 k^2}{2m} - \frac{\hbar^2}{2m} \frac{\partial^2}{\partial x^2} \right) i\Im(u_{k,\beta}(x)) - \frac{ik\hbar^2}{m} \frac{\partial}{\partial x} \Re(u_{k,\beta}(x)) \\
& \quad = E_{k,\beta} \Re(u_{k,\beta}(x)) + iE_{k,\beta} \Im(u_{k,\beta}(x)) \\
& \left(V_{lat} + \frac{\hbar^2 k^2}{2m} - \frac{\hbar^2}{2m} \frac{\partial^2}{\partial x^2} \right) \Re(u_{k,\beta}(x)) + \frac{kh^2}{m} \frac{\partial}{\partial x} \Im(u_{k,\beta}(x)) + \\
& \quad + i \left[\left(V_{lat} + \frac{\hbar^2 k^2}{2m} - \frac{\hbar^2}{2m} \frac{\partial^2}{\partial x^2} \right) \Im(u_{k,\beta}(x)) - \frac{kh^2}{m} \frac{\partial}{\partial x} \Re(u_{k,\beta}(x)) \right] \\
& \quad = E_{k,\beta} \Re(u_{k,\beta}(x)) + iE_{k,\beta} \Im(u_{k,\beta}(x))
\end{aligned}$$

$$\begin{aligned}
\left(V_{lat} + \frac{\hbar^2 k^2}{2m} - \frac{\hbar^2}{2m} \frac{\partial^2}{\partial x^2} \right) \Re(u_{k,\beta}(x)) + \frac{k\hbar^2}{m} \frac{\partial}{\partial x} \Im(u_{k,\beta}(x)) &= E_{k,\beta} \Re(u_{k,\beta}(x)) \\
\left(V_{lat} + \frac{\hbar^2 k^2}{2m} - \frac{\hbar^2}{2m} \frac{\partial^2}{\partial x^2} \right) \Im(u_{k,\beta}(x)) - \frac{k\hbar^2}{m} \frac{\partial}{\partial x} \Re(u_{k,\beta}(x)) &= E_{k,\beta} \Im(u_{k,\beta}(x)) \\
\left(-\frac{2m}{\hbar^2} V_{lat} - k^2 + \frac{\partial^2}{\partial x^2} \right) \Re(u_{k,\beta}(x)) - 2k \frac{\partial}{\partial x} \Im(u_{k,\beta}(x)) &= -\frac{2m}{\hbar^2} E_{k,\beta} \Re(u_{k,\beta}(x)) \\
\left(-\frac{2m}{\hbar^2} V_{lat} - k^2 + \frac{\partial^2}{\partial x^2} \right) \Im(u_{k,\beta}(x)) + 2k \frac{\partial}{\partial x} \Re(u_{k,\beta}(x)) &= -\frac{2m}{\hbar^2} E_{k,\beta} \Im(u_{k,\beta}(x)) \\
\frac{\partial^2}{\partial x^2} \Re(u_{k,\beta}(x)) &= \left[\frac{2m}{\hbar^2} (V_{lat} - E_{k,\beta}) + k^2 \right] \Re(u_{k,\beta}(x)) + 2k \frac{\partial}{\partial x} \Im(u_{k,\beta}(x)) \\
\frac{\partial^2}{\partial x^2} \Im(u_{k,\beta}(x)) &= \left[\frac{2m}{\hbar^2} (V_{lat} - E_{k,\beta}) + k^2 \right] \Im(u_{k,\beta}(x)) - 2k \frac{\partial}{\partial x} \Re(u_{k,\beta}(x))
\end{aligned}$$

$$\begin{aligned}
A'_0 &= A_1 \\
A'_1 &= \left[\frac{2m}{\hbar^2} (V_{lat} - E_{k,\beta}) + k^2 \right] A_0 + 2k A_3 \\
A'_2 &= A_3 \\
A'_3 &= \left[\frac{2m}{\hbar^2} (V_{lat} - E_{k,\beta}) + k^2 \right] A_2 - 2k A_1
\end{aligned}$$

with

$$A_0 = \Re(u_{k,\beta}(x)) \quad A_2 = \Im(u_{k,\beta}(x))$$

A.2 Infinite System Band Projection Operator

The goal is to find a computable expression for the infinite integral $\int_x x \varphi_k^*(x) \varphi_{k'}(x) dx$

$$\begin{aligned} \int_x x \varphi_k^*(x) \varphi_{k'}(x) dx &= \int_x x \underbrace{e^{-ikx} u_k^*(x) e^{ik'x} u_{k'}(x)}_{e^{i(k'-k)x} u_k^*(x) u_{k'}(x)} dx \\ &= \sum_{n \in \mathbb{Z}} \int_{x=0}^l (x + nl) e^{i(k'-k)(x+nl)} u_k^*(x+nl) u_{k'}(x+nl) dx \end{aligned}$$

with $l = \frac{2\pi}{\Delta k}$ and $\Delta k = \frac{2\pi}{a}$ sites

$u_k(x)$ has periodicity a

$e^{i(k'-k)(x+nl)} = e^{i(k'-k)(x+n \frac{2\pi}{\Delta k})}$ is the same for all n

$$\begin{aligned} \int_x x \varphi_k^*(x) \varphi_{k'}(x) dx &= \sum_{n \in \mathbb{Z}} \int_{x=0}^l (x + nl) e^{i(k'-k)x} u_k^*(x) u_{k'}(x) dx \\ &= \sum_{n \in \mathbb{Z}} \int_{x=0}^l x e^{i(k'-k)x} u_k^*(x) u_{k'}(x) dx + \\ &\quad \sum_{n \in \mathbb{Z}} \int_{x=0}^l (nl) \underbrace{e^{i(k'-k)x} u_k^*(x) u_{k'}(x)}_{\varphi_k^*(x) \varphi_{k'}(x)} dx \end{aligned}$$

$\varphi_k^*(x)$ is orthogonal to $\varphi_{k'}(x)$ if $k \neq k'$

$$\begin{aligned} \int_x x \varphi_k^*(x) \varphi_{k'}(x) dx &= \left(\sum_{n \in \mathbb{Z}} 1 \right) \left(\int_{x=0}^l x e^{i(k'-k)x} u_k^*(x) u_{k'}(x) dx \right) + \\ &\quad \underbrace{\delta_{k,k'} \left(\sum_{n \in \mathbb{Z}} nl \right) \left(\int_{x=0}^l \varphi_k^*(x) \varphi_k(x) dx \right)}_{=0} \\ \int_x x \varphi_k^*(x) \varphi_{k'}(x) dx &= \infty \int_{x=0}^l x e^{i(k'-k)x} u_k^*(x) u_{k'}(x) dx \end{aligned}$$

A.2.1 Accelerated Calculation

The expression $\int_{x=0}^l x e^{i(k'-k)x} u_k^*(x) u_{k'}(x) dx$ is to be optimized for numerical evaluation

$$\begin{aligned}
& \int_{x=0}^l x e^{i(k'-k)x} u_k^*(x) u_{k'}(x) dx \\
&= \sum_{n=0}^{\text{kSteps}-1} \int_{x=0}^a (x + a * n) e^{i(k'-k)(x+a*n)} u_k^*(x + a * n) u_{k'}(x + a * n) dx \\
&\quad u_k(x) \text{ has periodicity } a \\
&= \sum_{n=0}^{\text{kSteps}-1} \int_{x=0}^a (x + a * n) e^{i(k'-k)(x)} e^{i(k'-k)a*n} u_k^*(x) u_{k'}(x) dx \\
&= \sum_{n=0}^{\text{kSteps}-1} e^{i(k'-k)a*n} \int_{x=0}^a (x + a * n) e^{i(k'-k)(x)} u_k^*(x) u_{k'}(x) dx \\
&= \sum_{n=0}^{\text{kSteps}-1} e^{i(k'-k)a*n} \int_{x=0}^a x e^{i(k'-k)(x)} u_k^*(x) u_{k'}(x) dx \\
&\quad + \sum_{n=0}^{\text{kSteps}-1} (a * n) e^{i(k'-k)a*n} \underbrace{\int_{x=0}^a e^{i(k'-k)(x)} u_k^*(x) u_{k'}(x) dx}_{\delta_{k,k'} \int_{x=0}^a |u_k^2(x)| dx} \\
&= \left(\sum_{n=0}^{\text{kSteps}-1} e^{i(k'-k)a*n} \right) \left(\int_{x=0}^a x e^{i(k'-k)(x)} u_k^*(x) u_{k'}(x) dx \right) \\
&\quad + \underbrace{\left(\sum_{n=0}^{\text{kSteps}-1} a * n \right)}_{a * \frac{1}{2} * \text{kSteps} * (\text{kSteps} - 1)} \left(\delta_{k,k'} \int_{x=0}^a |u_k^2(x)| dx \right)
\end{aligned}$$

Thus

$$\begin{aligned}
\int_{x=0}^l x e^{i(k'-k)x} u_k^*(x) u_{k'}(x) dx &= \left(\sum_{n=0}^{\text{kSteps}-1} e^{i(k'-k)a*n} \right) \left(\int_{x=0}^a x e^{i(k'-k)(x)} u_k^*(x) u_{k'}(x) dx \right) \\
&\quad + \delta_{k,k'} * a * \frac{1}{2} * \text{kSteps} * (\text{kSteps} - 1) * \int_{x=0}^a |u_k^2(x)| dx
\end{aligned}$$

A.3 Calculation of State Position

A.3.1 Expectation Value of \hat{x}

$$\begin{aligned}
X(E) &= \langle E | \hat{x} | E \rangle \\
&= \int_x \langle E | x \rangle x \langle x | E \rangle dx \\
&= \int_x \sum_{l,\alpha} \sum_{l',\alpha'} \langle E | l, \alpha \rangle \langle l, \alpha | x \rangle x \langle x | l', \alpha' \rangle \langle l', \alpha' | E \rangle dx \\
&= \sum_{l,\alpha} \sum_{l',\alpha'} \langle E | l, \alpha \rangle \int_x \langle l, \alpha | x \rangle x \langle x | l', \alpha' \rangle dx \langle l', \alpha' | E \rangle \\
&= \vec{E}_{l,\alpha}^\dagger \cdot \hat{X}_{(l,\alpha),(l',\alpha')} \cdot \vec{E}_{l',\alpha'}
\end{aligned}$$

$\vec{E}_{l,\alpha}$ is a side product of the eigenvalue procedure.
 $\hat{X}_{(l,\alpha),(l',\alpha')}$ can be calculated once and then be reused for every trap strength.

A.3.2 Expectation Value of $\sum_\alpha \hat{x}_\alpha$

$$\begin{aligned}
X_\alpha(E) &= \langle E | \sum_\alpha \hat{x}_\alpha | E \rangle \\
&= \sum_{l,\alpha} \langle E | l, \alpha \rangle l a \langle l, \alpha | E \rangle
\end{aligned}$$

A.3.3 Relation between the Expectation Values of \hat{x} and $\sum_\alpha \hat{x}_\alpha$

beware $\sum_\alpha \hat{x}_\alpha \neq \hat{x}$

$$\begin{aligned}
X(E) &= \langle E | \hat{x} | E \rangle \\
&= \sum_{l,\alpha} \sum_{l',\alpha'} \langle E | l, \alpha \rangle \langle l, \alpha | \hat{x} | l', \alpha' \rangle \langle l', \alpha' | E \rangle \\
&= \langle E | \left(\sum_{l,l',\alpha} |l, \alpha\rangle \langle l, \alpha | \hat{x} | l', \alpha' \rangle \langle l', \alpha' | + \right. \\
&\quad \left. + \sum_{l,l',\alpha \neq \alpha'} |l, \alpha\rangle \langle l, \alpha | \hat{x} | l', \alpha' \rangle \langle l', \alpha' | \right) | E \rangle \\
&= \langle E | \left(\sum_\alpha \hat{x}_\alpha + \sum_{l,l',\alpha \neq \alpha'} |l, \alpha\rangle \langle l, \alpha | \hat{x} | l', \alpha' \rangle \langle l', \alpha' | \right) | E \rangle \\
&= X_\alpha(E) + \sum_{l,l',\alpha \neq \alpha'} \langle E | l, \alpha \rangle \langle l, \alpha | \hat{x} | l', \alpha' \rangle \langle l', \alpha' | E \rangle
\end{aligned}$$

A.4 Fast Calculation of the Localization

The localization of inhomogeneous eigenstates is to be computed for different inhomogeneous potential strength. Assuming the most straight forward approach of real space integration, for 100 different strength values, 30 eigenstates and 6 bands 18000 integrals would have to be evaluated.

The localization of the inhomogeneous eigenstates can be calculated more efficiently if $\langle l_0, \alpha | \hat{x} | l_0 + \Delta l, \alpha' \rangle$ is known:

$$\langle n | \hat{x} | n \rangle = \sum_{l_0, l'_0} \sum_{\alpha, \alpha'} \langle n | l_0, \alpha \rangle \langle l_0, \alpha | \hat{x} | l'_0, \alpha' \rangle \langle l'_0, \alpha' | n \rangle$$

Here only on the order of eigenstates² bands² summations have to be calculated but also $\langle l_0 | \hat{x} | l_0 + \Delta l \rangle$ has to be pre-calculated which can be sped up using the following method (band indices have been dropped):

$$\begin{aligned} \langle l_0 | \hat{x} | l_0 + \Delta l \rangle &= \int w_{l_0}^*(x) w_{l_0 + \Delta l}(x) x dx \\ &= \int w_{l_0, \Delta l}^{(prod)}(x) x dx \\ &= \int w_{0, \Delta l}^{(prod)}(x - l_0) x dx \\ &= \int w_{0, \Delta l}^{(prod)}(\bar{x}) (\bar{x} + l_0) d\bar{x} \\ &= \int w_{0, \Delta l}^{(prod)}(\bar{x}) \bar{x} d\bar{x} + l_0 \int w_{0, \Delta l}^{(prod)}(\bar{x}) d\bar{x} \\ &= \int w_{0, \Delta l}^{(prod)}(\bar{x}) \bar{x} d\bar{x} + l_0 \delta_{\Delta l, 0} \end{aligned}$$

Now only $\int w_{0, \Delta l}^{(prod)}(\bar{x}) \bar{x} d\bar{x}$ has to be calculated once for every Δl (and different band index combinations α, α'). As expected from the properties of the Wannier functions, elements with high Δl will be very small and a cut-off can be applied.

A.5 Exact Diagonalization

Starting point for the exact diagonalization procedure for a lattice system is the effective stationary Schrödinger equation for the u -functions obtained using the Bloch theorem

$$\left[-\frac{\hbar^2}{2m}(i\nabla + \vec{k})^2 + V(\vec{r}) \right] u_{\vec{k},\alpha}(\vec{r}) = E_{\vec{k},\alpha} u_{\vec{k},\alpha}(\vec{r})$$

With the potential $V(x)$ and thus the $u_{k,\beta}$ being periodic, it is possible to expand them in terms of Fourier coefficients:

$$u_{\vec{k},\alpha}(\vec{r}) = \sum_{n_1, n_2, n_3} c_{n_1, n_2, n_3}^{(\vec{k}, \alpha)} e^{i(n_1 \vec{b}_1 + n_2 \vec{b}_2 + n_3 \vec{b}_3) \vec{r}}$$

$$V(\vec{r}) = \sum_{n_1, n_2, n_3} V_{n_1, n_2, n_3} e^{i(n_1 \vec{b}_1 + n_2 \vec{b}_2 + n_3 \vec{b}_3) \vec{r}}$$

The \vec{b} 's above should be chosen to be the reciprocal lattice vectors to assure a small number of Fourier coefficients.

Plugging these series expansions into the effective stationary Schrödinger equation the following derivation can be conducted

$$\begin{aligned} & \left[-\frac{\hbar^2}{2m}(i\nabla + \vec{k})^2 + \sum_{n_1, n_2, n_3} V_{n_1, n_2, n_3} e^{i(n_1 \vec{b}_1 + n_2 \vec{b}_2 + n_3 \vec{b}_3) \vec{r}} \right] \times \\ & \quad \sum_{n_1, n_2, n_3} c_{n_1, n_2, n_3}^{(\vec{k}, \alpha)} e^{i(n_1 \vec{b}_1 + n_2 \vec{b}_2 + n_3 \vec{b}_3) \vec{r}} = \\ & \quad E_{\vec{k},\alpha} \sum_{n_1, n_2, n_3} c_{n_1, n_2, n_3}^{(\vec{k}, \alpha)} e^{i(n_1 \vec{b}_1 + n_2 \vec{b}_2 + n_3 \vec{b}_3) \vec{r}} \\ \\ & -\frac{\hbar^2}{2m}(i\nabla + \vec{k})^2 \sum_{n_1, n_2, n_3} c_{n_1, n_2, n_3}^{(\vec{k}, \alpha)} e^{i(n_1 \vec{b}_1 + n_2 \vec{b}_2 + n_3 \vec{b}_3) \vec{r}} + \\ & \sum_{n_1, n_2, n_3} V_{n_1, n_2, n_3} e^{i(n_1 \vec{b}_1 + n_2 \vec{b}_2 + n_3 \vec{b}_3) \vec{r}} \sum_{m_1, m_2, m_3} c_{m_1, m_2, m_3}^{(\vec{k}, \alpha)} e^{i(m_1 \vec{b}_1 + m_2 \vec{b}_2 + m_3 \vec{b}_3) \vec{r}} = \\ & \quad E_{\vec{k},\alpha} \sum_{n_1, n_2, n_3} c_{n_1, n_2, n_3}^{(\vec{k}, \alpha)} e^{i(n_1 \vec{b}_1 + n_2 \vec{b}_2 + n_3 \vec{b}_3) \vec{r}} \\ \\ & -\frac{\hbar^2}{2m} \sum_{n_1, n_2, n_3} (\vec{k} - n_1 \vec{b}_1 - n_2 \vec{b}_2 - n_3 \vec{b}_3)^2 c_{n_1, n_2, n_3}^{(\vec{k}, \alpha)} e^{i(n_1 \vec{b}_1 + n_2 \vec{b}_2 + n_3 \vec{b}_3) \vec{r}} + \\ & \sum_{n_1, n_2, n_3} \sum_{m_1, m_2, m_3} V_{n_1, n_2, n_3} c_{m_1, m_2, m_3}^{(\vec{k}, \alpha)} e^{i((n_1 + m_1) \vec{b}_1 + (n_2 + m_2) \vec{b}_2 + (n_3 + m_3) \vec{b}_3) \vec{r}} = \\ & \quad E_{\vec{k},\alpha} \sum_{n_1, n_2, n_3} c_{n_1, n_2, n_3}^{(\vec{k}, \alpha)} e^{i(n_1 \vec{b}_1 + n_2 \vec{b}_2 + n_3 \vec{b}_3) \vec{r}} \end{aligned}$$

For the second term on the left side

$$\vec{n} \rightarrow \vec{n} - \vec{m}$$

$$\begin{aligned}
& -\frac{\hbar^2}{2m} \sum_{n_1, n_2, n_3} (\vec{k} - n_1 \vec{b}_1 - n_2 \vec{b}_2 - n_3 \vec{b}_3)^2 c_{n_1, n_2, n_3}^{(\vec{k}, \alpha)} e^{i(n_1 \vec{b}_1 + n_2 \vec{b}_2 + n_3 \vec{b}_3) \vec{r}} + \\
& \sum_{n_1, n_2, n_3} \sum_{m_1, m_2, m_3} V_{n_1-m_1, n_2-m_2, n_3-m_3} c_{m_1, m_2, m_3}^{(\vec{k}, \alpha)} e^{i(n_1 \vec{b}_1 + n_2 \vec{b}_2 + n_3 \vec{b}_3) \vec{r}} = \\
& E_{\vec{k}, \alpha} \sum_{n_1, n_2, n_3} c_{n_1, n_2, n_3}^{(\vec{k}, \alpha)} e^{i(n_1 \vec{b}_1 + n_2 \vec{b}_2 + n_3 \vec{b}_3) \vec{r}} \\
& \sum_{n_1, n_2, n_3} \left[-\frac{\hbar^2}{2m} (\vec{k} - n_1 \vec{b}_1 - n_2 \vec{b}_2 - n_3 \vec{b}_3)^2 c_{n_1, n_2, n_3}^{(\vec{k}, \alpha)} + \right. \\
& \left. \sum_{m_1, m_2, m_3} V_{n_1-m_1, n_2-m_2, n_3-m_3} c_{m_1, m_2, m_3}^{(\vec{k}, \alpha)} \right] e^{i(n_1 \vec{b}_1 + n_2 \vec{b}_2 + n_3 \vec{b}_3) \vec{r}} = \\
& E_{\vec{k}, \alpha} \sum_{n_1, n_2, n_3} c_{n_1, n_2, n_3}^{(\vec{k}, \alpha)} e^{i(n_1 \vec{b}_1 + n_2 \vec{b}_2 + n_3 \vec{b}_3) \vec{r}}
\end{aligned}$$

This holds for all \vec{r} . Thus the equation can be separated

$$\begin{aligned}
& -\frac{\hbar^2}{2m} (\vec{k} - n_1 \vec{b}_1 - n_2 \vec{b}_2 - n_3 \vec{b}_3)^2 c_{n_1, n_2, n_3}^{(\vec{k}, \alpha)} + \sum_{m_1, m_2, m_3} V_{n_1-m_1, n_2-m_2, n_3-m_3} c_{m_1, m_2, m_3}^{(\vec{k}, \alpha)} = \\
& E_{\vec{k}, \alpha} c_{n_1, n_2, n_3}^{(\vec{k}, \alpha)}
\end{aligned}$$

Given the Fourier coefficients for a potential, the above formula which represents a whole system of equations can be used to obtain the Fourier coefficients of the u -functions. This equation is still very general. Especially separable potentials allow for further simplification. In order to be able to calculate anything, the Fourier coefficients for the potential need to be calculated.

To find the Fourier coefficients for a given real space potential the equation that constructs the real space potential from the coefficients has to be integrated over one unit cell ranging from $\vec{0}$ to \vec{a}

$$\begin{aligned}
V(\vec{r}) &= \sum_{n_1, n_2, n_3} V_{n_1, n_2, n_3} e^{i(n_1 \vec{b}_1 + n_2 \vec{b}_2 + n_3 \vec{b}_3) \vec{r}} \\
& \int_{z=0}^{a_3} \int_{y=0}^{a_2} \int_{x=0}^{a_1} V(\vec{r}) e^{-i(n'_1 \vec{b}_1 + n'_2 \vec{b}_2 + n'_3 \vec{b}_3) \vec{r}} dx dy dz = \\
& \int_{z=0}^{a_3} \int_{y=0}^{a_2} \int_{x=0}^{a_1} \sum_{n_1, n_2, n_3} V_{n_1, n_2, n_3} e^{i((n_1 - n'_1) \vec{b}_1 + (n_2 - n'_2) \vec{b}_2 + (n_3 - n'_3) \vec{b}_3) \vec{r}} dx dy dz = \\
& \int_{z=0}^{a_3} \int_{y=0}^{a_2} \int_{x=0}^{a_1} V_{n'_1, n'_2, n'_3} dx dy dz = \\
& a_1 a_2 a_3 V_{n'_1, n'_2, n'_3}
\end{aligned}$$

Thus the Fourier coefficients for the potential are

$$V_{n_1, n_2, n_3} = \frac{1}{a_1 a_2 a_3} \int_{z=0}^{a_3} \int_{y=0}^{a_2} \int_{x=0}^{a_1} V(\vec{r}) e^{-i(n_1 \vec{b}_1 + n_2 \vec{b}_2 + n_3 \vec{b}_3) \cdot \vec{r}} dx dy dz$$

As a short example, the Fourier coefficients for the simple 1-dimensional sine potential $V(x) = A \cos(bx)$ with unit cell size of $a = \frac{2\pi}{b}$ are

$$\begin{aligned} V_n &= (\delta_{n,1} + \delta_{n,-1}) A \frac{b}{2\pi} \int_{x=0}^a \cos(bx) \cos(bx) dx \\ &= (\delta_{n,1} + \delta_{n,-1}) \frac{A}{2} \end{aligned}$$

A.5.1 Localized States at Avoided Crossing

$$\hat{H} = \sum_n |n\rangle E_n \langle n|$$

Given the case that most states $|n\rangle$ are nicely localized and assignable to bands except for two states $|n_1\rangle$ and $|n_2\rangle$ whose energies are very close and whose expectation is similar for two different band projectors, see state 6, 7 in middle right plot in Figure 5.5. Using a superposition of these two states we may be able to derive states that can be assigned to bands more easily.

$$\begin{aligned} |n_1\rangle &= a|m_1\rangle + \sqrt{1-a^2}|m_2\rangle \\ |n_2\rangle &= \sqrt{1-a^2}|m_1\rangle - a|m_2\rangle \end{aligned}$$

$$\begin{aligned} \hat{H} &= \sum_{n \setminus \{n_1, n_2\}} |n\rangle E_n \langle n| \\ &+ (a|m_1\rangle + \sqrt{1-a^2}|m_2\rangle)E_1(a\langle m_1| + \sqrt{1-a^2}\langle m_2|) \\ &+ (\sqrt{1-a^2}|m_1\rangle - a|m_2\rangle)E_2(\sqrt{1-a^2}\langle m_1| - a\langle m_2|) \end{aligned}$$

$$\begin{aligned} \hat{H} &= \sum_{n \setminus \{n_1, n_2\}} |n\rangle E_n \langle n| \\ &+ E_1(a^2|m_1\rangle\langle m_1| + (1-a^2)|m_2\rangle\langle m_2| \\ &+ a\sqrt{1-a^2}(|m_1\rangle\langle m_2| + |m_2\rangle\langle m_1|)) \\ &+ E_2((1-a^2)|m_1\rangle\langle m_1| + a^2|m_2\rangle\langle m_2| \\ &- a\sqrt{1-a^2}(|m_1\rangle\langle m_2| + |m_2\rangle\langle m_1|)) \end{aligned}$$

assuming $E := E_1 \approx E_2$ the Hamiltonian becomes

$$\begin{aligned} \hat{H} &= \sum_{n \setminus \{n_1, n_2\}} |n\rangle E_n \langle n| \\ &+ E(|m_1\rangle\langle m_1| + |m_2\rangle\langle m_2|) \end{aligned}$$

The band projector can now be defined in terms with the states m_1 and m_2 instead of the states n_1 and n_2 . This should allow for a clear band assignment and thus for nicely localized Wannier states.

Using the new band projectors, \hat{H} will not be strictly block diagonal in the generalized Wannier basis. This is because a Wannier state in one band will have contributions from $|n_1\rangle$ and $|n_2\rangle$ which each have parts in different bands (which are defined through m_1 and m_2). The size of the matrix \hat{H} in the generalized Wannier basis increases by 1 in each direction. Consequently, in a Hubbard-like model, further elements might have to be taken into account.

Bibliography

- [ASSK⁺06] Marco Anderlini, Jennifer Sebby-Strabley, Jens Kruse, James V Porto, and William D Phillips. Controlled atom dynamics in a double-well optical lattice. *Journal of Physics B: Atomic, Molecular and Optical Physics*, 39(10):S199, 2006.
- [BDH12] U. Bissbort, F. Deuretzbacher, and W. Hofstetter. Effective multi-body induced tunneling and interactions in the Bose-Hubbard model of the lowest dressed band of an optical lattice. 2012, arXiv:1108.6047.
- [Bis07] Ulf Bissbort. Stochastic mean field theory for the disordered bose-hubbard model, 2007.
- [Bis12] Ulf Bissbort. Dynamical Effects and Disorder in Ultracold Bosonic Matter. PhD thesis, Johann Wolfgang Goethe-Universität, 2012.
- [Blo05] I. Bloch. Ultracold quantum gases in optical lattices. *Nat Phys*, 2005.
- [BPC⁺07] Christian Brouder, Gianluca Panati, Matteo Calandra, Christophe Mourougane, and Nicola Marzari. Exponential localization of wannier functions in insulators. *Phys. Rev. Lett.*, 98:046402, Jan 2007.
- [BWP⁺09] J. Biddle, B. Wang, D. J. Priour, Jr., and S. Das Sarma. Localization in one-dimensional incommensurate lattices beyond the Aubry-andr model. *Phys.Rev.*, A80:021603, 2009.
- [DZS⁺03] B. Damski, J. Zakrzewski, L. Santos, P. Zoller, and M. Lewenstein. Atomic bose and anderson glasses in optical lattices. 2003, arXiv:cond-mat/0303065.
- [EOD⁺12] M. Egorov, B. Opanchuk, P. Drummond, B. V. Hall, P. Hannaford, and A. I. Sidorov. Precision measurements of s-wave scattering lengths in a two-component Bose-Einstein condensate. 2012, arXiv:1204.1591.
- [GTVG97] L. Guidoni, C. Triché, P. Verkerk, and G. Grynberg. Quasiperiodic optical lattices. *Phys. Rev. Lett.*, 79:3363–3366, Nov 1997.
- [HH93] A. Hemmerich and T. W. Hänsch. Two-dimesional atomic crystal bound by light. *Phys. Rev. Lett.*, 70:410–413, Jan 1993.

- [HQ04] Chris Hooley and Jorge Quintanilla. Single-atom density of states of an optical lattice. *Phys. Rev. Lett.*, 93:080404, Aug 2004.
- [HZH94] A. Hemmerich, C. Zimmermann, and T. W. Hänsch. Multiphoton transitions in a spin-polarized 3d optical lattice. *Phys. Rev. Lett.*, 72:625–628, Jan 1994.
- [JInA13] Aitor Bergara, Giulio Pettini, Michele Modugno, Julen Ibañez Azpiroz, Asier Eiguren. Self-consistent tight-binding description of Dirac points moving and merging in two dimensional optical lattices. 2013, arXiv:1306.1796.
- [KH91] L. S. Kuzmin and D. B. Haviland. Observation of the bloch oscillations in an ultrasmall josephson junction. *Phys. Rev. Lett.*, 67:2890–2893, Nov 1991.
- [KS82] S. Kivelson and J. R. Schrieffer. Fractional charge, a sharp quantum observable. *Phys. Rev. B*, 25:6447–6451, May 1982.
- [LCV⁺92] B. Lounis, J.-Y. Courtois, P. Verkerk, C. Salomon, and G. Grynberg. Measurement of the friction coefficient in 1d corkscrew optical molasses by stimulated rayleigh spectroscopy. *Phys. Rev. Lett.*, 69:3029–3032, Nov 1992.
- [MMY⁺12] N. Marzari, A. A. Mostofi, J. R. Yates, I. Souza, and D. Vanderbilt. Maximally localized Wannier functions: Theory and applications. 2012, arXiv:1112.5411.
- [MSV03] N. Marzari, I. Souza, and D. Vanderbilt. An Introduction to Maximally-Localized Wannier Functions. *Highlight of the Month - Psi-k Newsletter*, 2003, 57:129-168, 2003.
- [MYL⁺08] Arash A. Mostofi, Jonathan R. Yates, Young-Su Lee, Ivo Souza, David Vanderbilt, and Nicola Marzari. wannier90: A tool for obtaining maximally-localised wannier functions. *Computer Physics Communications*, 178(9):685 – 699, 2008.
- [PC89] M. Prentiss and A. Cable. Slowing and cooling an atomic beam using an intense optical standing wave. *Phys. Rev. Lett.*, 62:1354–1357, Mar 1989.
- [SBM⁺11] J. Simon, W. S. Bakr, R. Ma, M. E. Tai, P. M. Preiss, and M. Greiner. Quantum Simulation of Antiferromagnetic Spin Chains in an Optical Lattice. 2011, arXiv:1103.1372.
- [SH07] Michiel Snoek and Walter Hofstetter. Two-dimensional dynamics of ultracold atoms in optical lattices. *Phys. Rev. A*, 76:051603, Nov 2007.
- [SZL⁺07] C. Sias, A. Zenesini, H. Lignier, S. Wimberger, D. Ciampini, O. Morsch, and E. Arimondo. Resonantly enhanced tunneling of bose-einstein condensates in periodic potentials. *Phys. Rev. Lett.*, 98:120403, Mar 2007.

- [UJM⁺13] T. Uehlinger, G. Jotzu, M. Messer, D. Greif, W. Hofstetter, U. Bissbort, and T. Esslinger. Artificial graphene with tunable interactions. 2013, arXiv:1308.4401.
- [Wan37] G.H. Wannier. The Structure of Electronic Excitation Levels in Insulating Crystals. Phys. Rev., 52(3):191–197, 1937.
- [WS13] Patrick Windpassinger and Klaus Sengstock. Engineering novel optical lattices. Reports on Progress in Physics, 76(8):086401, 2013.

Acknowledgments

I would like to thank Prof. Dr. Walter Hofstetter for welcoming me into his working group. He generously gave me the opportunity and confidence to work on this theoretical subject and kept me motivated when things looked unfavorable. Furthermore, I would like to thank Prof. Dr. Roser Valenti also, for taking the time to examine this thesis. You each sparked my interest in theoretical physics and in this field of research.

Thank you very much, Ulf Bissbort, for the time you invested to supervise this project. Your detailed advise left me stunned and extremely jealous after nearly every discussion. Many wonderful discussions, not always on topic, were held with the other members of the working group as well. I thank you for your advice and also for the time we all shared together. It was always great fun and I will miss you once our ways part.

The same is true for my other dear friends throughout the university and my whole family. If you hadn't stood by me, even in times when the work caused me to become grouchy, reaching this point would have been unlikely.

Cynthia and Thomas, special thanks for dealing with my errors even though you probably had much better things to do.

Doris, Cynthia and Tobias, spending my vacation with you was great fun and rekindled my motivation for this work. Thank you!

Last, I would like to thank my father who should have seen the results of his efforts.

Erklärung nach §30 (11) Ordnung für den BA- und MA-Studiengang

Hiermit erkläre ich, dass ich die Arbeit selbstständig und ohne Benutzung anderer als der angegebenen Quellen und Hilfsmittel verfasst habe. Alle Stellen der Arbeit, die wörtlich oder sinngemäß aus Veröffentlichungen oder aus anderen fremden Texten entnommen wurden, sind von mir als solche kenntlich gemacht worden. Ferner erkläre ich, dass die Arbeit nicht - auch nicht auszugsweise - für eine andere Prüfung verwendet wurde.

Frankfurt, den